Fabrication and characterization of the nanofluids by the electrical explosion of the wire in liquid method

Eunju Park

Department of Materials Science Engineering

Graduate school of UNIST

Fabrication and characterization of the nanofluids by the electrical explosion of the wire in liquid method

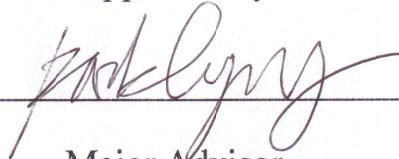A dissertation

Submitted to the Graduate School of UNIST

in partial fulfillment of the requirements

for the degree of Doctor of Philosophy

Eunju Park
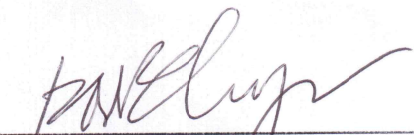
12.01.2014

Approved by

_____

Major Advisor

Hyung Wook Park

UΠiST

Fabrication and characterization of the nanofluids by the electrical explosion of the wire in liquid method

Eunju Park

This certifies that the dissertation of Eunju Park is approved.

12.01. 2014

Thesis Supervisor: Hyung Wook Park

In Cheol Bang

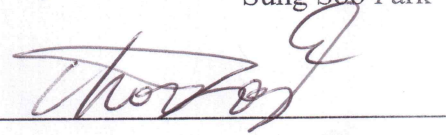Young-Bin Park

Sung Soo Park

Hae-Jin Choi

Abstract

Although nanofluids have superior and unique properties, the problem of dispersion stability and the mass production of nanofluids are still limited in the industrial applications. For this study, nanofluids were prepared using the electrical explosion of wire in liquids (EEWL) method. EEWL enables the manufacture of high-purity nanoparticles without the chemical additives. Other advantages of this method are its simple evaporation and condensation processes, short production times, and the feasibility for mass production. The EEWL method has been employed in the production of pure metallic nanofluids as well as their oxides. In this study, silver, copper oxide and aluminum oxide nanofluids were synthesized under various experimental parameters, such as voltage, capacitance, length of the wire and basefluid. The size of nanoparticles depends on the deposited energy value in the wire. The phase and morphology of nanoparticles are influenced by the basefluid and the additives. The nanoparticles synthesized by the EEWL process are spherical in shape. Copper oxide and aluminum oxide nanoparticles are synthesized in the water due to a chemical reaction with oxygen and hydroxyl. In the case of copper, the copper oxide nanoparticles were synthesized to be spherical in shape in the water as basefluid, whereas the 3D copper oxide structure particles were synthesized by adding sodium hydroxide (NaOH) or ammonia ($NH_3 \cdot H_2O$) in the water. In this study, the metallic and oxide nanofluids were prepared in the various base fluids. The structure and morphology were investigated using various analysis tools, such as X-ray diffraction, X-ray photoelectron spectroscopy, high-resolution transmission electron microscopy, and field emission scanning electron microscopy. The optical band gap was determined using ultraviolet/visible spectroscopy. The impact of deposited energy in the wire on the size and shape of the nanoparticles were analyzed by using TEM analysis. In order to determine the optimized experimental conditions of nanofluids production, the investigation of the effects of experimental parameters are very important. As a method for the optimization of the process conditions, we used design of experiments (DOE) and analysis of calculated deposited energy values in the wire by measuring the voltage and current oscillograms. Through production of the silver nanofluids, optimized conditions can be determined by the MINITAB tool. The energy used in the explosion has to be experimentally quantified using the voltage and current oscillograms because it is difficult to directly measure the energy and to theoretically calculate it. Furthermore, the explosion phenomena can be explained by the analysis of the voltage and current oscillograms.

The thermal conductivity and the viscosity of aluminum oxide nanofluids were measured and compared with the prediction models. The experimental results are similar to the prediction model, the increasing of the thermal conductivity and the viscosity could not be confirmed because of the very small concentration of nanoparticles.

A pool boiling experiment was performed to investigate the effect of nanofluids on critical heat flux

(CHF) enhancement. The nanofluids for experiments were prepared into two groups; 1) the water-based silver, copper oxide and aluminum oxide nanofluids synthesized by electrical explosion of the wire in liquid method and 2) xGnPs and xGnPs oxide nanofluids prepared by sonication. The silver, copper oxide and aluminum oxide nanofluids prepared by the electrical explosion of the wire in liquid process caused significant CHF enhancement during pool boiling experiments: 187% at 0.001 vol% for aluminum oxide, 58% at 0.001 vol% for silver, and 99% at 0.001 vol% for copper oxide nanofluids. The xGnPs oxide nanofluids dispersed with 0.005 vol% particles showed the largest CHF enhancement (189%). Deposition of nanoparticles on the wire surface occurs during nucleate boiling, and it can change the surface properties. In this study, the CHF phenomenon was also predicted using Kandlikar's CHF model. The CHF results of silver, copper oxide and aluminum oxide nanofluids are in accord with the trend of the theoretical results. However, in case of the xGnPs and xGnPs oxide nanofluids, the CHF is enhanced with increasing of the contact angle value while CHF by Kandlikar's model is enhanced with decrease the contact angle.

Contents

List of Figures

List of Tables

Nomenclature

W	the energy deposited in the wire
$V(\tau)$	the voltage with time integration
$i(\tau)$	the current with time integration
α	the absorption coefficient
hv	the photon energy
n	the nature of the transition
E_g	the optical band gap
k_{eff}	the effective thermal conductivity
k_p	the thermal conductivity of the particle
k_b	the thermal conductivity of the base liquid
Φ	the particle volume fraction in the liquid
C	a modified constant
c_{BF}	the specific heat of the base fluid
a, b	empirical constants
f	the volume fraction
ρ_p	particle density
μ	viscosity of base fluid
d_p	diameter of particle
T	the absolute temperature (K)
q"	heat flux
A	area
S	the thermal activity
δ	the heater dimension
ρ_v	the gas density
ρ_l	the liquid density
h_{fg}	the latent heat from the liquid state to the gas state
σ	the surface tension
θ	the receding contact angle
φ	the surface angle

Chapter 1. Introduction

1.1. Background

Metal nanoparticles have the unique properties such as physical, chemical and biological compared to the micro and macro-size particles, due to the high surface-to-volume ratio. Nanofluids have attracted a wide range of fields for application, such as catalysis, electronics, biological, sensor, ink printing and heat transfer [1-6] .

Nanofluids are extensively playing an important role in the development of advanced nanotechnology. Development of many industrial and new technologies is limited in the agglomeration of the nanoparticles. In one such case, the most attractive property of nanofluids is the enhancement of the thermal conductivity. The thermal conductivity of nanofluids depends on many parameters including the thermal conductivity of the base fluid and the nanoparticles, the volume fraction, the size, the shape, the clustering of the nanoparticles and the temperature. However, there is a lack of agreement between experimental results from other studies [7]. To reconcile these discrepancies, it is essential to identify the effects of various parameters and investigate the interaction among the parameters systematically.

There are two methods for the production of the nanofluids: the one-step and two-step methods. With the two-step approach, the nanoparticles are produced by physical and chemical methods and then are dispersed in a basefluid, but the aggregation of nanoparticles appears easily due to their high surface energy. The two-step method is useful for the preparation of nanofluids with a high concentration; however it needs sufficient energy for the breakdown of the agglomeration between the nanoparticles. The one-step method is a process of combining the production of nanoparticles and dispersion in liquid. In the one-step method, agglomeration of the nanoparticles is prohibited and the long-term stability of nanofluids is possible because of the avoiding of steps such as the drying, storage, and handling of nanoparticles. A disadvantage of the conventional method is that it is impossible to do mass production for industrial applications. Electrical explosion of the wire in liquid (EEWL), a physical synthesis technique, is a promising one-step method. The electrical explosion of the wire in liquid technique enables the manufacture of high-purity nanoparticles without any chemical additives or surfactant. Other advantages of this method are its simple process consisting of evaporation and condensation, short production times, and the feasibility for mass production. This method has been employed in the production of pure metallic nanoparticles as well as their oxides and other compounds. Figure 1-1 shows the method of nanofluids and its background conditions by using

the electrical explosion of the wire in liquids that are used in this study. The investigations have been carried out to determine the effect of various experimental parameters on the characteristics of nanofluids. Some of these parameters include the kind of basefluid, the viscosity of the liquid, and the energy deposited into the wire. Figure 1-1 illustrates the nanoparticles formation by transfer of the electric energy into heat. The exploding wire phenomenon depends upon a very fast current rise, on the order of a few microseconds. The wire was heated by the pulse current passing through it. The wire was replaced to liquid column of metal. The surface of the liquid column was condensed to a solid by the surrounding media. The wire was expanded and broken instability. Then, a sudden flash of light is observed by disruption of the arcs formed between the broken wires. Finally the generated metal vapors and ions were condensed by the surrounding media and the nanoparticles were formed.
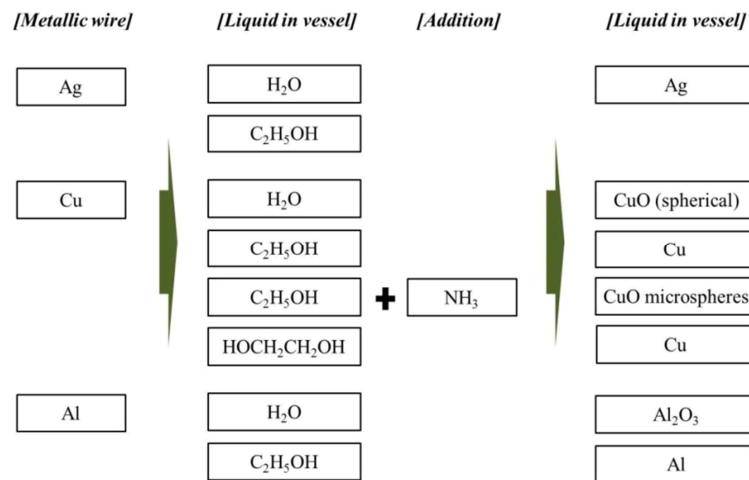
Figure 1-1. Nanofluids produced by electrical explosion of the wire in liquids
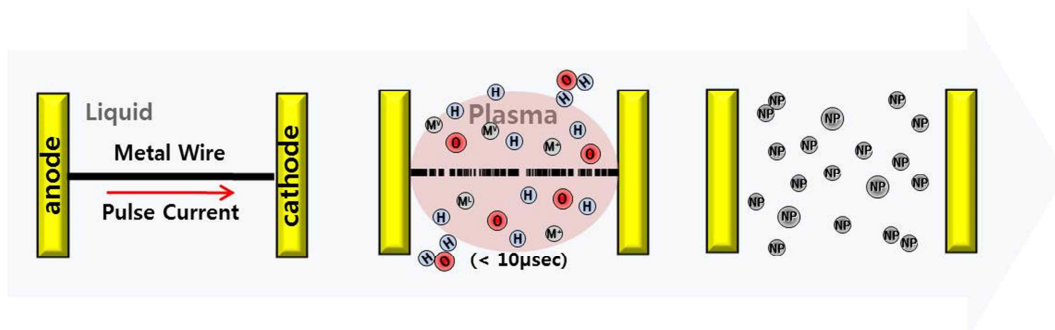
Figure 1-2. Illustration of model of nanoparticles formation by wire explosion

2

It is difficult to clearly understand the electrical explosion of the wire in liquids process, which involves heating and evaporation, followed by condensation of the vapor molecules. The process is activated by energy deposited into the wire. Energy stored in the capacitors is used as the explosion energy of the wire. The parameter conditions of the explosion are selected on the basis of the used energy efficiency charged in the capacitors and the energy density applied in the wire. The energy applied in the wire is one of the important parameters for determining the resistance change and thermodynamic state of the wire when the wire explodes and characteristic of the nanoparticles. The energy used in the explosion has to be quantified experimentally using the voltage and current oscillograms because it is difficult to calculate theoretically. The effect of parameters on particles formation can be investigated through measurements of voltage and current. Dispersion stability was examined by observing the mobility of particles in the liquids. Through a variety of experimental conditions, the optimization conditions can be found out.

The possibility of application to thermal fluids or catalyst was examined using high purity nanofluids produced by the EEWL process.
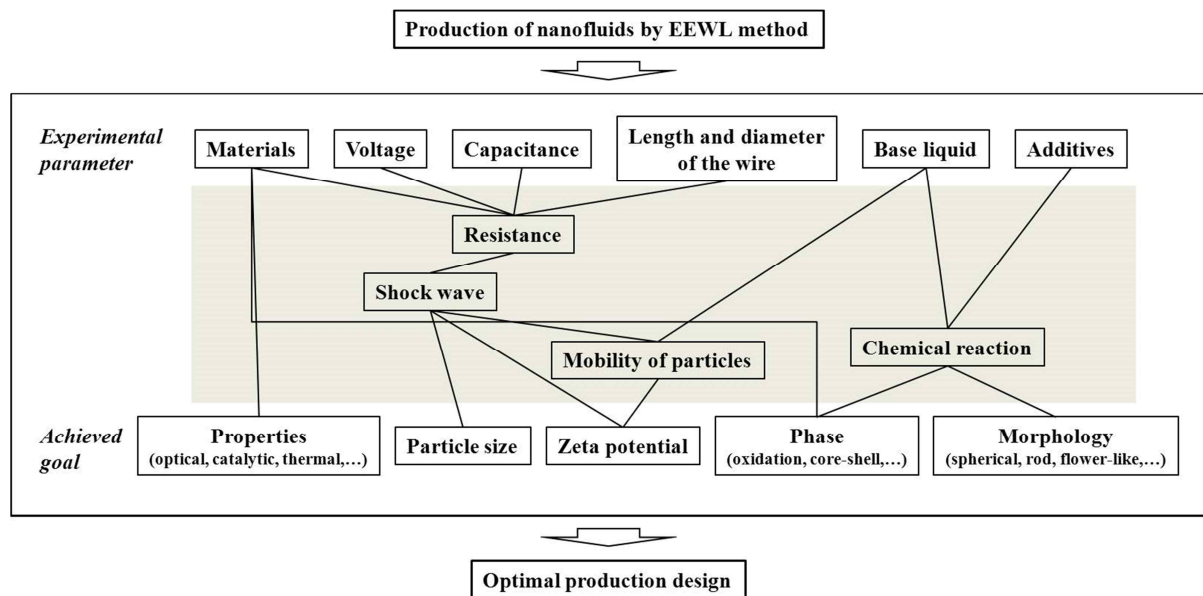
Figure 1-3. Interaction diagram for optimization design between experimental parameters and characteristic

3

1.2. Research Objectives

The electrical explosion of the wire in liquid method has been used for the production of nanofluids due to several advantages: (i) high purity, (ii) high energy efficiency, and (iii) the possibility of mass production. The electrical explosion of the wire in liquid method has been studied due to its physical phenomena during explosion of the wire. Changing the size and shape of the nanoparticles has different characteristics because their electronic structure, bonding, surface energy, and chemical relativities are related to their surface morphology. Copper oxide is a technologically important material for various applications, such as catalysis, batteries, magnetic storage media, solar energy conversion, gas sensing and field emission transistors. Copper oxide nanostructure is expected to be used for lithium-ion batteries or gas sensors because of the ease of synthesis, and its high-quality and low-cost. Hierarchical copper oxide microsphere can also be synthesized using the electrical explosion of the wire in liquids method. In this regard, the diverse types of nanostructured copper oxide with 3D hierarchical micro/nanostructures were wynthesized. An understanding of the fundamental physical and chemical properties of copper oxide micro/nanostructures is also essential for their application. Investigations have been carried out to determine the effect of various experimental parameters on the characteristics of nanofluids synthesized by the electrical explosion of the wire in liquids method. Experimental parameters are: (i) electrical circuit parameters (voltage, capacitance, and inductance), (ii) the properties of the exploding wire (diameter, length, and defects), (iii) sublimation of the metal, and (iv) properties of the liquid (viscosity, thermal conductivity, and breakdown strength). It is important to understand the effect of each experimental parameter on the characteristics of nanofluids to optimize process parameters. In this study, the design of experiments (DOE) method and analysis of voltage and current oscillograms at the wire explosion were used for optimization of the process parameters. The deposited energy in the wire affects the characteristics of nanofluids in substances. However, there is no way the energy can be measured directly. Therefore, the deposited energy in the wire was determined by multiplying the voltage and current.

In the field of industrial applications, nanofluids, despite some limitations, have excellent properties. The dispersion stability of nanofluids is the main reason for the problem. In this study, nanofluids will prepare to use for the applications. To do that, the basic experiment should be performed with the aim of application. The pool boiling experiments were preceded using silver, copper oxide and aluminum oxide nanofluids produced by the electrical explosion of the wire in liquids method. Several studies have shown that the nanofluids could significantly increase the critical heat flux (CHF) under pool boiling. The reasons of the increasing were related to the nanoparticles deposited on system surface. However, the effect of nanofluids on the CHF enhancement on the basis of the underlying physics is

not yet clear. In this study, we found out the mechanism of the CHF enhancement using various nanofluids.

Silver

Processing parameter	Products	Characterization	Optimization	Application
Capacitance Voltage Length of wire Liquid Liquid volume	Ag	Size, Zeta potential Phase	Design of Experiments (DOE)	CHF enhancement (Pool boiling)

(a)

Al

Processing parameter	Products	Characterization	Optimization	Application
Capacitance Length of wire Liquid	Al Al$_2$O$_3$	Size, Zeta potential Phase Thermal conductivity Viscosity	Analysis of VI oscillograms	CHF enhancement (Pool boiling)

(b)

Cu

Processing parameter	Products	Characterization	Application
Liquid Additives	Cu CuO	Size, Zeta potential Phase Thermal conductivity Viscosity	- CHF enhancement (Pool boiling) - Lithium storage capability enhancement

(c)

Figure 1-4. Experimental design for various nanofluids

1.3. Dissertation organization

The introduction of this study is presented in Chapter 1. Chapter 2 describes the review of literature relating to the electrical explosion of the wire in liquid method and the pool boiling CHF enhancement. The production process and characterization of prepared nanofluids by the electrical explosion of the wire in liquid method is presented in Chapter 3 and 4. Chapters 3 and 4 are divided according to the shape of particles. The effect of various experimental parameters on the characteristics of nanofluids synthesized by the electrical explosion of the wire in liquids method and thermophysical properties of nanofluids are described in Chapter 5. Chapter 6 describes pool boiling experiments using various metallic and carbon-materials nanofluids. Finally, the conclusions and

recommendations are described in Chapter 7. This dissertation is laid out as follows in Figure 1-5.
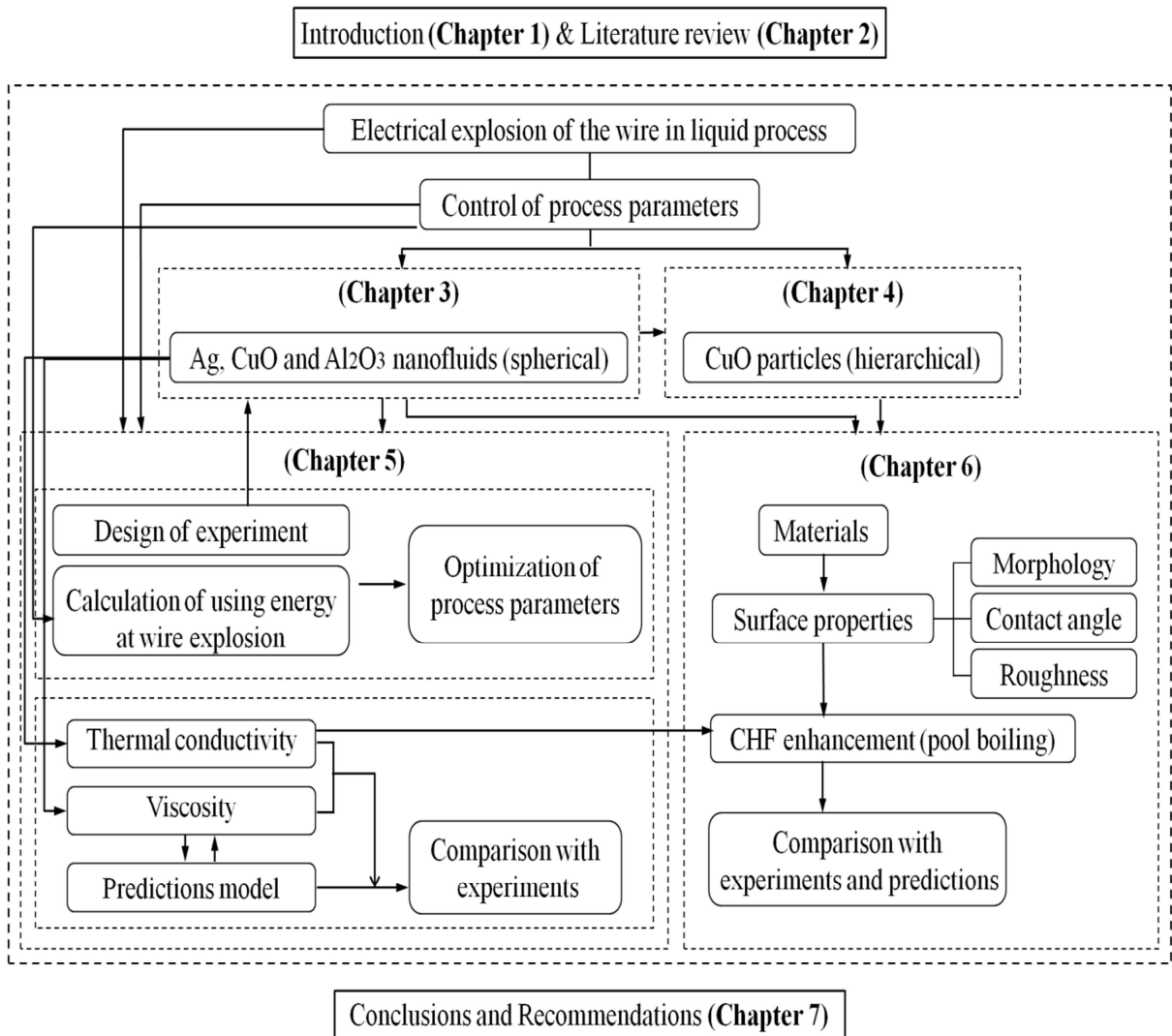
Figure 1-5. Flow chart of dissertation organization

Chapter 2. Literature Review

This chapter presents the review of literature survey of the areas of studies. The literature review is divided into three groups: (i) production of nanofluids by the electrical explosion of the wire in liquid process, (ii) thermophysical properties of nanofluids, and (iii) critical heat flux(CHF), one of application field of nanofluids. The reviews on the electrical explosion of the wire process will include the results of the recent studies of the nanoparticles production with various experimental parameters. Thermophysical properties will include the research on thermal conductivity and viscosity of various nanofluids. The literature review of the critical heat flux will include the research on the enhancement of critical heat flux in pool boiling experiment using nanofluids.

2.1. Electrical explosion of the wire in liquid process

Electrical explosion of the wire(EEW) is a pulsed method that has been known since 1774[8]. It was proceed in the following. A pulsed high-density current in the capacitor, passes through a wire. Then, the wire was heated and exploded by a high rate injection of energy. The explosion of the wire was accompanied with a bright flash of light, a shock wave, the evaporation of the metal, and dispersion of the surrounding medium. Characteristic of particles depend on the explosion conditions.

The production of particles by the electrical explosion of the wire method was first proposed by Abrams[9] in 1946. The electrical explosion of the wire has been studied due to several advantages; (1) high purity high energy efficiency and (2) mass production[10].

Sarathi et al. [11, 12] described the mechanism of nanoparticle formation. There are five stages which are: (1) charging in capacitor, (2) superheating by discharging high current through the wire, (3) decomposition of gas and evaporation of metallic wire surface by deposition of energy in the wire, (4) transition from a liquid to a vapor phase and (5) particle formation. In stage 1, closing the switch, the voltage occurs across the wire and the current will be controlled by RLC circuit. The wire is superheated reaching the boiling point before changing from liquid to vapor phase in stage 2. According to the nucleation mechanism of the wire explosion, the deposited energy during resistive heating cannot exceed the sublimation energy of materials. Next stage, the concentric magnetic field is developed due to current flow in the exploding wire. Figure 2-1[13] shows the characteristic variation in the magnetic pressure. It is realized that the magnetic pressure is maximum at the center

and is minimum near the surface of the wire and hence a surface layer evaporates and plasma is formed before explosion. The magnetic pressure generated compression of the liquid core of the wire. It follows the substance of the liquid core does not reach boiling condition, and the equilibrium pressure of the vapor coexisting with liquid core exceeds the saturation vapor pressure [14]. In stage 4, the metallic wire is vaporized by the deposited energy. The material resistance is determined by the induced energy and 'an integral of the specific current action' (h). The integral of the specific current action (h) can be defined as [15],

$$h = \int_{T0}^{T} \frac{c \, dT}{\rho(\omega)} = \int_{\omega_0}^{\omega} \frac{d\omega}{\rho(\omega)} = \int j^2 dt \approx j^2 t \qquad (2\text{-}1)$$

Then, the nanoparticles are produced and collected in final stage.

When the explosion of the wire occurs, minimum deposited in the wire for evaporation will be equal to the sublimation (Ws) of the material. By Sindhu et al.[13], the particle size decreases substantially with increasing super heating of the metal by injecting energy in excess of wire, i.e., k=W/Ws, where W is the injecting energy into the wire and Ws is the sublimation energy of the wire. Figure 2-2 shows the voltage and current oscillograms measured at different levels of deposited energy. The EEW process can be classified into two stages: the heating stage and the stage of the explosion.
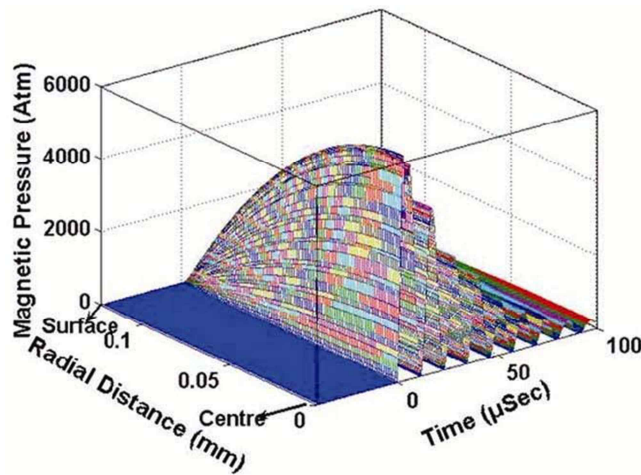
Figure 2-1. Characteristic variation in the magnetic pressure developed due to current flow in exploding conductor[13]

8
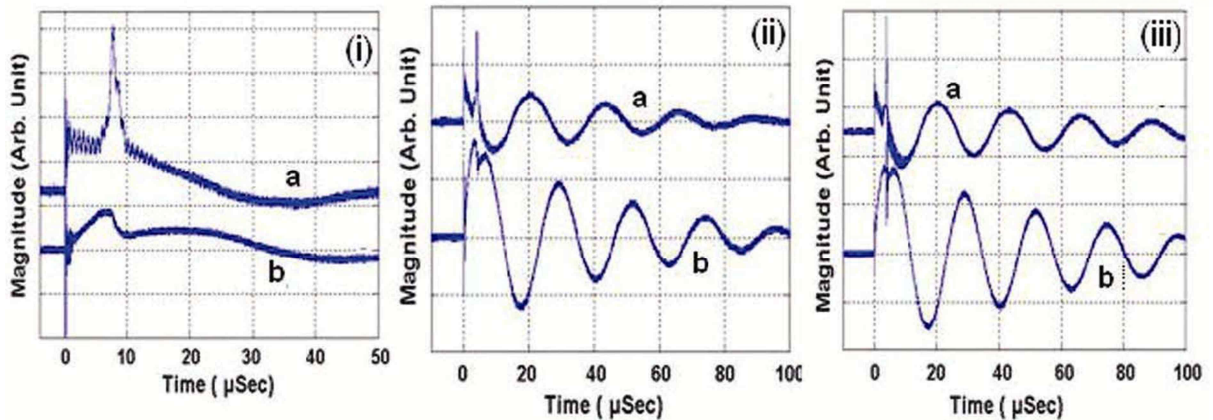
Figure 2-2. Voltage and current oscillograms for different level of deposited energies, (i) w/ws=1, (ii) w/ws=2, (iii) w/ws=3, (a) voltage and (b) current[13]

Electrical explosion of the wire has been employed in the production of pure metallic nanoparticles as well as their oxide, carbide, and nitrides by surrounding atmosphere[16-20]. Previous studies showed that the size distribution, morphology, and phase of particles depend on the induced energy in the wire[21], the heating rate[22], the ambient gas pressure[23, 24], the reactivity of the ambient gas[10, 22], and the diameter of the wire[10]. Cho et al[25] estimated the energy deposition at various discharge conditions, and discussed the effect of energy deposition on the particle size distribution of Cu nanoparticles prepared in the N_2 gas. Energy deposition was increased with increasing current rise. Fast rising pulsed current delivers the high energy in the wire due to inductive energy contribution. Under the conditions of high pressure and fast current rise, the energy deposition exceeds the vaporization energy, but submicron-sized particles still exist. Lee et al.[26] studied the effect of different pressures of air on the characteristics of copper and copper oxide nanoparticles. By adopting the log-normal distribution, median diameter of the particles were decreased with decreasing the air pressure. Sindhu et al.[27] produced aluminum nanoparticles in nitrogen argon and helium atmospheres and analyzed the impact of deposited energy into the conductor on the size and shape of the nanoparticles. Deposited energy is nearly the same in N_2, Ar and He atmospheres. Figure 2-3(a) shows typical variation in the saturation ratio of the vaporized aluminum formed after explosion in different ambiences. The saturation ratio of metal vapors depends on the cooling rate of the ambience. A homogeneous nucleation was generated by the fast cooling of vapors. Figure 2-3 (b) shows the nucleation rate of the aluminum nanoparticles formed in different ambient. The small nucleus was formed at the point of high saturation ratio and nucleation rate.

9
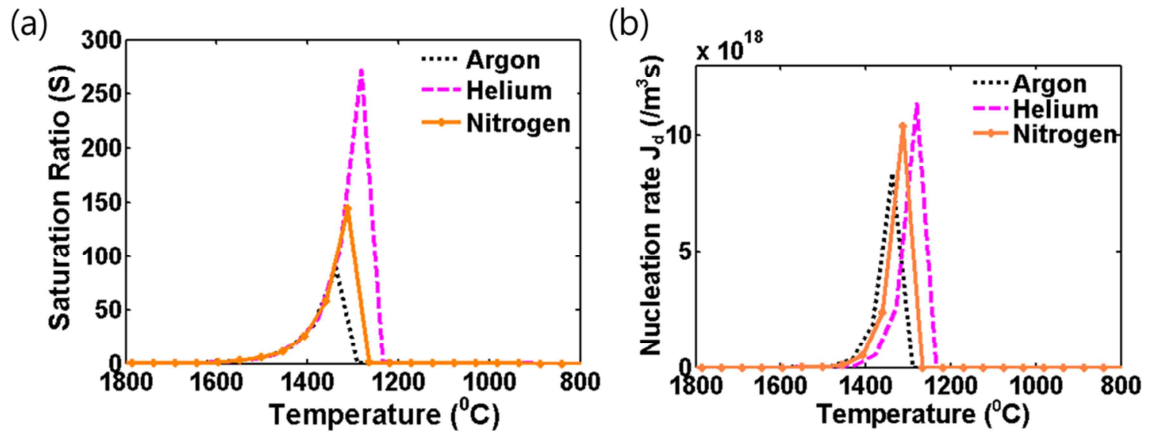
Figure 2-3. Variation of (a) saturation ratio (S) and (b) nucleation rate (J) with temperature in different ambiences[27]

Bora et al.[28] also investigated the mechanism of nanoparticle formation under different gases by optical emission spectroscopy. They synthesized Cu nanoparticles with different pressure of Ar and N_2 atmosphere. Time difference of arc plasma formation was observed between Ar and N_2 ambience. As a result, different pressure of different gases causes the variation of particle size. Size of nanoprticles formed in Ar increases with increasing pressure, while an opposite trend was observed for the nanoparticles produced in N_2 and He. Antony et al.[29] produced aluminum nanoparticles in different inert gas ambience. Their results also showed the same trend about the size of nanoparticles on pressure of Ar, N_2 and He. And they measured the plasma temperature in different ambient by the optical-emission spectroscopy. The intensity of plasma increases with an increase in the ambient pressure. Tungsten carbide nanoparticles were produced in different carburizing medium by Debalina et al.[30] They said that thermal conductivity of the gas plays a major role on the size of the particle. When the thermal conductivity of the gas, the local plasma temperature is high and leads to decrease the particle size. Song et al.[31] synthesized iron oxide nanoparticles for arsenic removal. The explosion of iron wire in air produced magnetic iron oxide nanoparticles compared of magnetite (55.8 wt%) and maghemite (44.2%) without antiferromagnetic, hematite or wüstite phase. The electrical explosion of the wire in liquids method is a useful alternative method for the production of pure metal, chemical compounds and magnetic nanofluids, and these nanofluids would have application such as arsenic removal. Other studies are shown in Table 2-1.

Numerous researches proceeded under gas ambient condition. Several studies are introduced under liquid conditions. Wada et al.[32] synthesized titanium oxide in air and water medium. In air atmosphere, TiO_2 in anatase and rutile phases with well-crystallized spherical particles was observed while unknown phase of Ti-O was recovered in the water. Grinenko et al.[33] were analyzed a number of theoretical approaches on the parameters of a discharge channel consisting of strongly coupled plasma in process of underwater electrical wire explosion. The analysis is based on experimental results obtained from Cu nanoparticles. Good agreement between numeric magneto-hydrodynamics (MHD) calculation and experimental results was obtained. Silver nanoparticles were synthesized in air and water by Cho et al.[34]. This study shows that the enhancement of energy deposition in water medium, due to longer plasma formation time, leads to decrease of particle size. The silver nanoparticles produced in water have smaller particle size compared with that in air. Krasik et al.[35] obtained the experimental and simulations results concerning underwater electrical wire explosion. According the results, the input energy density can be substantially increased as well as the pressure of the generated shock waves (SW) by increasing the power deposition rate. Figure 2-4 shows the dependence of the deposited energy on the wire diameter.

Table 2-1. Previous works on electrical explosion of the wire

authors	material	Product	ambient	Control parameters	Average size
Karioris and Fish[36]	Au, Ag, Al, Cu, Fe, W, Mo, Ni, Th, U, Pt, Mg, Pb, Sn Ta	Au, Ag, Al, Cu, Fe, W, Mo, Ni, Th, U, Pt, Mg, Pb, Sn Ta	Air	Capacitance Applied voltage Wire mass Ambient gas	30-50nm
Phalen et al. [37]	Ag	Ag	Air	Voltage (0-30kV)	$0.3\mu m$
R.Sugunakar Reddy et al. [38]	Zr	ZrN	N_2		
Goloverda G. et al. [39]	Fe_3O_4	Fe_3O_4	DEG		4nm
I.V.Beketov et al. [40]	Fe, Ni	Fe, Ni, $FeCl_2$,	Hexane, toluene, chloroform, polystyrene in toluene In an inert gas	Additives in and inert atmosphere	50-80 nm
Dong-Woo joh et al. [41]	Ni	Ni, Pt	$Pt(NH_3)_2(NO_2)_2$ solution		26nm, 2.7nm
Kyungsun Song et al. [31]	Fe	Magnetite and maghemite	air	For arsenic removal	34nm
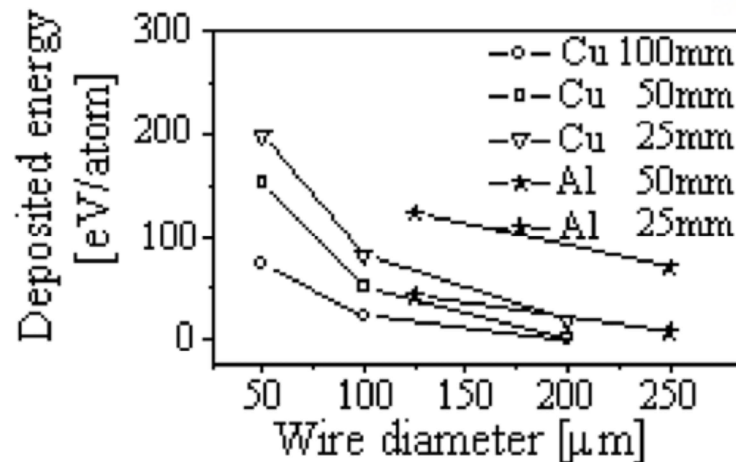
Figure 2-4. Dependence of the average deposited electrical energy per atom on the wire diameter for different wire lengths and material[35]

Kwon et al.[42] investigated and analyzed of aluminum nanoparticles produced in various ambient. In electrical explosion of the wire process, is required the passivation of the particles surface due to self-ignition of metallic. The oxide layers are formed in surface of nanoparticles by passivation. They investigated the difference of the gas-, solid- and liquid-passivated aluminum nanoparticles. Figure 2-5 shows the TEM images of air-passivated and liquid-passivated aluminum nanoparticles. The agglomeration was determined by the explosion process itself and aerodynamics of particles at the formation in a chamber. The necks between spherical particles formed at above the aluminum melting point, because the shape of aluminum liquid droplet was close to spherical at the moment when liquid jet of aluminum melt passed through tem. Organic coated particles had two layers.

Jiang et al.[43] and Cho et al.[44] investigated the process of discharge of the wire in gas and water, respectively. Figure 2-6 shows high-speed photographs obtained under the air condition. In the early stage of the discharge, the current flows through the wire. At a certain moment, the bright points seen on Figure 2-6 (a). The entire wire is evaporated and plasma is expanded in radial direction within 10 ns after the appearance the bright points [Figure 2-6 (b) and (c)]. The expansion of the plasma results in a large volume of the metallic vapors, as shown in Figure 2-6 (d). High-speed photographs of silver wire explosion in water obtained by Cho[44] are shown in Figure 2-7. A round shaped bright area and an annular shaped relatively dark area were formed 0.6 ms after the discharge by shock wave. After 2.7 ms, it was observed that a cloud was formed inside the shell which expanded into a longish shape. The cloud is composed of the particles condensed of the vapor. The shell collapsed and the particles were dispersed into the water after 12 ms.

13
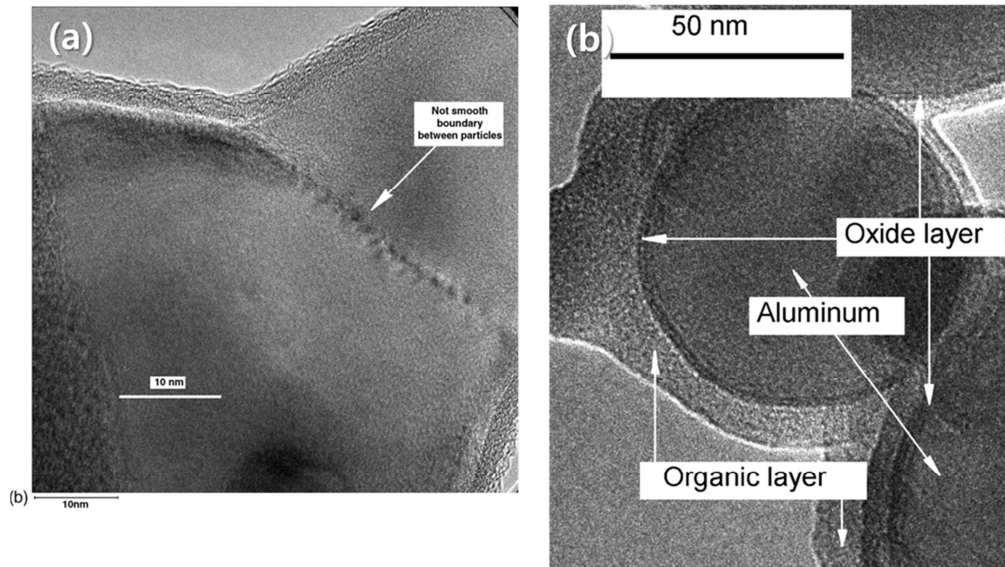
Figure 2-5. TEM images of (a) air-passivated and (b) organically passivated aluminum nanoparticles[42]
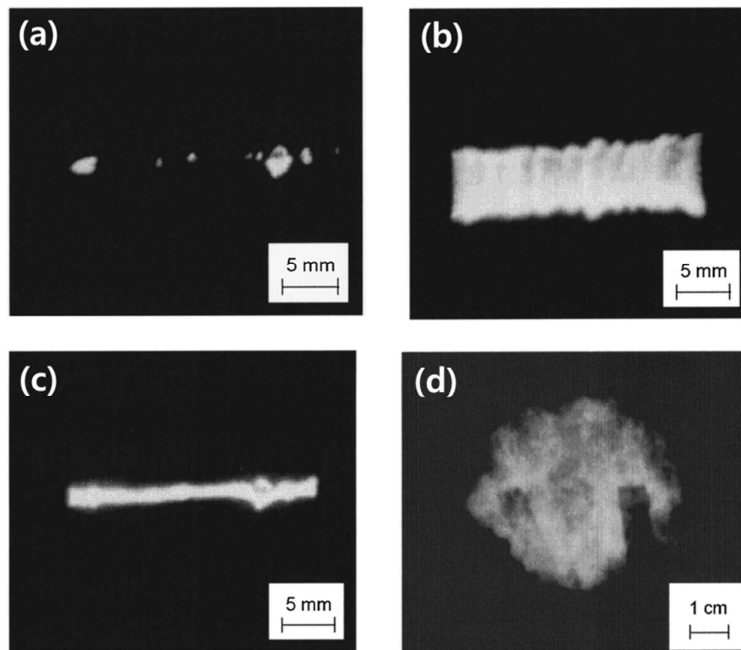
Figure 2-6. High-speed photographs of wire explosion in air (a) t=4.55μs, (b)t=4.65μs, (c) t=5.9μs, and (d) t=350μs [43]
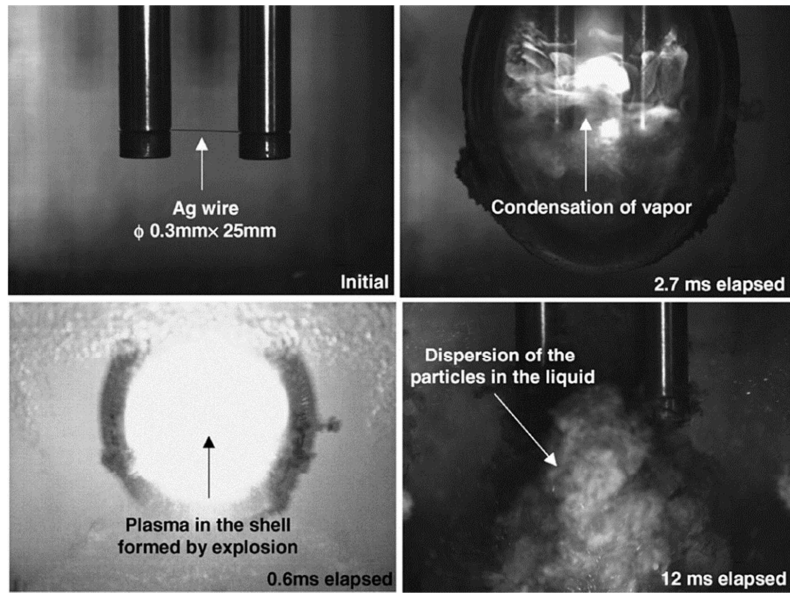
Figure 2-7. High-speed photographs of silver wire explosion in water (Φ 0.3x25mm, 10μF, 12kV,

3000 pps of frame speed, 300μs of exposure[44]

2.2. Heat transfer of nanofluids

2.2.1. Thermal conductivity of nanofluids

Convective heat transfer can be improved by enhancing the thermal conductivity of nanofluids. Numerous theoretical and experimental studies of nanofluids containing metal, metal oxide, and carbide nanoparticles have been conducted. The nanofluids can be improving heat transfer capabilities compared to conventional fluids dispersed coarse-grained or micro-sized particles due to larger relative surface area of nanoparticles. Alumina (Al_2O_3) nanofluids have used many researchers in their experimental investigations due to the most common and inexpensive. Masuda et al. reported a 30% increase in the thermal conductivity of water with 4.3 vol% of Al_2O_3. Eastman et al[45]. measured the thermal conductivity of Al_2O_3 nanofluids with water and its showed 60% improvement of thermal conductivity with only 5 vol% of nanoparticles. Experimental results by Wang et al.[46] showed 12% improvement for 3 vol% Al_2O_3nanofluids. Xie et al[47]. investigated the effect of pH on the thermal conductivity of nanofluids. They found that the pH value at largest difference from isoelectric point resulted in enhancement of the effective thermal conductivity. Several experimental investigation of thermal conductivity is summarized in Table 2-2.

2.2.2. Viscosity of nanofluids

Viscosity is one of the important properties of nanofluids for thermal applications. The pumping power depends on the viscosity of nanofluids. There are the several reports for the effective viscosity of nanofluids as shown in Table 2-3. Prasher et al.[48] measured the viscosity for various shear rates, temperature, diameter and volume fraction of Al_2O_3 nanoparticles. Viscosity of nanofluids is a strong function of volume fraction of nanoparticles compared to temperature and diameter of nanoparticles. However, Nambure et al.[49] found that viscosity decreases with increasing of diameter of nanoparticles. Chen et al.[50] measured the effect of concentration and temperature on viscosity with multi walled carbon nanotubes (MWCNT). They reported that viscosity increases with temperature after 55 at 0.4 vol% ~ volume fraction. Kole and Dey[51] presented the experimental results on viscosity of the Al_2O_3 nanofluids dispersed in commercial car coolant. Viscosity of Al_2O_3 nanofluids increases with increasing concentration of nanoparticles and decreases with increasing temperature. Table 2-3 shows a list including investigations about the effects on viscosity of nanofluids.

Table 2-2. Summary of experimental studies on thermal conductivity

	particles	particles size (nm)	Base fluid	Observations
Masuda et al.[52]	Al_2O_3	13	Water	30% enhancement for 4.3vol% Al_2O_3/water
Lee et al.[53]	Al_2O_3	33	Water	15% enhancement for 4.3vol% Al_2O_3/water
Liu et al.[54]	CuO	50-100	Water	23% enhancement for 0.1vol% CuO/water
Eastman et al.[45]	Al_2O_3/CuO/Cu	33/36/18	Water/HE-200 oil	60% enhancement for 5vol% CuO/water
Wang et al.[55]	Al_2O_3/CuO	28/23	Water/EG/PO/EO	12% enhancement for 3vol% Al_2O_3/water
Xie et al.[47]	Al_2O_3	12.2-302	Water/EG/PO	pH value
Li and Peterson[56]	Al_2O_3/CuO	36/29	Water/oil	30% and 52% enhancement with increase temperature for 6vol% and 10vol % of Al_2O_3 and CuO
Das et al.[57]	Al_2O_3/CuO	38.4/28.6	Water	Increasing with increase of temperature

Table 2-3. Summary of experimental studies on viscosity

Reference	Particles	Particles size (nm)	Base fluid	Observations / Strong function of
Prasher et al.[48]	Al_2O_3	27/40/50	PG	volume fraction
Namburu et al.[49]	SiO_2	20/50/100	EG/Water (60:40)	particles size
Chen et al.[50]	MWCNT	15	Water/EG/Gly	volume fraction (> 0.4vol%) and temperature (>55℃)
Kole and Dey[51]	Al_2O_3	<50	Car engine coolant	volume fraction and at low temperature
Wang et al.[55]	Al_2O_3	28	Water/EG	Mechanical blending than coating particle with polymers and filtration
Tseng and Lin[58]	TiO_2	7-20	Water	Increasing 1200 times for 12 vol% of TiO_2 with water
Nguyen et al.[59]	Al_2O_3	36,47	Water	Increasing 5.3 times for 12 vol% of Al_2O_3 with water
Lee et al.[60]	SiC	<100	Water	Increasing 102 % for 12 vol% of SiC with water
Chen et al.[61]	TiO_2	25	EG	Independent of temperature
Murshed et al.[62]	TiO_2, Al_2O_3	15 80	Water	Increasing 86% and 82% for 5 vol% of TiO_2 and Al_2O_3 with water, respectively
Anoop et al.[29, 63]	Al_2O_3	45,95,100,150	Water, EG	Increasing with decrease of particle size
He et al.[64]	TiO_2	95,145,210	Water	Increasing with increase of particle size and volume fraction
Yang et al.[65]	Graphite	20-40 in thickness	ATF and synthetic base oils	Decreasing with increase of temperature

2.3. Pool boiling CHF enhancement of nanofluids

The critical heat flux (CHF) enhancement can contribute to increasing the safety and economic competitiveness of thermal system. There are many application areas involving CHF, such as nuclear power plants, fusion, and electronics cooling. Nanofluids have been shown to have nucleate boiling critical heat flux comparing with pure base fluid. Over the past decade, numerous experimental and analytical studies of CHF of nanofluids have been conducted. Several studies have shown enhancement of CHF. Studies of CHF enhancement in pool boiling are summarized in Table 2-4. You et al.[66] showed the CHF increasing (~200%) using water-based alumina (Al_2O_3) nanofluids at less than 0.01 vol% in concentration comparing pure water. And they found a thin layer deposited nanoparticles on the heater surface after pool boiling. Shi et al.[67] reported the enhancement of CHF with iron (Fe) and alumina (Al_2O_3) nanofluids. The enhancement is affected on increasing of thermal conductivity and lowered surface tension. Wen and Ding[68] conducted the pool boiling experiments using γ- Al_2O_3 and TiO_2 on a stainless steel disc. They are CHF enhancement above 50% with no deposited particles on the heater surface while Truong[69] found high enhancement up to 68% of CHF with particle deposition. Kim et al.[70] investigated with varying the concentration of nanoparticles and reported CHF enhancement with increasing the concentration of nanoparticles up to a certain point. Liu et al.[71] showed 25-50% increasing of CHF using copper oxide (CuO) nanofluids up to 1wt% in concentration.

There are the other factors affecting on the characteristics of CHF enhancement:

1) the nanoparticle concentration,[66, 70, 71]

2) the nanoparticle material and size[72]

3) the heater size,[73]

4) the system pressure,[71, 74, 75]

5) the existence of additives.[76, 77]

Enhancement of the CHF with nanofluids is dependent on nanoparticle concentration. Figure 2-8 shows the several experimental results for the CHF of nanofluids with various nanoparticles concentration in pool boiling. CHF is enhanced with increasing the particles concentration to a certain concentration.

Table 2-4. Summary of studies on CHF with nanofluids in pool boiling

Reference	Nanofluids	Heater type	Results
Witharana[78]	Au, SiO_2/water, EG	Cu block (D=100mm)	15-20% enhancement
Das et al.[57]	Al_2O_3/water	Cartridge heaters(smooth/rough)	10-40% enhancement
Vassallo et al.[79]	SiO_2/water	NiCr wire (φ=1mm)	60% enhancement
Tu et al.[80]	Al_2O_3/water	Vapor deposited heater (26x40mm)	64% enhancement
Wen et al.[68]	Al_2O_3, TiO_2/water	Stainless steel disc (D=150mm)	40%, 50% enhancement
Bang and Chang[81]	Al_2O_3/water	Rectangular (4x100mm)	20% enhancement
Liu et al.[71]	CuO/water	Grooved Cu block	25-50% enhancement
Shi et al.[67]	γ-Al_2O_3, Fe/water	Cu block (D=60mm)	60% enhancement
Coursey and Kim[82]	Al_2O_3/water, ethanol	Glass, Au and Cu surfaces	40% enhancement
Ahn et al.[83]	MWCNTs/PF-560	Nanostructured Cu block	19-33% enhancement
Kim et al.[84]	TiO_2, Al_2O_3/water	Cu and Ni disks (φ=20mm)	40% enhancement
Kwark et al.[85, 86]	Al_2O_3, CuO, Diamond/water	Cu plate ($40x40mm^2$)	80% enhancement
Park et al.[87]	Graphene, Graphene oxide	NiCr wire	84%, 179% enhancement
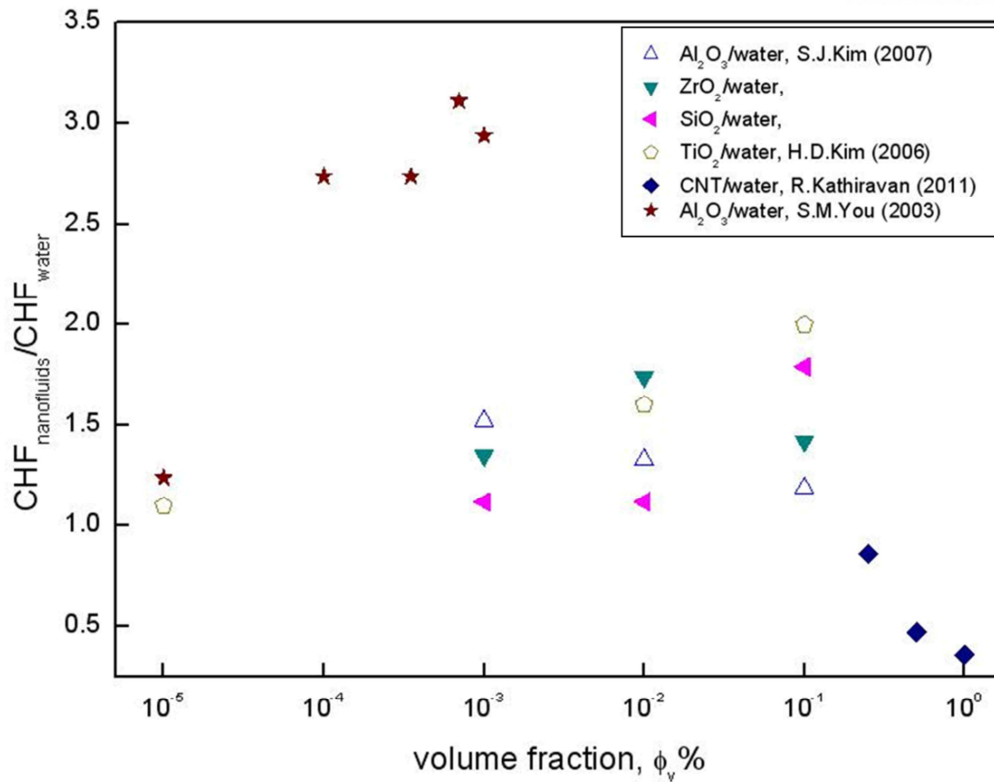
Figure 2-8. CHF increase for different nanofluids [66, 88-90]

The several results of table 2-4 show the different enhancement values even though the nanofluids with the same nanoparticle material are prepared in water without additives and are tested with flat-plate heaters. The enhancement of CHF is not only influenced by the nanoparticle material, but dispersion state of the nanofluids and the geometry of the heaters are influence also.

Moreno et al. shows the nearly identical CHF enhancement with the different particle size while Jo et al. determined that the CHF decreases with increasing particle size.

Many previous studies conducted the nucleate boiling experiments with wires or flat plates. Figure 2-9 shows the experimental results for both flat plates and thin wires under atmospheric condition and without additive. Compared with flat plate, the CHF with thin wires increased as much as 1.5-2.5 times. Nucleate boiling with flat plates generates by the hydrodynamic mechanism, while boiling phenomenon with thin wires is caused by the local dryout mechanism[91].

21
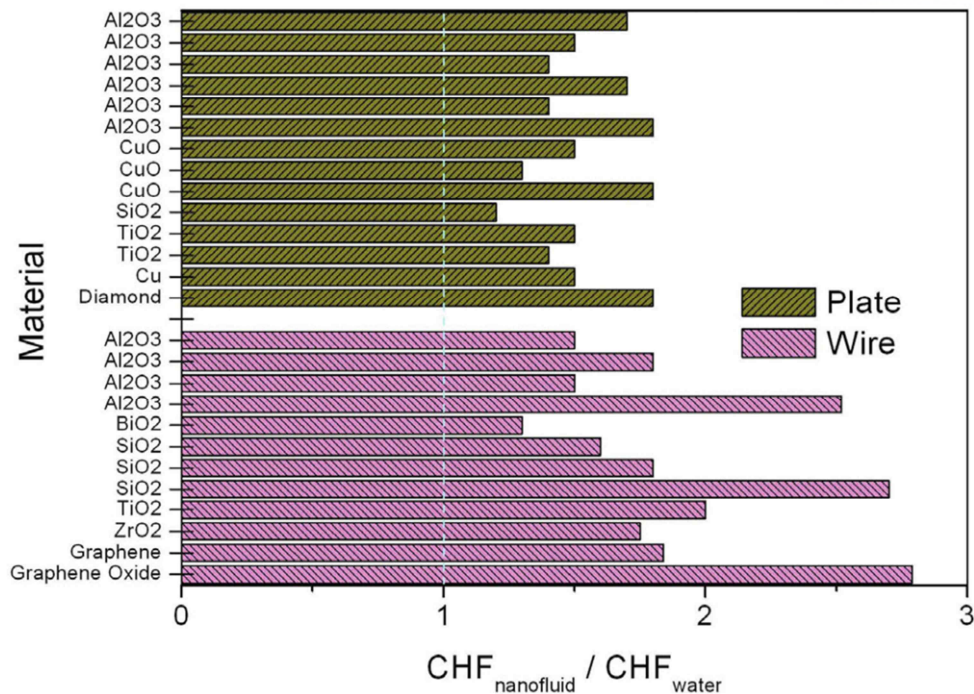
Figure 2-9. Experimental results of measured CHF values for both flat plates and thin wires [91]

Several studies examined the pressure dependency of CHF enhancement in nanofluids. The CHF enhancement decreases with increasing the system pressure due to dry patches. Ionic additives and surfactants affect nucleate boiling by changing of the surface tension. However, the effect of additives on CHF of nanofluids is still not clear.

Some groups [76, 81] noted that the nanofluids significantly changed the surface roughness. Porous surface is affected to CHF phenomena by the trapping of liquid and the breakup of voids on the heater surface.

Common consensus is that nanoparticles enhance the CHF by

1)   changing the morphology and wettability of the heated surface due to the deposited nanoparticles[88, 92-94] and

2)   depositing a layer on the heater, affecting the surface roughness depending on the nanoparticle size and concentration[95, 96].

Kwark et al.[97] investigates the mechanism responsible for the deposition of nanoparticle on the heater surface. The deposition of nanoparticles is generated by the vapor bubbles microlayers

22

evaporate as shown in Figure 2-10. Vapor bubbles grow and leave behind nanoparticles on the heater surface.
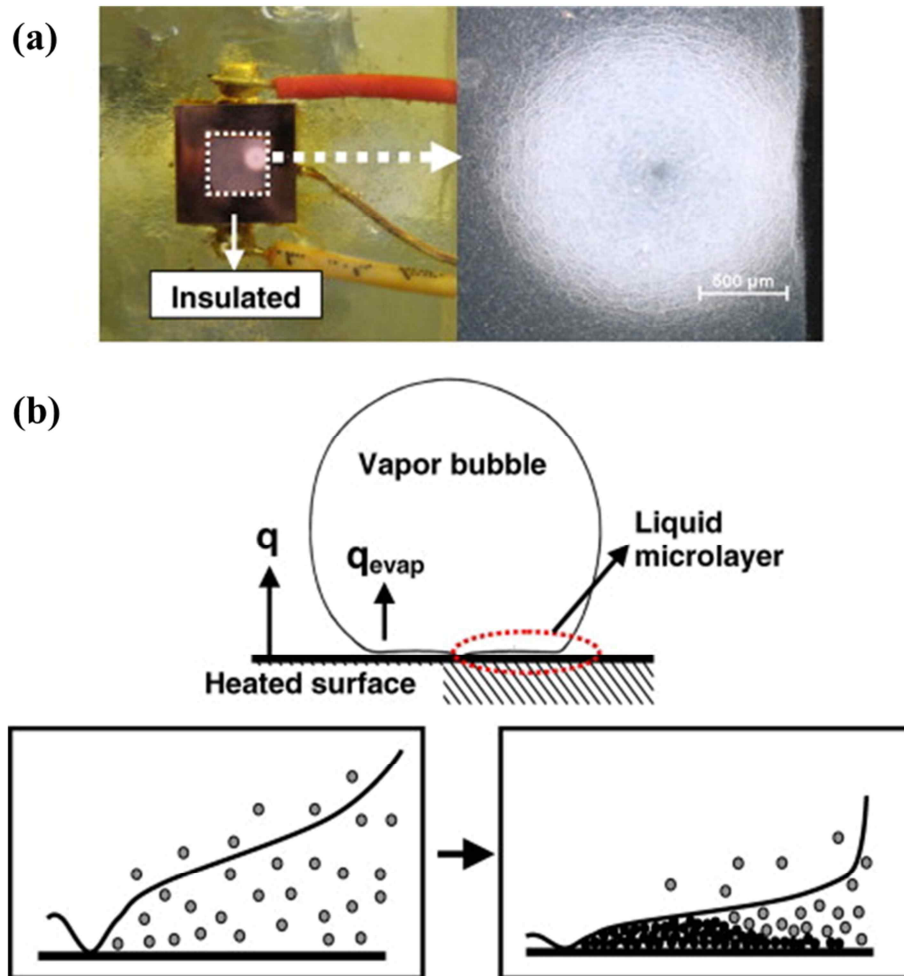
Figure 2-10. (a) Images of nanoparticle coating on the heater surface from a single bubble and (b) the mechanism of the particle deposition during the boiling process[97]

Theoretical studies have been conducted to incorporate the changed surface properties caused by deposited nanoparticles compared with experimental results. According numerous previous studies [88, 98-101], the mechanisms of CHF enhancement can be divided into four categories: 1) hydrodynamic instability, 2) macrolayer dryout, 3) bubble interaction model, and (4) hot/dry spot model. Hydrodynamic instability model of Zuber[102] is the most widely used to interpret CHF phenomena. However, Zuber's model does not consider the surface effects. Kim and Kim[103]

explained hot/dry spots model to understanding CHF phenomena. The hot spots can cause a boiling crisis and CHF. The rewetting capability and the irreversible growth of hot spots are important characteristics to delay of CHF. They examined the effect of the surface wettability and capillarity of the deposited nanoparticles layer on CHF. The CHF was enhanced with decreasing of the contact angle as shown in Figure 2-11. However, the two samples of A and B shows different CHF results at a contact angle close to 20°. Thus, the significant CHF enhancement is depending on increasing of the wettability and capillarity due to the deposited nanoparticles on the surface. Park et al.[87] reported the CHF enhancement of water-based graphene, graphene oxide and alumina nanofluids. Graphene and graphene oxide nanofluids enhanced the CHF performance without increasing of wettability and capillarity of the surface deposited with the nanoparticles as shown in Figure 2-12. They explained the CHF enhancement of graphene oxide as regards the changed critical instability wavelength due to ordered porous surface structure.

The formation of a porous nanoparticle layer on the heater is one of the most influential consequences of nanofluids boiling. However, the properties of nanofluids depend on the size, shape, and dispersibility of the particles, and many researchers using low concentrations (less than 1 vol%) of nanoparticles in water as a base fluid have found that the thermal properties were unchanged.
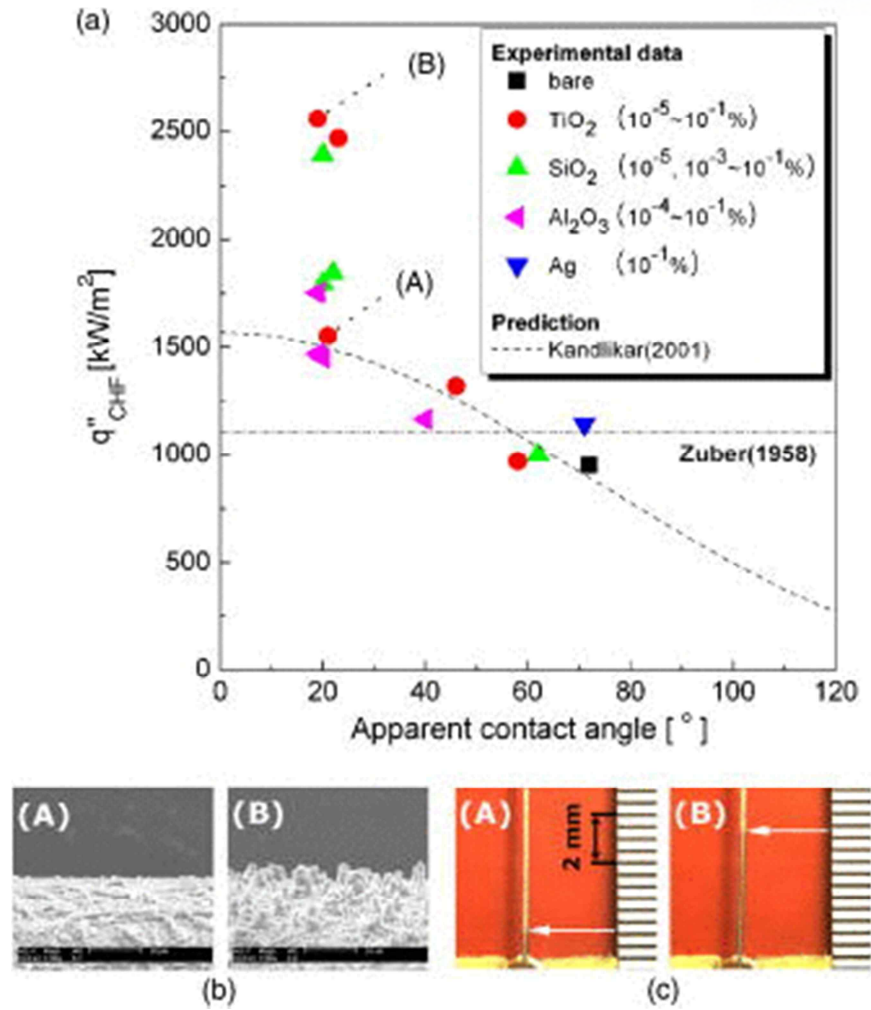
Figure 2-11. (a) Relation between CHF and the contact angle on surface of deposited with nanoparticles, (b) morphologies of heater surface after boiling, and (c) maximum capillary wicking height of pure water for surfaces boiled in (A) 10^{-3}% and (B) 10^{-1}% TiO$_2$ nanofluids, with the same contact angles of ~20° [103]
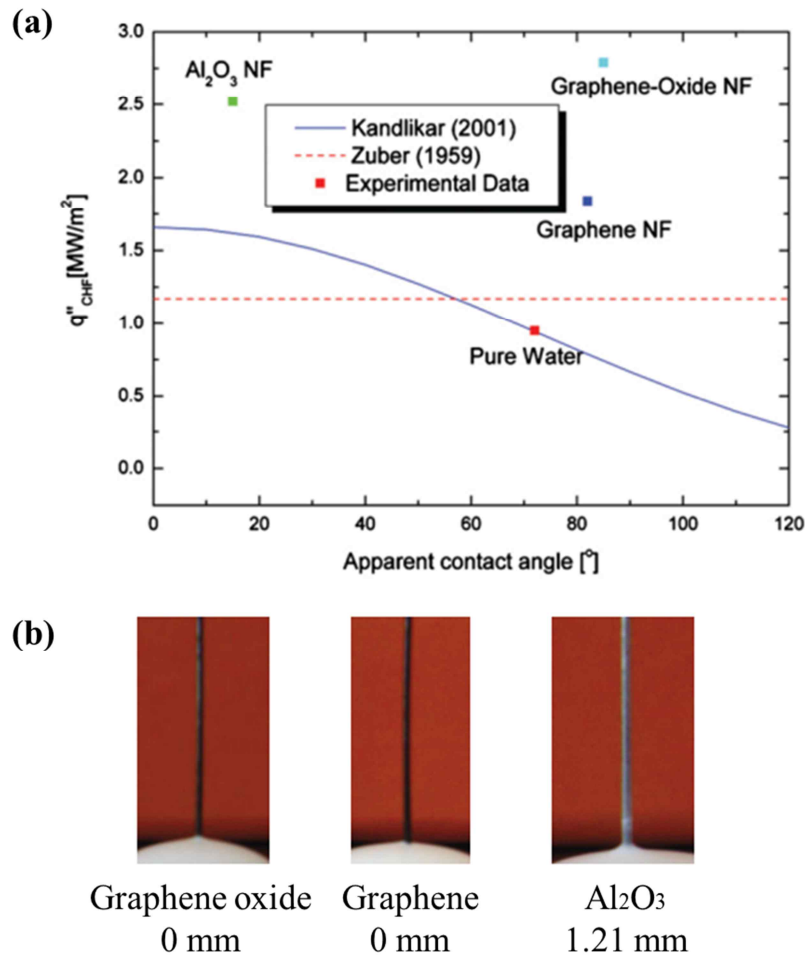
Figure 2-12. (a) Relation between CHF and the contact angle on surface of deposited with nanoparticles and (b) maximum capillary wicking height of pure water for surfaces boiled of graphene oxide, graphene and alumina nanofluids[87]

2.4. Summary

Based on the literature reviews relating to the electrical explosion of the wire in liquid method, heat transfer of nanofluids, and, a part of application area, the researches on CHF enhancement has been summarized in this chapter. Most of studies on the electrical explosion of the wire in liquid method have reported the effect of parameters on formation of the nanoparticles produced by the electrical explosion of the wire in liquid method. They tried to explain the mechanism of nanoparticles formation using visualization method.

The thermal conductivity and the viscosity is important characteristic of the nanofluids for thermal

applications. Thus, numerous researches have reported about the effect of nanofluids with factors, such as the size and volume fraction of the nanoparticles and temperature on the thermal conductivity and viscosity. The investigations used Al_2O_3, CuO, SiO_2 and MWCNT nanoparticles dispersed in working fluids such as the water, EG, or oil. One field of nanofluids application is CHF enhancement. Nanofluids have an influence on CHF enhancement, but the reasons still remain uncertain state.

Chapter 3. Preparation and characterization of the silver, copper oxide and aluminum oxide nanofluids by the electrical explosion of the wire in liquid method

3.1. Introduction

To be used in the nanofluids applications, it is important that nanofluids are prepared a homogeneous dispersion state maintained stability over long periods of time. Maintaining homogeneity of the nanofluids is still a technical challenge because of strong van der Waals interactions between nanoparticles. The electrical explosion of the wire in liquid (EEWL) method has involved two process as the top-down and bottom-up process. In the top-down process, the wire is broken up into supersaturated vapor by the joule heating of the wire. After then, it is bottom-up process, in which the nanoparticles will be formed through the nucleation and growth of nuclei from the supersaturated vapor. This method can adjust the size, the shape, and the dispersion stability of the nanofluids through control the applying energy in the wire, liquid, and temperature.

In this chapter, there are three parts concerning the silver, copper oxide, and aluminum oxide nanofluids synthesized by the electrical explosion of the wire in liquid method. First, the investigations are carried out the effect of experimental parameters on explosion phenomenon of the wire by analysis of voltage and current oscillograms. Then, we investigated the morphologies and phase of nanofluids with different base liquids. Finally, we examined the capacitance, liquid type, and materials influence on size and dispersion stability of nanofluids. Furthermore, the effect of pH and the difference of the electrical explosion of the wire and sonication method are studied in this part.

3.2. Experimental Setup

A schematic illustration of the experimental system is shown in Figure 3-1. The system is consisted of a vessel for liquid media for the explosion process and a simple discharge circuit that included a high-voltage power supply, the capacitors, and a switch. Metallic wire was placed between the two electrodes. A vessel is filled with the base liquid. The capacitor was charged using an applied voltage. The amount of stored energy (W) in the capacitor was $0.5CV^2$, where C is the capacitance and V is the charged voltage. A current stored in capacitors flows through the wire in the form of pulses when the switch was closed. The current deposited electrical energy in the wire because of its finite resistance.

Thus, the wire located between the two electrodes melted, vaporized, and the high-temperature plasma generated by the electrical energy deposited in the wire. Finally, nanoparticles formed by interaction with the liquid. A current transformer (Pearson model 1330) and a high-voltage probe were used to measure the current and voltage oscillograms, respectively.

Many parameters, such as applied voltage, capacitance, materials, properties of the wire (diameter, length, and defect), additives, and kind of media, can affect the size, shape and dispersion stability of nanoparticles produced by electrical explosion of the wire in liquid.

Nanofluids produced using pure silver, copper and aluminum (> 99.0%) wire in various liquids (deionized water, ethanol, and ethylene glycol) at different capacitances (7.5, 15, and 30μF). The production conditions for the nanofluids followed a statistical design of experiments (DOE). The morphology, size and shape of the nanoparticles were investigated by the high-resolution transmission electron microscopy (HR-TEM). The size distribution and zeta potential of the nanofluids were measured by dynamic light scattering (DLS) method.
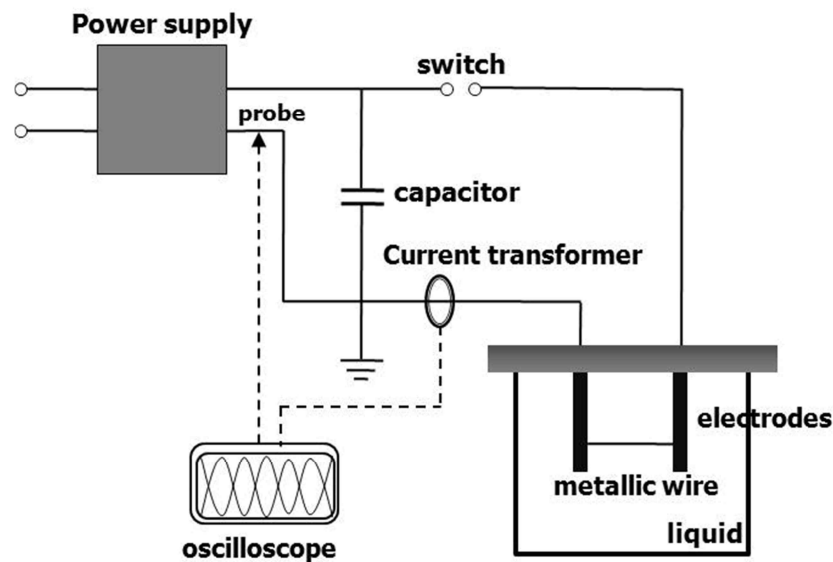
Figure 3-1. Schematic diagram of the experimental system for the EEWL process

3.3. Results and Discussion

3.3.1. Voltage-current oscillograms

Figure 3-2 (a) and (b) shows the voltage and current oscillograms with no explosion and explosion. When the capacitor was discharged, the current increased, and after a certain time, a sudden current drop and sharp rise in voltage occurred. The current drop and voltage rise stemmed from an increase in the resistivity of the wire because of vaporization. The resistance increased several orders of magnitude, and the current in the circuit was interrupted. The inductive energy stored in the stray inductance of the circuit generated a high voltage, which was higher than the initial voltage of the capacitor. Once vaporization occurred, an arc discharge formed between the electrodes, and the current flowed through the low-resistance arc plasma. Thus, the wire was heated and vaporized by the energy deposited in the wire until the arc discharged.

In this process, the energy deposited in the wire can be calculated by time integration using the measured voltage and current oscillograms of the power dissipated in the wire according to the following equation:

$$W = \int_0^t V(\tau) \times i(\tau) d\tau \qquad (3.1)$$

where, W is the energy deposited in the wire, V is the voltage, and $i(\tau)$ is the time integration.
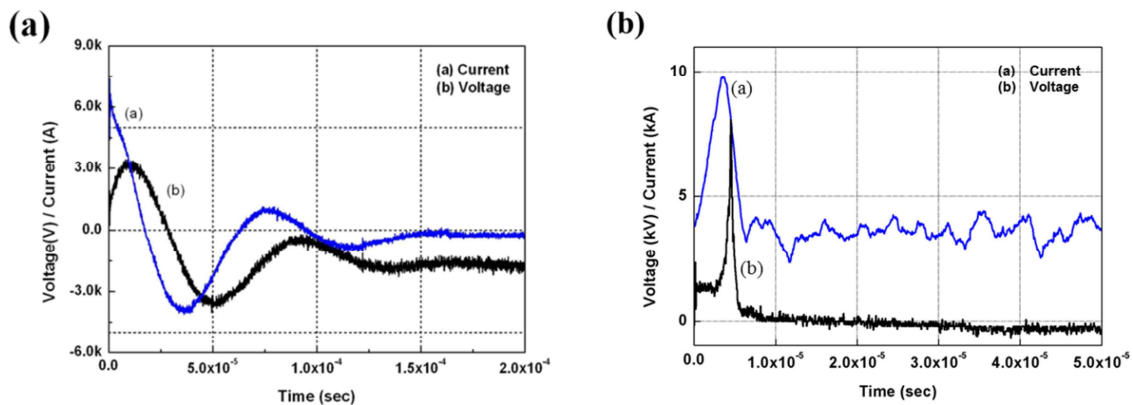
Figure 3-2. Typical voltage and current oscillograms for (a) shorting circuit and with (b) explosion

The particle size is the hardest determined by the evaporation and condensation rate of the wire. Figure 3-3 shows the voltage and current oscillograms generated at explosion of silver wire under various capacitances. When the energy was stored at capacitor, the explosion occurs. Both the voltage and the current declined to zero after the first pulse current. In general, in explosion of wire process, the re-strike region exists in ringing type. The re-strike phenomenon occurs, or it does not. The phenomenon is attributed to the level of deposited energy. Under the same discharge voltage, the explosion of wire generated faster with and the introduced energy into wire was larger with $30\mu F$ than other capacitances.

In Figure 3-4 (a) and (c), the amount of current increases as the capacitance was increased. The energy was deposited in the wire during the voltage rise. The deposited energy in the wire under $30\mu F$ in capacitance is greater than $7.5\mu F$. In Figure 3-4, faster current rise can be adjusted by changing the capacitance and lead to the higher energy deposition in the wire. The formation of plasma seems to be the effect of liquid through the voltage peaks. In water, the voltage peak is sharper.

(a)

(b)

(c)
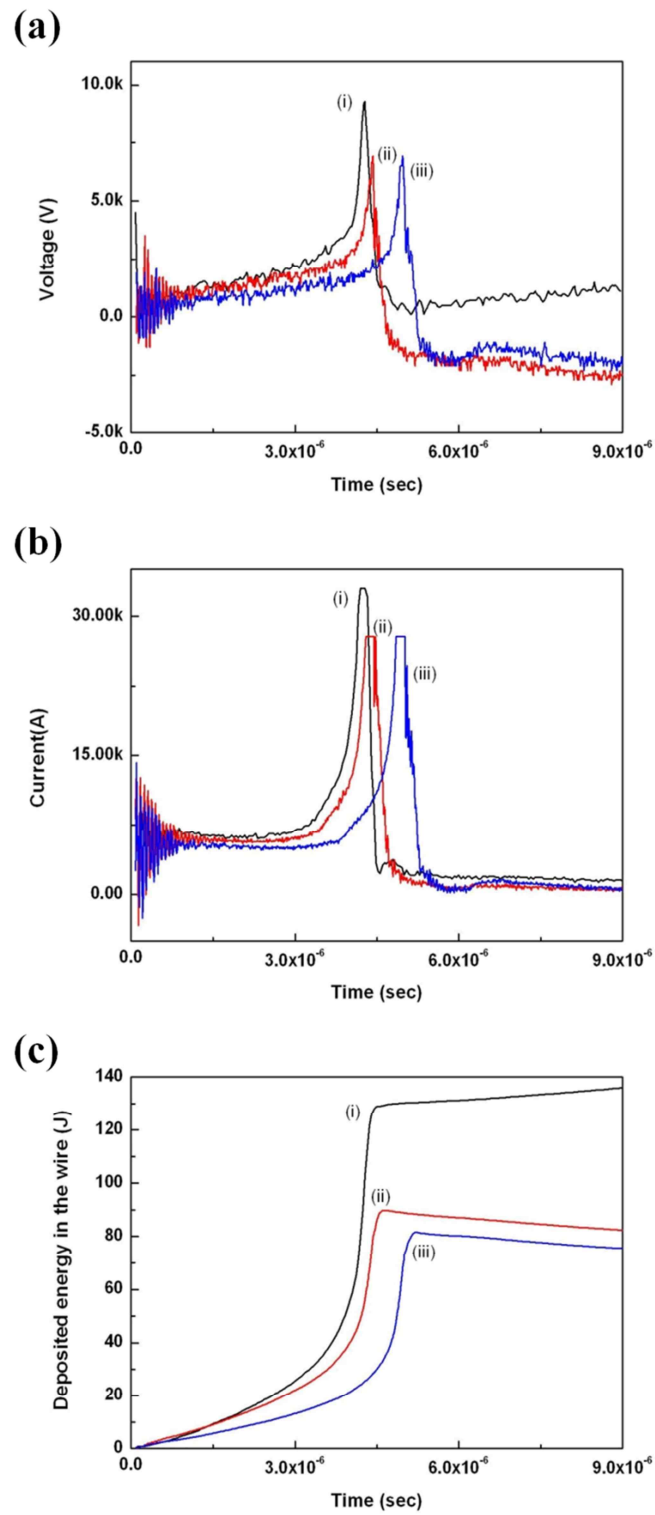
Figure 3-3. Voltage (a), current (b), and deposited energy in the wire (c) under different capacitances
((i) 30μF, (ii) 15μF, and (iii) 7.5μF)
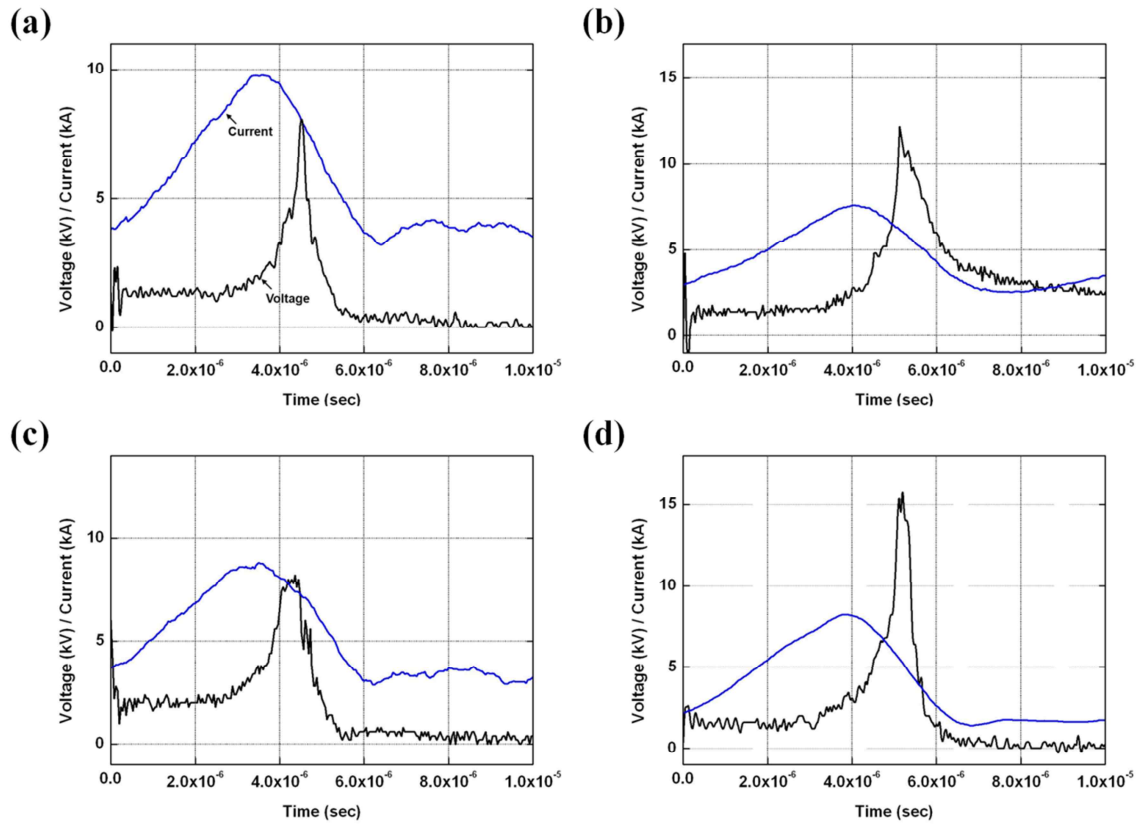
Figure 3-4. Voltage and current oscillograms under various conditions as a function of time: (a) Case 1 (30 μF, 28 mm, water), (b) Case 2 (7.5 μF, 28 mm, ethanol), (c) Case 3 (30 μF, 38 mm, ethanol), and (d) Case 4 (7.5 μF, 38 mm, water)

3.3.2. Morphology and Phase of Nanoparticles

Silver, copper, and aluminum oxide nanofluids were produced by the electrical explosion of the wire in liquids method. As shown in Figure 3-5, nanofluids are in difference colors with difference materials and liquids. The colors of nanofluids have a relation with surface Plasmon. Oscillating electric fields of light ray propagation near nanoparticles in the nanofluids interact with the free electrons causing a concerted oscillation of electron charge that is in resonance with the frequency of visible light. These resonant oscillations are known as surface plasmon. Figure 3-6 shows the aggregated nanoparticles of various nanofluids. In the water-based silver nanoparticles, nanoparticles are aggregated and growth. Figure 3-7 shows the morphologies of nanoparticles dispersed in the nanofluids. The nanoparticles prepared by electrical explosion of the wire in liquid process are usually spherical in shape, and the particle size distribution in broad. The reasons are that energy can be applied to the whole wire and the some defect may exist inside wire, so that the size of vapor is not homogeneous. And the condensation velocity of vapors in vessel is different. The results of selected area electron diffraction (SADP) of the water-based nanoparticles present a single crystalline diffraction pattern without uncrystallized particles. The analysis of SADP performed to prove the phase of nanoparticles and it was obtained in local nanoparticle. Several nanoparticles have some defects in the crystalline. Under non-equilibrium process conditions, the nanoparticles can have some defects such as twin and dislocations. In the case of Al_2O_3, the nanoparticles have very clean surface because it was covered with oxide layer. The effect of base liquid on nanoparticles shape can be confirmed with the TEM images of aluminum water-based and aluminum ethanol-based nanoparticles, as shown in Figure 3-7 (e) and (f).
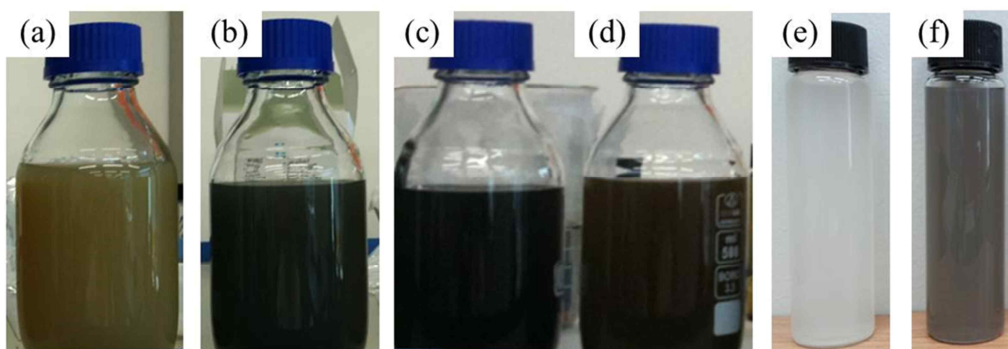
Figure 3-5. Photographs of nanofluids produced by electrical explosion of the wire in liquids (a) water-based silver, (b) ethanol-based silver, (c) ethylene glycol-based copper, (d) water-based copper, (e) water-based aluminum, and (f) ethanol-based aluminum nanofluids
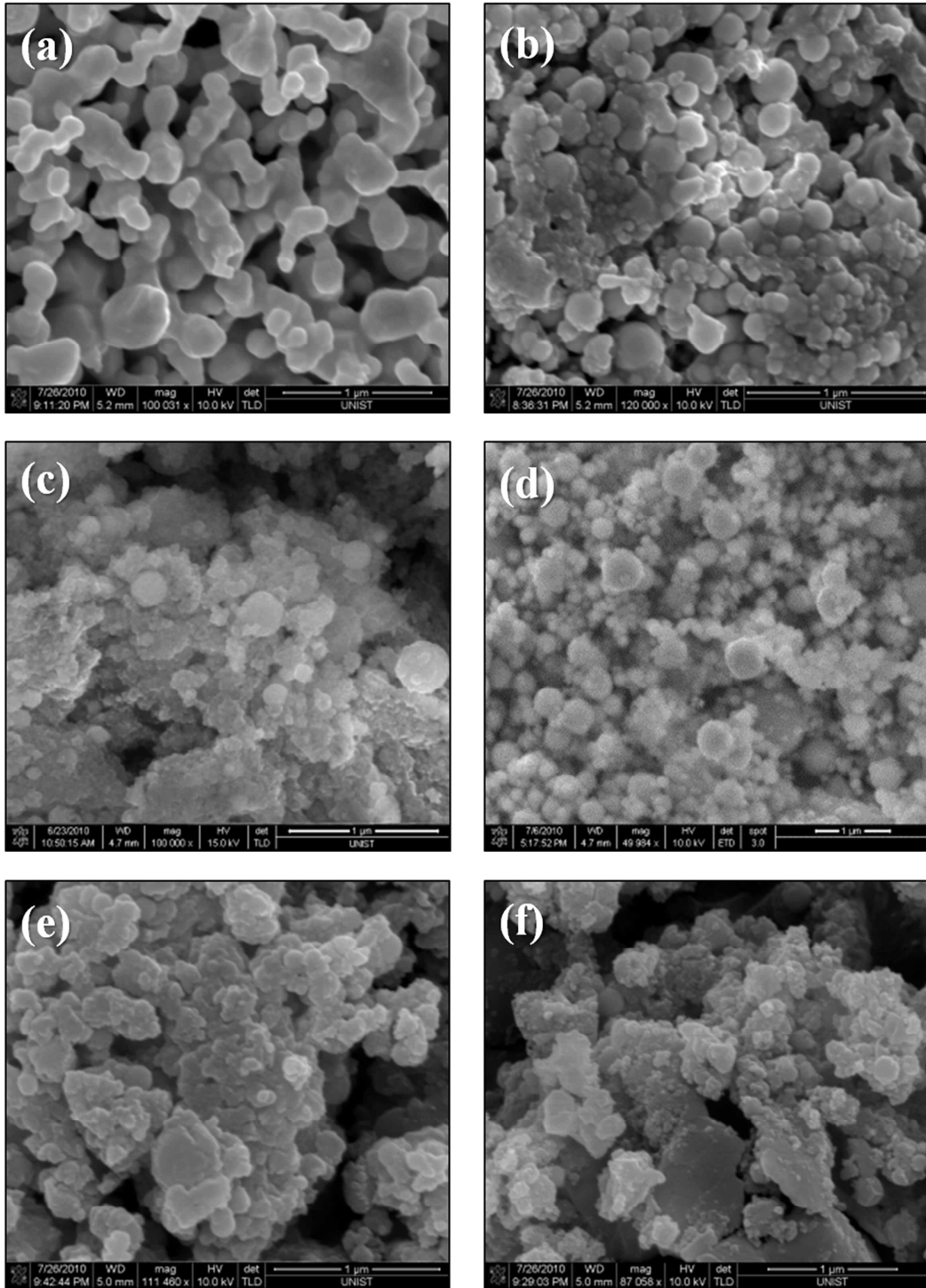
Figure 3-6. SEM images of (a) water-based silver, (b) ethanol-based silver, (c) water-based copper, (d) ethylene glycol-based copper, (e) water-based aluminum, and (f) ethanol-based aluminum nanoparticles
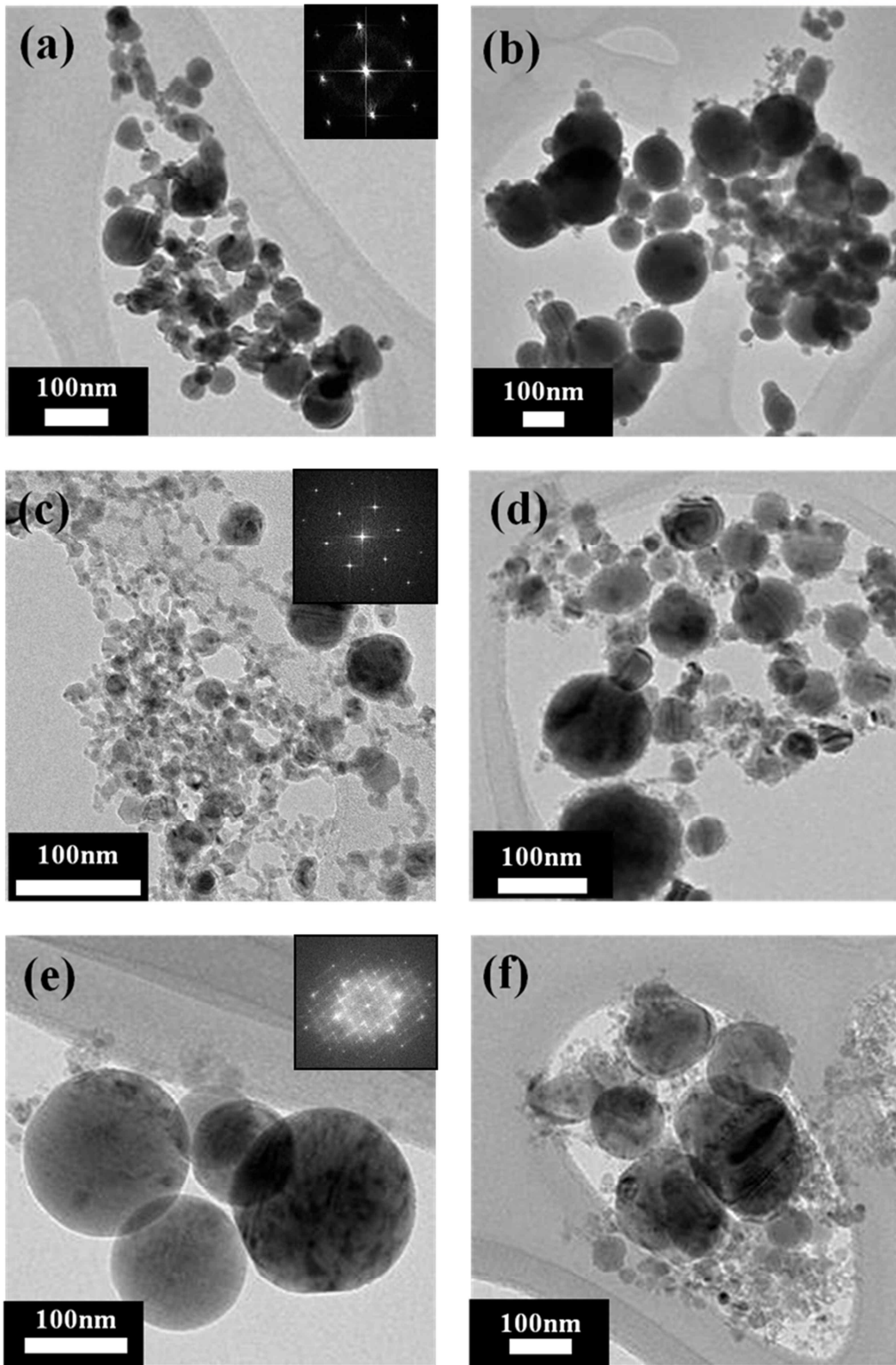
Figure 3-7. TEM images of (a) water-based silver, (b) ethanol-based silver, (c) water-based copper, (d) ethylene glycol-based copper, (e) water-based aluminum, and (f) ethanol-based aluminum nanoparticles

Figure 3-8 shows the XRD pattern of the water-based silver and copper oxide nanoparticles produced via the EEWL process. XRD patterns of silver and copper oxide particles obtained by EEWL, which reveals a face centered cubic (fcc) structure (JCPDS 04-0783, a=4.086 Å) and a monoclinic structure (JCPDS 03-1005, JCPDS 05-0661, a = 4.684 Å, b = 3.425 Å, c = 5.129 Å, β = 99.47°), respectively. The diffraction pattern of silver nanoparticles revealed only the presence of silver phase. In the case of copper, three phases (Cu, CuO and Cu_2O) exist in XRD pattern. Copper oxide composite was determined concentration of Cu^+ and Cu^{2+} ions generated by ionization at wire explosion.
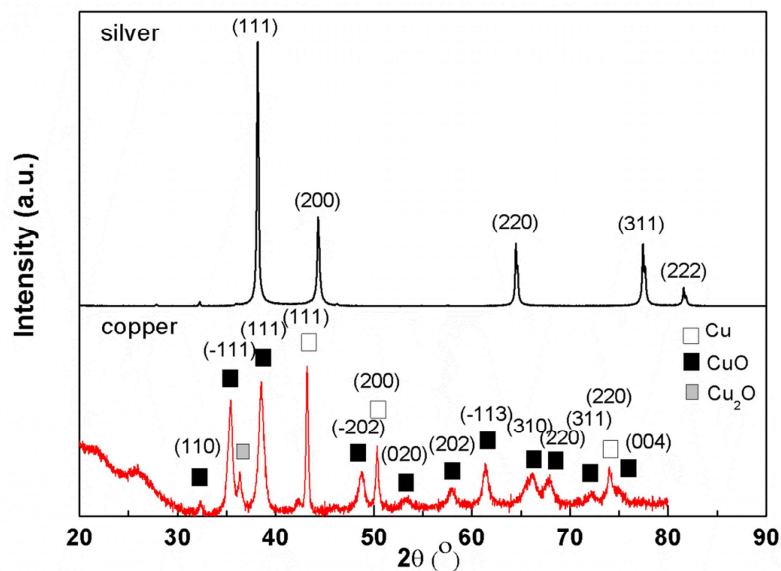
Figure 3-8. XRD patterns of water-based silver and copper oxide produced by EEWL.

Table 3-1 presents the composition concentration results of silver, copper oxide and aluminum oxide nanoparticles by energy dispersive spectroscopy (EDS). The phase of the produced nanoparticles changed with the liquid because of different oxidizing environments. In ethanol, the aluminum particles contained oxide at 12 at% compared with the nanoparticles produced by EEWL in water. We made other aluminum oxide nanofluids by a two-step method to confirm the phase of the nanoparticles produced in water. The aluminum oxide nanofluids prepared by sonication was γ–alumina (99.9% purity, 40–80 nm average size). We confirmed that oxide portion in water-based aluminum oxide nanofluids produced by EEWL is similar to other one produced by two-step method.

Oxidation state of nanoparticles has relevance to ionization tendency of metal. In contrast, copper oxide and silver nanofluids have little or no oxide portion.

Table 3-1. EDS results of silver, copper oxide and aluminum oxide produced by EEWL

Material	Type	Base liquid	Synthesis Method	Element	Weight%	Atomic%
Al	Wire	Water	EEWL	O K	44.68	57.66
				Al K	55.32	42.34
	Powder	Water	sonication	O K	43.90	56.89
				Al K	56.10	43.11
	Wire	Ethanol	EEWL	O K	7.67	12.30
				Al K	92.33	87.70
Cu	Wire	Water	EEWL	O K	4.49	15.74
				Cu K	95.51	84.26
Ag	Wire	Water	EEWL	C K	6.03	36.55
				Ag L	93.97	63.45

3.3.3. Size and Dispersion Stability

Table 3-2 shows the particles size and zeta potential of water-based silver, copper oxide and aluminum oxide nanoparticles produced by the EEWL method. The measuring theory is the dynamic light scattering (DLS). Dynamic light scattering is one of the most popular light scattering techniques for measuring the size of nanoparticles. The nanoparticles have the random movement called Brownian motion by collisions between the particles and solvent molecules. This DLS technique can measure the speed of particles undergoing Brownian motion. The reason for the size difference between TEM images and DLS results is, particles in TEM images can see the individual nanoparticles but DLS system is unable to see the aggregated particles. Average particle size of silver and alumina are 123 nm and 345.5 nm respectively but have similar zeta potential value. Zeta potential is widely used to determine the stability of nanofluids. Actually, zeta potential is a technique for measuring the surface charge of nanoparticles in solution. Nanoparticles have a surface charge that attracts a thin layer of ions of opposite charge to the particles surface. This electric potential of the double layer is known as the zeta potential. Zeta potential is an important tool for understanding the

surface state and predicting the stability of the nanoparticles. Nanoparticles having high zeta potential value (usually, up to ±25mV) have high degree of stability. The nanoparticles having low zeta potential value will aggregate due to Van der Waals inter-particle attractions. The zeta potential is more related to surface charge than the particles size. In these experiments, all nanofluids have high degree of stability.

Table 3-2. Average particle size and zeta potential of water-based silver, copper oxide and aluminum oxide nanofluids

Wire material	Average particle size (nm)	Zeta potential (mV)
Silver	123.5	–37
Copper	160	26
Aluminum	345.5	37.4
Alumina (two-step)	608.8	29.5

As the discharge energy is increased the deposited energy in the wire is increased. The faster current rise gives the higher energy deposition as shown in Figure 3-3. Current can be increased by changing the charging voltage and the capacitance. Average particle size could be decreased by the higher deposited energy. The capacitance has relevance to melting and evaporating rate of the wire at explosion. It means that the particle size of silver nanoparticles is affected by capacitance. The particle size is smaller with large capacitance as shown in Table 3-3. Figure 3-9 shows the TEM images of silver nanoparticles synthesized by different charging voltages. When the applied voltage was 5kV, the deposited energy was higher as 68J than 26.4 J at 3kV. The diameter of water-based silver nanoparticles decreases from 115.8 nm to 66.8 nm when the applied voltage increases from 3kV to 5kV (Table 3-4).

Table 3-3. The average particle size and zeta potential values of water-based silver nanofluids under various capacitances

capacitance	Average particle size	Zeta potential
7.5 μF	123.7 nm	-43.0 mV
15 μF	119.8 nm	-47.5 mV
30 μF	116.6 nm	-46.6 mV
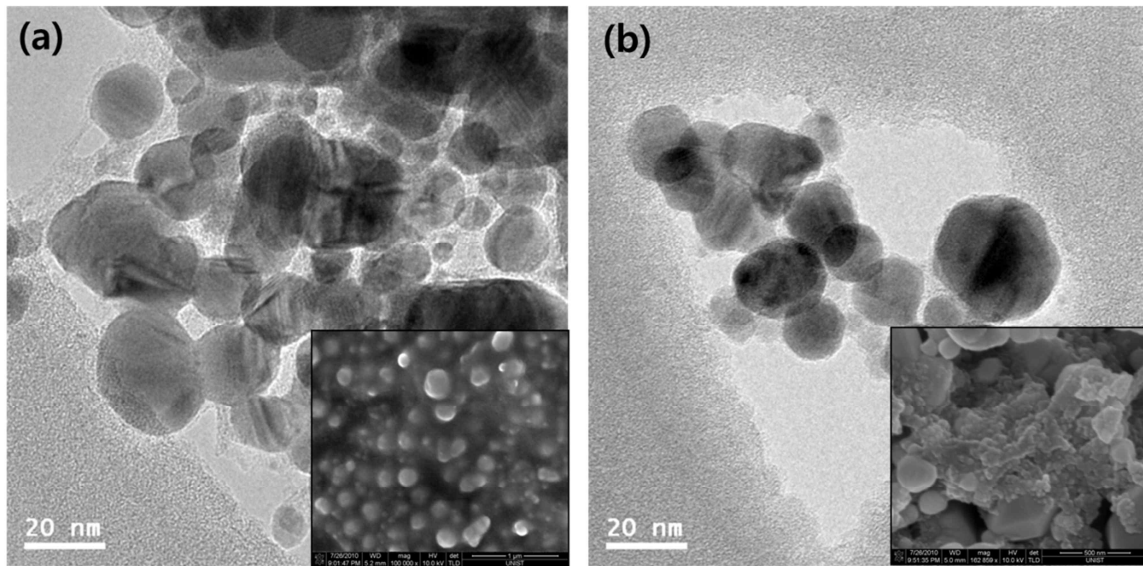
Figure 3-9. TEM images of silver nanoparticles synthesized in DI water at (a) 3kV, and (b) 5kV (7.5μF and 28mm)

Table 3-4. The average particle size and zeta potential values of the silver nanofluids under different applied voltage and base fluid (7.5μF and 28mm)

Charging voltage	Base fluid	Average particle size	Zeta potential
5 kV	DI water	66.8 nm	-28.2 mV
3 kV	DI water	115.8 nm	-29.3 mV
3 kV	Ethanol	262.5 nm	-19.7 mV

40

The silver nanoparticles synthesized in water have the higher zeta potential value than synthesized in ethanol. Figure 3-10 shows the infrared (IR) spectrum of the silver nanofluids. The IR spectrum indicates the details of functional groups present in surface of nanoparticles synthesized by EEWL. A significant strong O-H absorption peak appeared at 3377 cm^{-1} in the spectrum of nanofluids synthesized in water. The H-O-H bending peak occurred at 1641 cm^{-1} due to water molecules. In ethanol, the C-H peak was observed at 2977 cm^{-1} due to the presence of CH$_3$ groups.

The zeta potentials of the silver nanofluids synthesized in water and ethanol were -29.3 mV and -19.7 mV, respectively. Silver nanoparticles were charged the negative surface in base fluid. When the current charged in the wire, the water molecules can dissociate into hydrogen, oxygen, and radical hydroxides. In case of water, hydrogen and oxygen started interacting with surface of the silver nanoparticles. Hydrogen with a form of molecular or atomic cannot continue to be adsorbed on the silver surface while oxygen can be absorbed on the surface [104-109]. Therefore, this leads to the formation of hydrogen bond with the neighboring water molecules and preventing agglomeration and sedimentation of nanoparticles. The negatively charged surface of silver nanoparticles was by the oxygen which can create hydrogen bonds with water molecules. The model of silver nanoparticles synthesized in water and ethanol is shown in Figure 3-11.
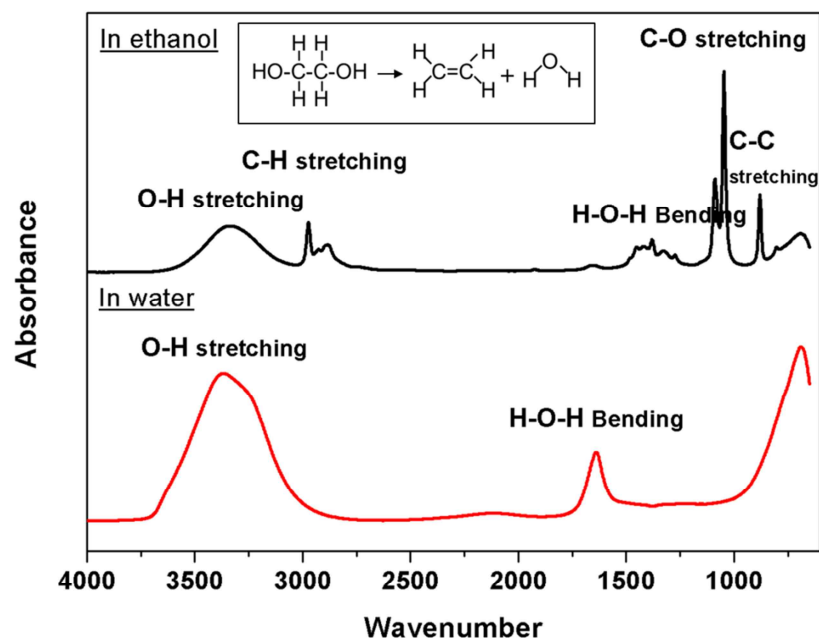
Figure 3-10. IR spectrum of the silver nanofluids synthesized in water and ethanol
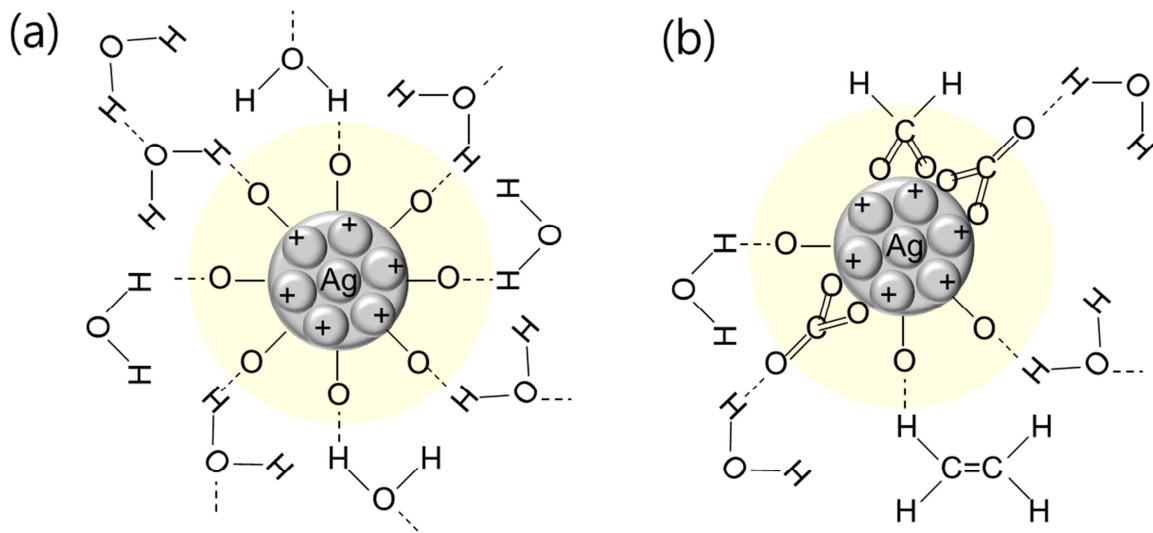
Figure 3-11. Model of silver nanoparticles synthesized (a) water and (b) ethanol (yellow area means zeta potential)

Figure 3-12 shows the morphology of aluminum oxide nanofluids observed by the TEM. The liquid type had the greatest effect among the EEWL conditions. The capacitance and length of wire outweigh its relatively low impact on the particle formation. The nanoparticles formed in ethanol were much larger (ca. 3000 nm) and had a negative zeta potential compared with those formed in water, as shown in Table 3-5. There are two reasons for the large particles. First, coagulation of alumina primary nanoparticles led to larger agglomerates. Second, the distribution of the nanoparticles is not mono-sized. Particles larger than 100 nm resulted from liquid droplet formation during the explosion. The average particle sizes were 313.8 and 317.6 nm with zeta potentials of 26 and 19.9 mV, respectively, for the nanoparticles formed in water. There is difference of deposited energy in wire at explosion in Figure 3-4 (a) and (c), but the average particle size is almost no difference. The smaller the capacitance, it takes to explode of wire. As early as the rise in the current through the wire, the greater part of the wire turns into vapor and plasma state. The nanoparticles synthesized in water have positive charge in zeta potential due to oxide surface.
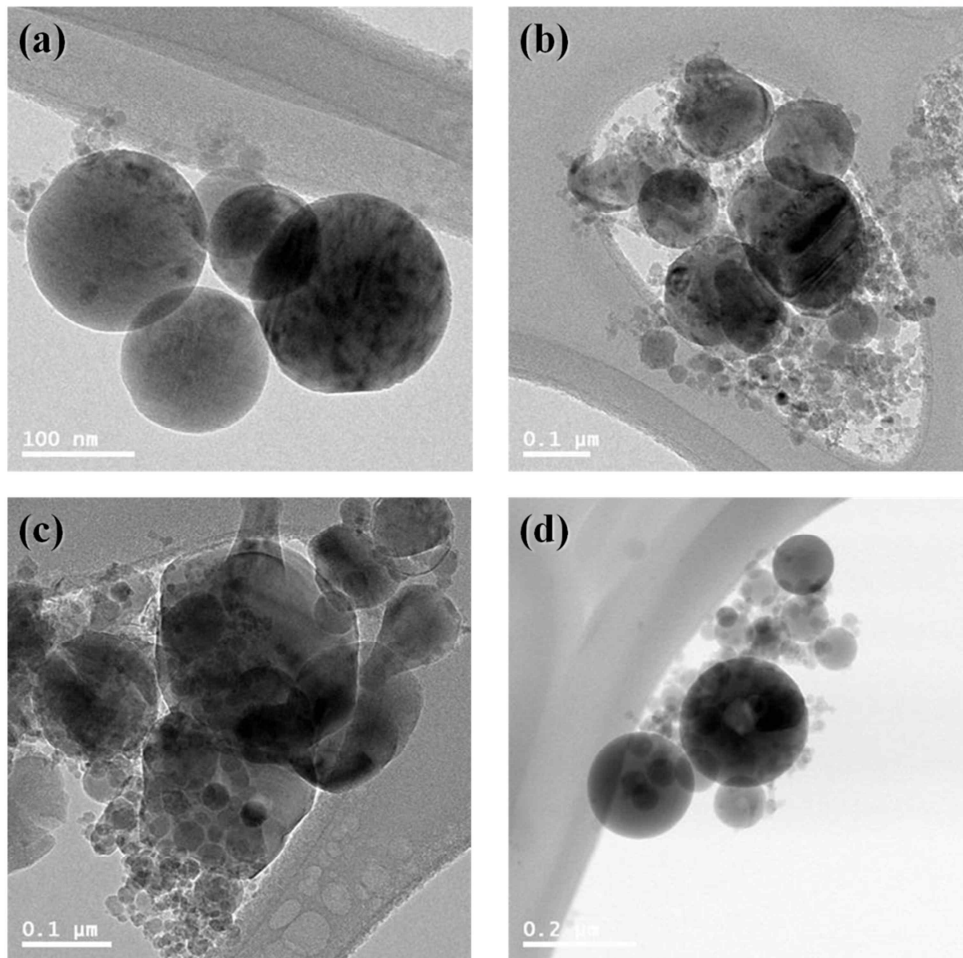
Figure 3-12. TEM images and size distribution calculated with TEM images of aluminum oxide nanoparticles: (a) Case 1 (30μF, 28mm, water), (b) Case 2 (7.5μF, 28mm, ethanol), (c) Case 3 ((30μF, 38mm, ethanol), and (d) Case 4 (7.5μF, 38mm, water)

Table 3-5. Average size and zeta potential of the aluminum oxide nanofluids by EEWL

	Conditions	Average particle size (nm)	Zeta potential (mV)
Case 1	30 µF, 28 mm, water	313.8	26
Case 2	7.5 µF, 28 mm, ethanol	3718	-10.4
Case 3	30 µF, 38 mm, ethanol	3043	-9.39
Case 4	7.5 µF, 38 mm, water	317.6	19.9
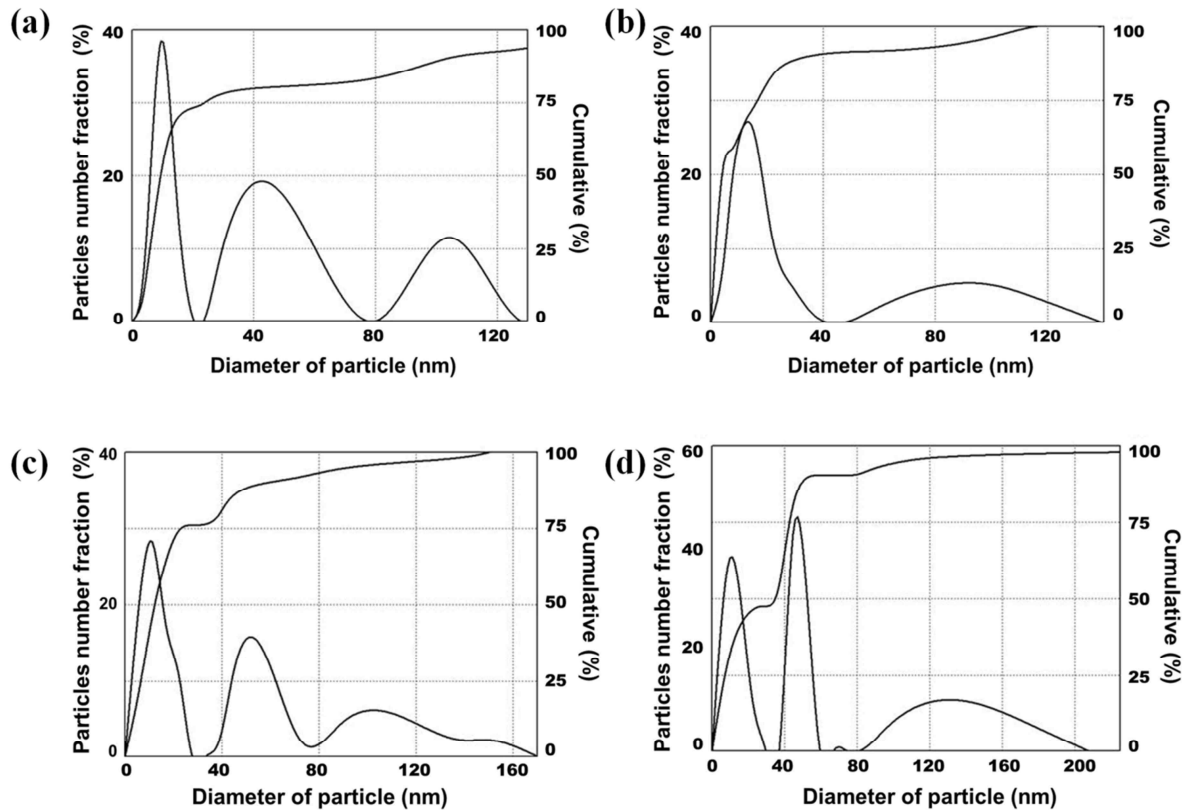
Figure 3-13. Particle size distribution calculated with TEM images of aluminum oxide nanoparticles: (a) Case 1 ($30\mu F$, 28mm, water), (b) Case 2 ($7.5\mu F$, 28mm, ethanol), (c) Case 3 (($30\mu F$, 38mm, ethanol), and (d) Case 4 ($7.5\mu F$, 38mm, water)

Figure 3-13 shows the particle size distribution calculated with the TEM images of the aluminum oxide nanoparticles. There are the particles up to 100nm in size which are originated from the liquid droplet or strongly agglomerated particles. Moreover, liquid particles coalesce. Regarding the properties of oxide particles, the oxide nanoparticles synthesized are weakly aggregated. The particles have almost spherical shape and clear surface. In ethanol-based aluminum nanoparticles were observed non-spherical shape.

Particle size and dispersion stability are influenced by basefluid. Figure 3-14 shows high-speed photographs obtained under the water and ethanol. In the early stage of the discharge, the current

flows through the wire. The first image of Figure 3-14 (b) shows the distortion of the wire. The entire wire is evaporated and a sudden flash of light is next observed by shock wave. The expanding plasma is reduced to a point within 1.5ms after the discharging. The reduced plasma size of in water was smaller than in ethanol. The voltage peak is dependent on the thermal conductivity and viscosity of basefluid as shown Table 3-6. In water, the voltage peak was shaper and higher than one in ethanol (Figure 3-4). A cloud formed by nanoparticles was observed after 5.5ms and 6ms. A particle cloud in water was nearly perfectly spherical compared with others. The nanoparticles were dispersed into the basefluid by shock. The nanoparticles were spread onto the bottom in ethanol while the nanoparticles were dispersed with a cone. Therefore, the dispersion stability of nanoparticles synthesized in water is superior in ethanol.
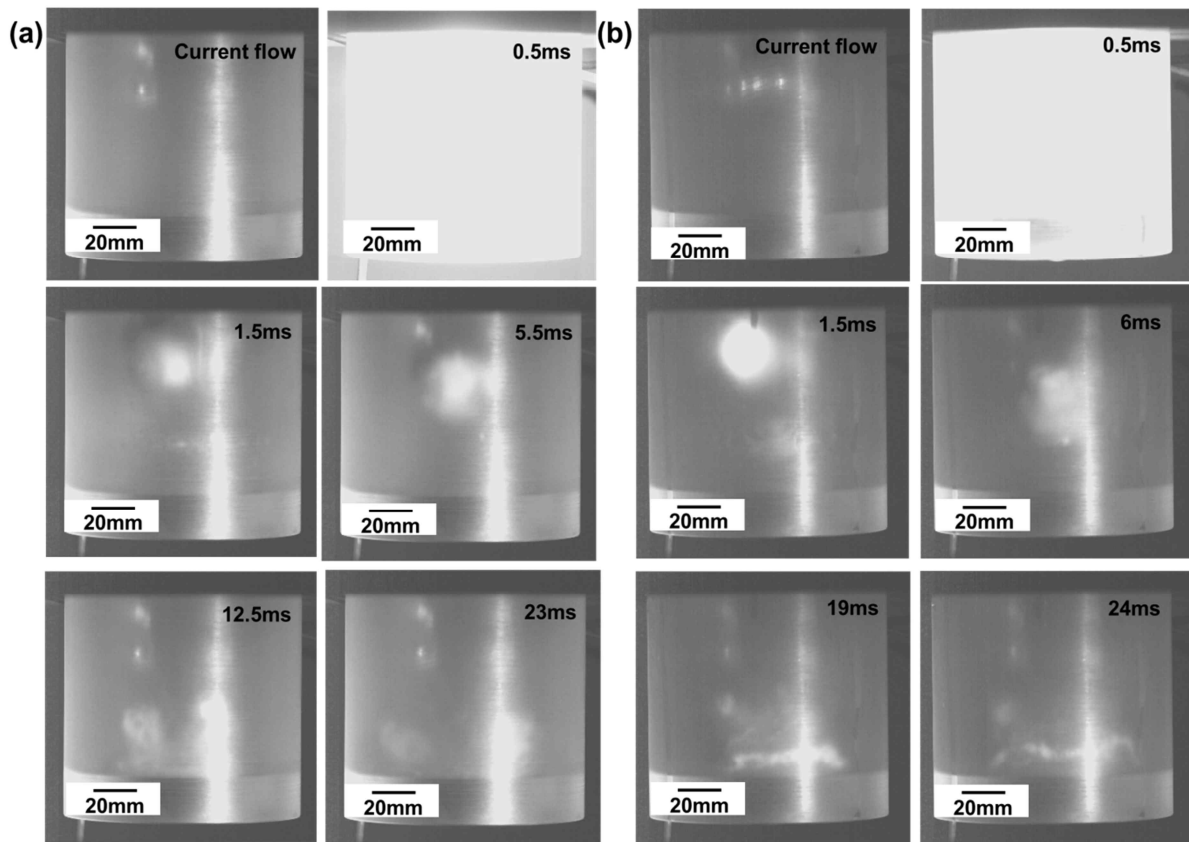
Figure 3-14. High-speed photographs of aluminum wire explosion in (a) water and (b) ethanol (φ=0.1mm, 30μF, and 1.4kV)

Table 3-6. Thermal conductivity and viscosity of basefluid at 25℃

	Thermal conductivity (W/mK)	Viscosity (mPa.s)
Water	0.609	0.894
Ethanol	0.171	1.074

pH is a key parameter for the production of stable nanoparticle dispersions. We measured the pH and the zeta potential of each sample to understand dispersion stability of nanofluids. The samples with different pH were prepared adding 0.1M HCl or 0.1M NaOH. A large absolute zeta potential at different pH values will keep the nanoparticles in a stable, dispersed state with no agglomeration. The isoelectric point (IEP) is the pH at which the zeta potential is zero. A little farther away from the IEP, the nanofluids are more stable. In case of water-based copper oxide nanofluids, could not measure the zeta potential due to buffer of nanoparticles.

The water-based silver nanofluids prepared by EEWL process has yellow coloring, as shown in Figure 3-15 (a). The stability of nanofluids has a little difference with pH value. As pH value is below 3, the nanofluids was settled the nanoparticles at bottom of bottle by agglomeration. Therefore, in the case a pH of 2, zeta potential was no measured. A large absolute zeta potential at different pH values will keep the nanoparticles in a stable, dispersed state with no agglomeration. The IEP of water-based nanofluids prepared by the EEWL process was nowhere to be found. In the Figure 3-15 (b), there is no observable change in the size and zeta potential as a function of pH. All zeta potential has a negative value lager than -40 mV and average diameter is about 115 to 118nm except a pH of 3, what is sufficient to maintain in a stable nanofluids. Silver nanofluids are stable due to the repulsive force by the bonding between water molecules and oxygen atom on the surface of silver nanoparticles in plasma. The zeta potential is related to the charge of particle surface.

Figure 3-16 shows the comparison of zeta potential value of water-based aluminum oxide nanofluids prepared by EEWL (one-step) and sonication (two-step) as a function of pH. The isoelectric point (IEP) of the aluminum oxide nanofluids prepared by EEWL was at pH 6.7 where the zeta potential was at its lowest value. However, the most stable dispersion was obtained at pH 3 (in shown Figure 3-16). In the two-step method, the IEP was at pH 9.5. In nanofluids prepared by two-step method is stable in a wide range below IEP having a value of more than 20 mV. In more than pH 9, the nanofluids by one-step method are more stable.
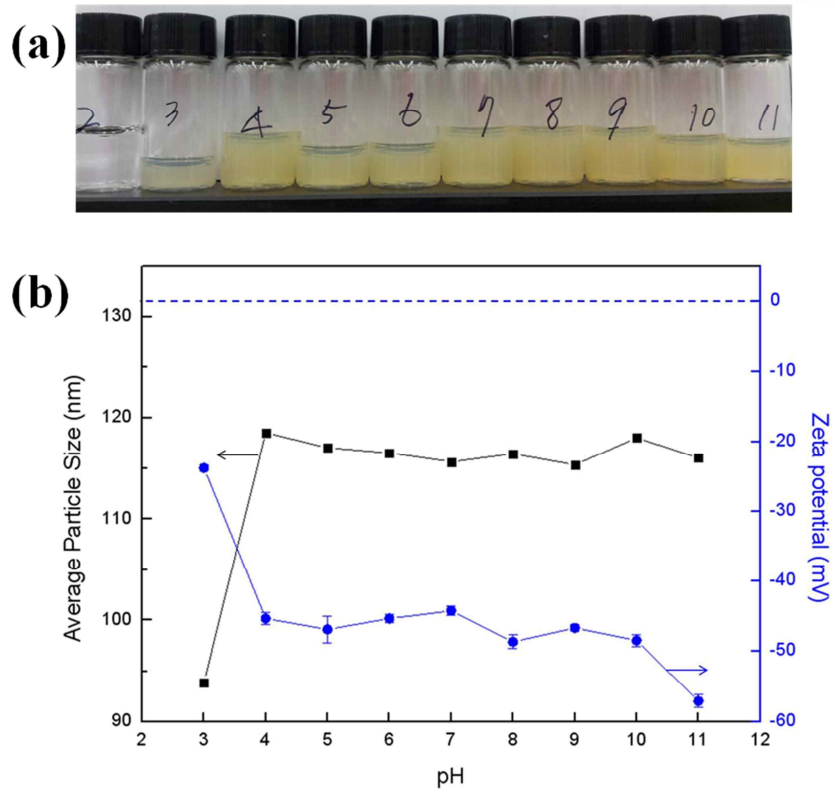
Figure 3-15. (a) Photo of visualization, and (b) zeta potential and average particle size of water-based silver nanofluids as a function of pH
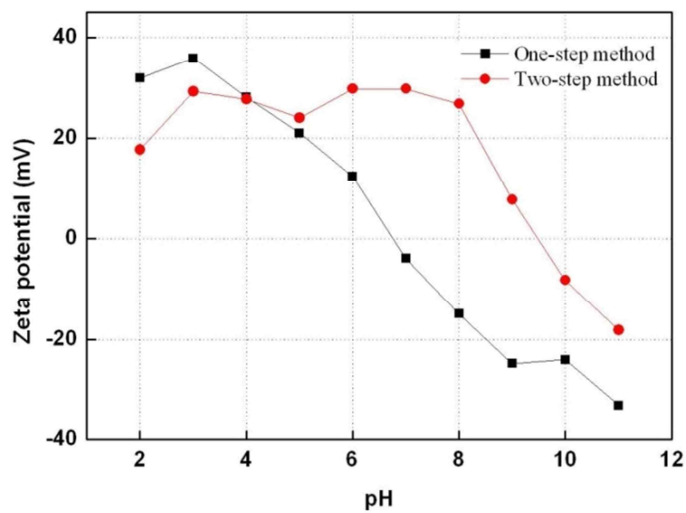
Figure 3-16. Variation in zeta potential of the water-based aluminum oxide nanofluids prepared by EEWL (one-step) and sonication (two-step) as a function of pH

A Turbiscan was used to evaluate the stability of the nanofluids. Particle size variation caused by coagulation of nanoparticles leads to a decrease or increase in the backscattering flux (%) or transmission flux (%) over the entire height of the sample. Generally, the backscattering flux profile decreases with variation in particle size. However, in the Rayleigh diffusion zone where the particles are smaller than the wavelength used in the Turbiscan, the backscattering flux increases by Rayleigh diffusion such as these nanofluids. As shown in Figure 3-13, the results of all water-based nanofluids only show sedimentation form. Based on the slope of the mean value kinetics shown in Figure 3-17 (c), nanoparticle aggregation occurred more rapidly in ethanol than in water. However, the backscattering flux for nanoparticles in water was less after 24 h. The water-based aluminum oxide nanofluids were more stable than the ethanol-based ones.
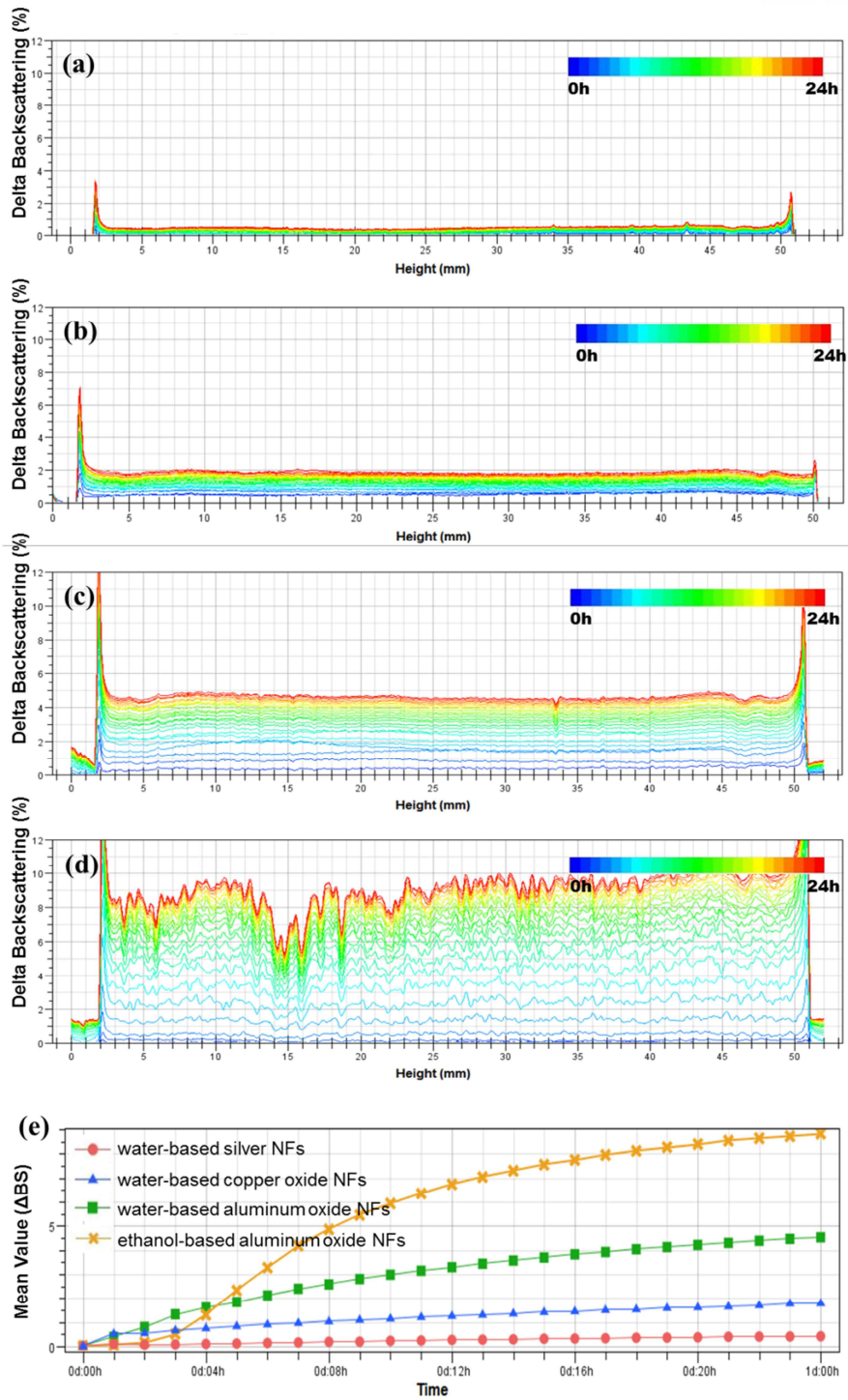
Figure 3-17. Backscattering intensity profiles and mean value kinetics of nanofluids: (a) water-based silver, (b) water-based copper oxide, (c) water-based aluminum oxide nanofluids, (d) ethanol-based aluminum nanofluids and (e) Mean values. These data are represented as a function of time (ca. 24 h) and of sample height (0–53 mm)

3.4. Summary

In this study, we produced silver, copper oxide and aluminum oxide using by the electrical explosion of the wire in liquid technique without any additives. With increasing capacitance, the used energy is the highest and the explosion rate is the fastest. It leads to decreasing the particle size in nanofluids. The nanoparticles produced by the electrical explosion of the wire in liquid process are spherical in shape and have a broad size distribution. Electrical explosion of the wire in liquids method can control the oxidation of nanoparticles by liquid type. The aluminum nanoparticles prepared in water and ethanol were oxidized to different degrees. Those dispersed in ethanol contained only 12 at% oxygen, which is better phase control than with other methods. And compared with nanofluids produced by sonication method, the EEWL nanofluids were well dispersed in the base liquid. It is difficult to dispersion in water dried nanoparticles due to their high specific surface area. To disperse the dried nanoparticles, it needs sufficient energy for breakdown the agglomeration.

The energy used explosion of silver wire is 129.1J in water in the capacitance $30 \mu F$. This has an efficiency of 95.6%. In the case $30 \mu F$, the used energy is the highest and the explosion rate is the fastest. It is conduced to decreasing the particle size of silver. The silver nanoparticles have negatively charged surface by the bonding of oxygen atoms and water molecules. The zeta potential of water-based silver nanofluids shows a negative value and -57 mV. In pH of 3 to 11, the silver nanofluids have a fixed in zeta potential and particle size and the IEP was non-existent. In contrast, the isoelectric point (IEP) of the water-based aluminum oxide nanofluids was at pH 6.7 where the zeta potential was at its lowest value.

Chapter 4. Preparation and characterization of hierarchical copper oxide microspheres by the electrical explosion of the wire in liquid

4.1. Introduction

Copper oxide is separated two phase, cupric oxide (CuO) and cuprous oxide (Cu_2O). CuO and Cu_2O are *p*-type transition metal oxide semiconductor with a band gap of approximately 1.2 eV and 2.2. eV, respectively.[110] It has applications including catalysis, gas sensing, solar cells, biosensors, and lithium batteries.[111-116] Much copper oxide research has focused on shape-controlled hierarchical copper oxide structures, including nanorods, nanoplates, microflowers, and nanowires. Hierarchical copper oxide microspheres have attracted much interest because of the large surface area, large electrical conductivity, and large capacitance due to the unique structural properties.[117-119] The properties of the hierarchical copper oxide microspheres depend strongly on the microstructure; i.e., the orientation, size and morphology.

Hierarchical copper oxide microspheres have been synthesized by various techniques, including the hydrothermal method, the facile solution oxidative method, and electro-deposition, all of which are generally considered "bottom-up" approaches.[120-123] With such approaches, it is important to understand the nuclei formation and growth mechanism. Jiang *et al.*[124] reported the synthesis of flower-like, plume-like and spindle-like CuO nanostructures via the hydrothermal method. The structures could be controlled by varying the reaction parameters, including the reactant concentration, the temperature, and the reaction time. Chen *et al.*[125] prepared CuO nanorods with a small diameter via a low-temperature solution method. Mukherjee *et al.*[122] fabricated nanowhisker-like CuO thin films via an electrochemical technique, and the grain shape changed from cubic to nanowhiskers following annealing. Most of these synthesis methods require a precursor and high temperatures, and progress slowly at low temperatures. In addition, the methods require surfactants to induce the self-assembly. However, the method using in this work, electrical explosion of the wire in liquids, have the huge advantages for synthesis of copper oxide having various shape. This method can synthesize under a second without preparation of precursor and heating.

Electrical explosion of wire in liquids (EEWL) is a single-step physical synthesis technique that can be used to fabricate metal-oxide nanostructures.[126] This method enables the synthesis of high-purity nanoparticles without requiring a surfactant. Many different metallic wires and liquids can be used with this process, whereby a metal wire is heated using a pulsed electric current. During this Joule heating of the wire, it melts, accompanied by thermal expansion and evaporation of the wire

surface.

The particle size can be controlled by adjusting deposited energy in the wire with process parameters. The deposited energy in the wire was determined by the stored energy in capacitor, properties of materials and wires, and liquid types. A short-lived solid–liquid plasma is generated, in which the temperature can reach approximately 4000ºC. The resulting vapor-phase metal condenses at the interface with the surrounding liquid. The nucleation and growth of the particles occurs over a very short timescale, and a variety of particles can be synthesized, including pure metals and metal oxides. In this work, we synthesized hierarchical copper oxide microspheres via EEWL. The pH effect of Cu^+ and Cu^{2+} on the morphology was varied, and the formation mechanism and properties of copper oxide microspheres are discussed.

4.2. Experimental Setup

Deionized (DI) water was used as the base liquid, and 5, 10, 15 ml of 0.1 M sodium hydroxide (NaOH) and 25-30% ammonia solution ($NH_3 \cdot H_2O$) were added. The volume of liquid was 200 ml (including the NaOH and $NH_3 \cdot H_2O$). The synthesis conditions are listed in Table. 4-1. All copper oxide solutions were prepared with the same number of explosions and using 0.001 vol% copper oxide concentration solution without alkaline solution.

Table 4-1. The conditions used for synthesis of copper oxide microspheres

Contents	Values
Capacitance	30μF
Charging voltage	3kV
Material	Copper wire (99 %)
Wire diameter	0.1 mm
Wire length	30 mm
Liquid	Deionized water
Additions	NaOH, $NH_3 \cdot H_2O$
Liquid volume	200 mL

The structure of the copper oxide microspheres was analyzed using X-ray diffraction (XRD) with a high-power X-ray diffractometer (Rigaku, Japan) at a scan rate of $0.02°s^{-1}$ with a range of 20–80° and with a Cu-Kα source (λ = 1.5406 Å). The morphology of the hierarchical copper oxide microspheres

was observed using field emission scanning microscopy (FE-SEM) (FEI Nanonova230) and high-resolution transmission electron microscopy (HR-TEM) (JEOL JEM-2100F). Elemental compositions were measured by X-ray photoelectron spectroscopy (XPS, K-alpha, UK) by using Al Kα X-ray source. The optical band gap was determined from ultraviolet/visible (UV-vis) absorption spectroscopy (Agilent Cary5000) in the wavelength range 250–1000 nm.

4.3. Results and Discussion

4.3.1. Synthesis of hierarchical copper oxide structure

All samples were prepared via the same procedure, and the quantity of NaOH or NH_3H_2O was varied. Figure 4-1 shows photographs of the copper oxide colloidal dispersions. The aqueous copper oxide colloidal dispersion was brown, and changed to blue when ammonia was added, due to the more stable dispersion and low concentrations of copper oxide particles. With the exception of the dispersion with added ammonia, the copper oxide particles were agglomerated and settled after 1 day.
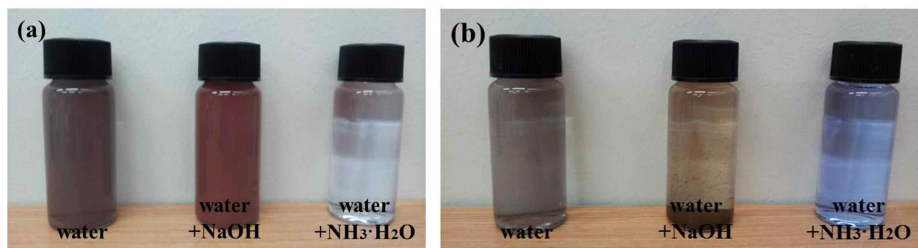
Figure 4-1. Photographs of (a) the copper oxide nanofluids dispersions immediately following synthesis and (b) after 1 day

Figure 4-2 shows FE-TEM and TEM images of the copper oxide nanoparticles produced in water together with histograms of the particle size distribution. The nanoparticles were 5–10nm in diameter, and approximately spherical, as shown in Figure 4-2 (b); however, there was some agglomeration due to the large surface area. The mean diameter of the copper oxide nanoparticles was 163.3 nm via aggregation of nanoparticles, which was measured using dynamic light scattering (DLS), as shown in Figure 4-2 (c).
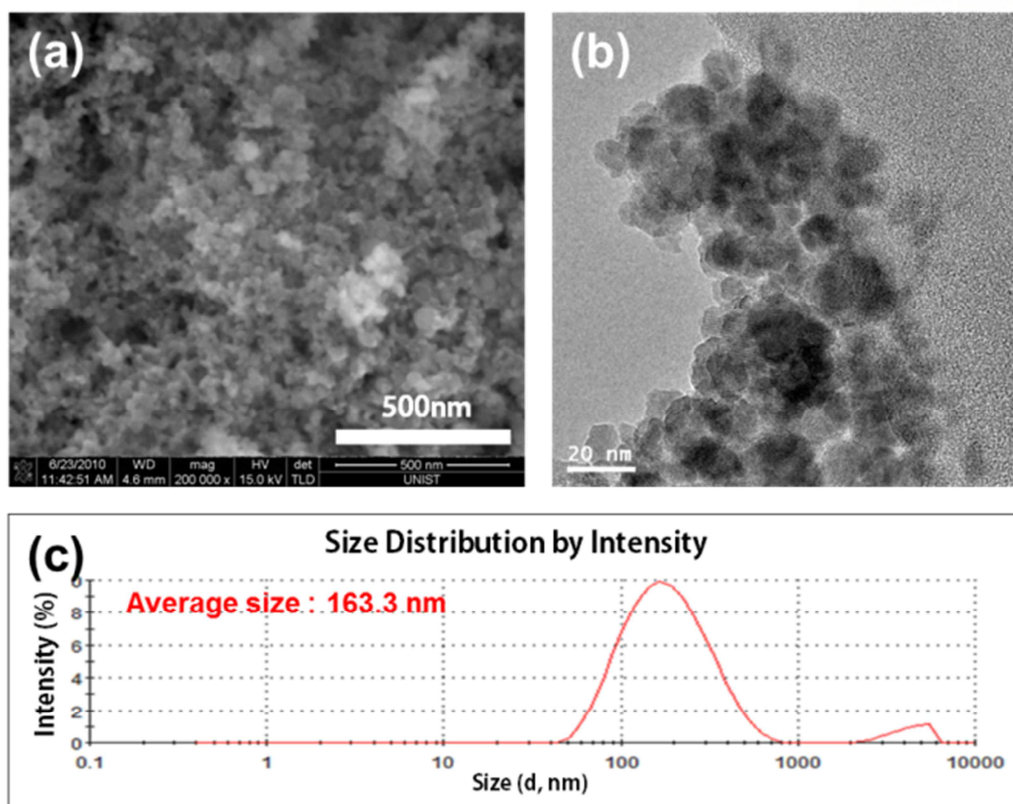
Figure 4-2. Morphology and size distribution of water-based copper oxide nanoparticles. (a) SEM image, (b) TEM image, and (c) size distribution as measured by dynamic light scattering

Figure 4-3 shows FE-SEM images of copper oxide prepared with various quantities of NaOH. With the addition of 5 ml of NaOH solution, aggregated needle-like structures were formed, as shown in Figure 4-3 (a) and (b). By increasing the quantity of NaOH to 10 and 15 ml, leaf-like and flower-like structures were observed, which were composed of needle-like building blocks. The size of leaf-like and flower-like structures increased with the amount of NaOH. Figure 4-3 (c) and (e) show leaf-like structures, which had smooth walls, and a high aspect ratio. Hierarchical copper oxide nanoflowers composed of nanosheet building blocks were formed when 10 and 15 ml of NaOH were added, as shown in Figure 4-3 (d) and (f), respectively.

Figure 4-4 shows FE-SEM images of the copper oxide samples prepared with 5, 10, and 15 ml of $NH_3 \cdot H_2O$. The morphology changed substantially, compared with NaOH to $NH_3 \cdot H_2O$. When 5 ml of $NH_3 \cdot H_2O$ were added, self-assembled copper oxide foil structures were observed. When 10 ml of $NH_3 \cdot H_2O$ were added, hierarchical copper oxide microspheres were observed, consisting of leaf-like building blocks. These microspheres were formed via the following process. First, leaf-like copper oxide particles were formed via the aggregation of nanoparticles. These leaf-like copper oxide

particles then self-assembled into flower-like structures, and larger flower-like copper oxide structures formed large flower-like copper oxide via Ostwald ripening. Figure 4-4 (c) and (d) show the morphology when 15ml of $NH_3 \cdot H_2O$ were added. There were two different regions: one was flower-like and the other formed 100-nm-diameter hexagonal copper oxide rods, which were approximately 916 nm long. Foil structure of Figure 4-4 (a) are similar the results of Liu et al.[127] They also studied about fabrication of CuO hierarchical nanostructure. CuO flower-like structures composed of hierarchical 2D nanosheets and spherical architectures are constructed into different alkaline solutions (NaOH and $NH_3 \cdot H_2O$).
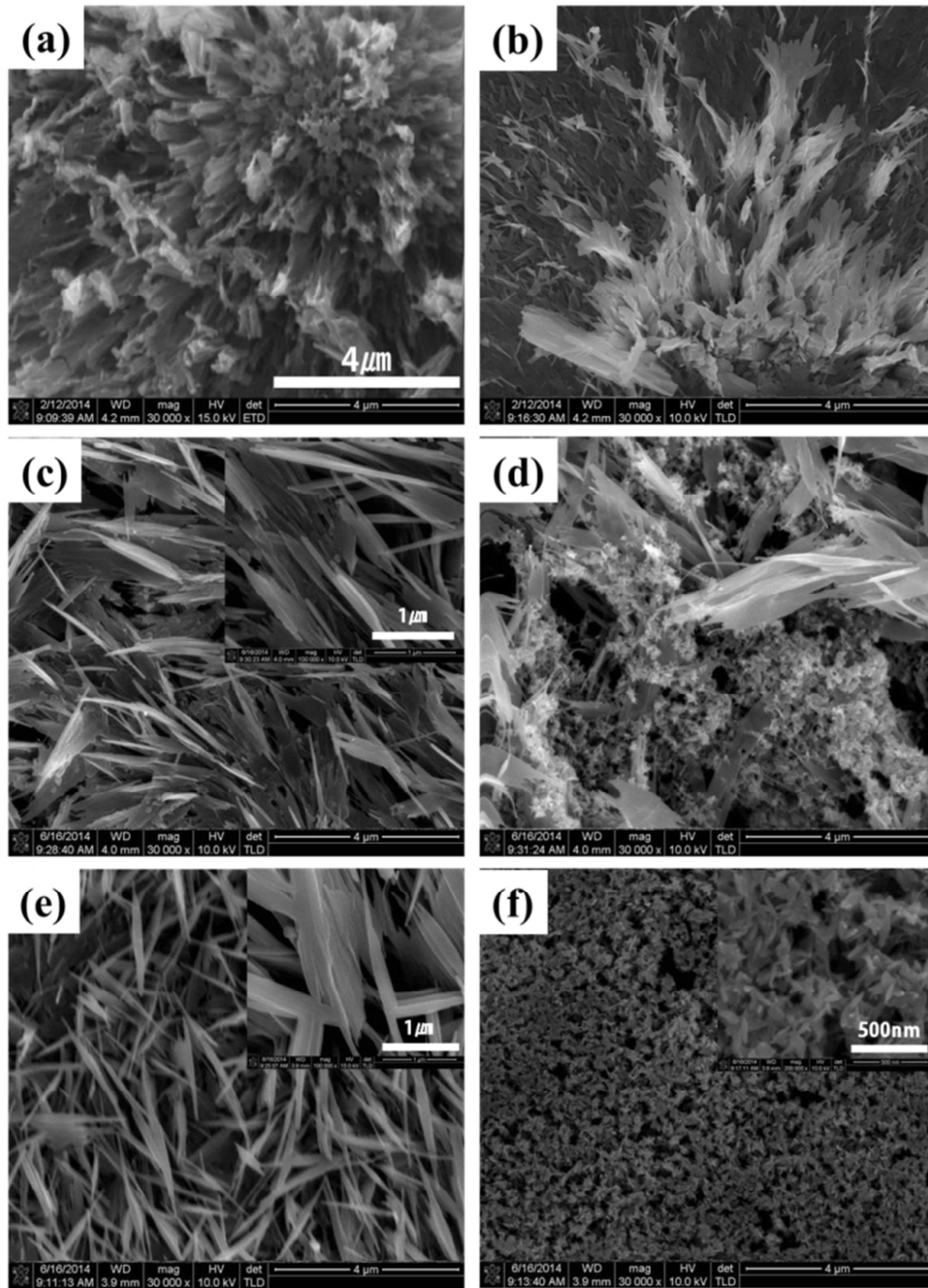
Figure 4-3. Morphologies of copper oxide microspheres obtained with (a) and (b) 5 mL of NaOH, (c) and (d) 10 mL of NaOH, and (e) and (f) 15 mL of NaOH
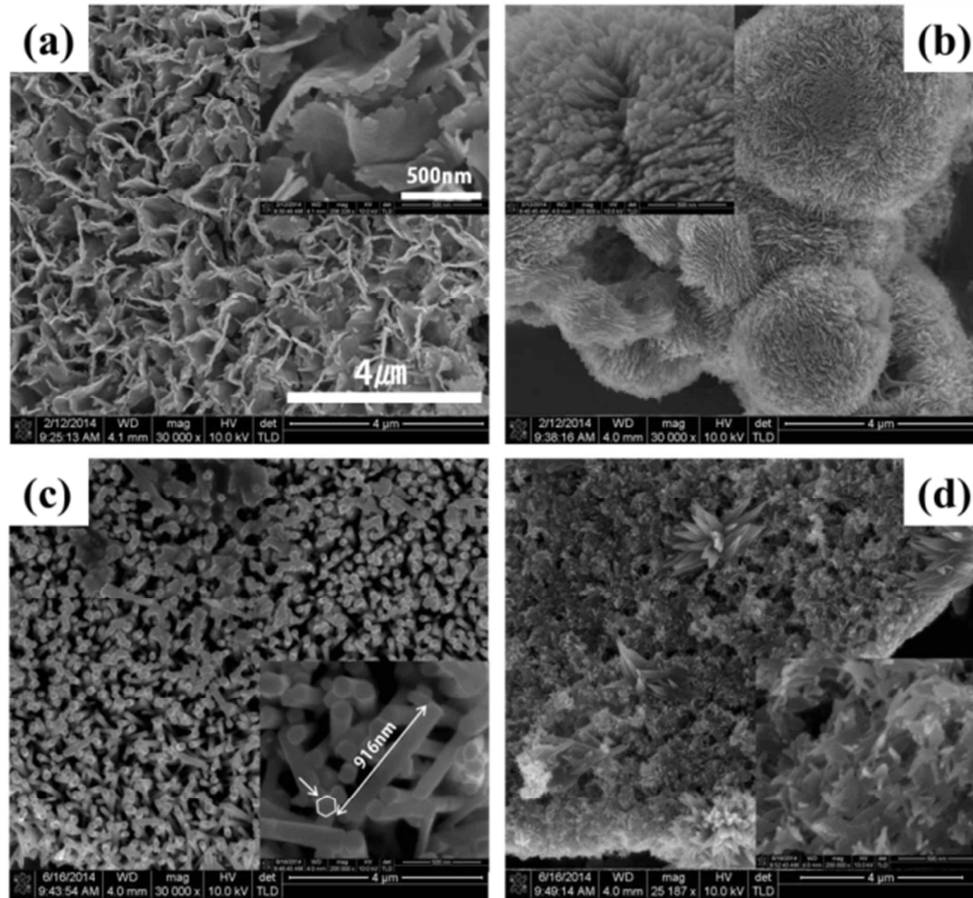
Figure 4-4. Morphologies of copper oxide microspheres obtained with different quantities of
$NH_3 \cdot H_2O$. (a) 5 ml, (b) 10 ml, and (c) and (d) 15 ml

The XPS spectrum of the CuO/Cu_2O composite is presented in Figure 4-5. In Figure 4-5 (a), the four peaks indicate the presence of the Cu^+ and Cu^{2+}. The Cu^+ and $Cu2^+$ ions are contributed to formation of CuO or Cu_2O. In case of two samples adding $NaOH$ and $NH_3 \cdot H_2O$, the binding energies of Cu 2p3/2 peak are slightly shifted to higher binding energy by 1.2 eV and 0.4 eV, respectively, than no additives sample. Oxidation states of Cu can be distinguished by satellite peaks of Cu2p. CuO has satellite peak at around 943 eV. The peak positions and intensities mean the different compositions. The O 1s peaks of three samples are presented in Figure 4-5 (c). The inserted image in Figure 4-5 (c) indicates distributable energy band of oxide (O^{2-}), hydroxide or hydroxyl groups (OH^-), and water (H_2O) in O 1s spectrum [ref]. O1s spectrum of no additives copper oxide is composed of two overlapping peaks corresponding to O^{2-} and OH^-. Copper oxide particles adding $NaOH$ and $NH_3 \cdot H_2O$ have OH- and H_2O. In the case of adding $NaOH$, the portion of H^- and H_2O is significantly high than adding $NH_3 \cdot H_2O$. The O1s peaks are the byproducts of formation copper oxide after chemical reaction. The detailed atomic concentrations of copper oxide composite are shown in table 4-2.
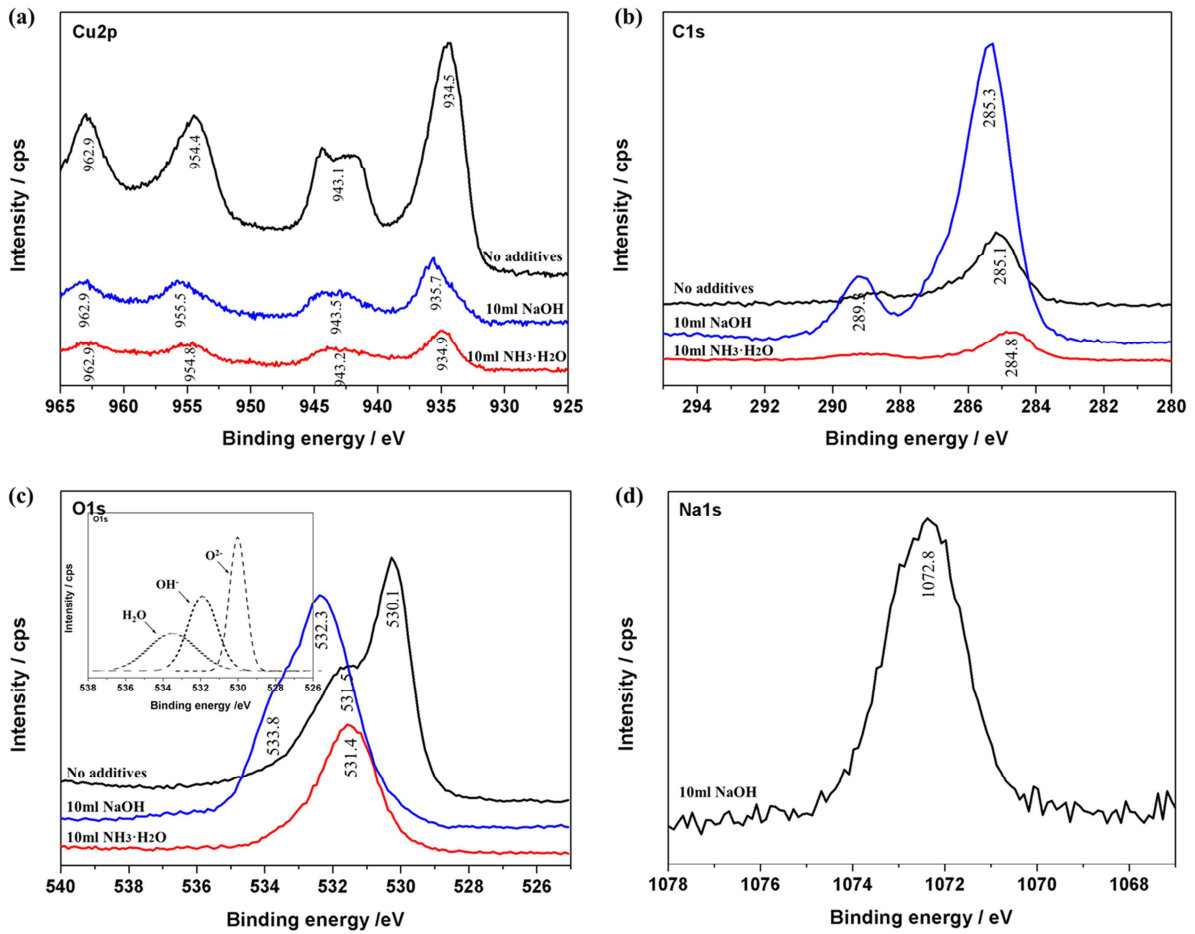
Figure 4-5. XPS spectra of the copper oxide particles produced under different liquid condition. (a) Cu2p spectrum, (b) C1s spectrum, (c) O1s spectrum and (d) Na1s spectrum

Table 4-2. Atomic concentration of Cu/CuO/Cu$_2$O composite in XPS spectra

	No additives (at%)	NaOH (at%)	NH$_3$·H$_2$O (at%)
Cu2p	21.2	1.84	9.86
O1s	46.06	27.88	38.32
C1s	32.74	68.41	51.82
Na1s	-	1.87	-

4.3.2. Growth mechanism

Size distribution of the nanoparticles was effected by absence of additives, as shown in TEM images of Figure 4-6. The nanoparticles produced via EEWL without additives are aggregated and grown up for stabilization thermodynamically. Using additives, the nanoparticles were aggregated in a specific direction due to a functional group formed by the effect of the additives.

The chemical reactions during the formation of the copper oxide structures were as follows:

$$Cu^{2+} + 4OH^- \rightarrow [Cu(OH)_4]^{2-}, \qquad\qquad\qquad (4.1)$$

$$[Cu(OH)_4]^{2-} \rightarrow CuO + 2OH^- + H_2O, \qquad\qquad\qquad (4.2)$$

$$Cu^{2+} + 4NH_3 \rightarrow [Cu(NH_3)_4]^{2+} \qquad\qquad\qquad (4.3)$$

$$[Cu(NH_3)_4]^{2+} + OH^- \rightarrow CuO + 4NH_4OH \qquad . \qquad\qquad (4.4)$$
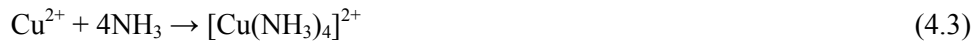
The copper wire and solutions were ionized, generating plasma during the explosion of the wire. In plasma, there are the Cu^+ and Cu^{2+} ions resulting from Cu dissociation. When NaOH is added to water, Cu^{2+} ions combine with OH^- to form $[Cu(OH)_4]^{2-}$ (eq. (1)). The concentration of Cu^{2+} and OH^- determines the formation of $[Cu(OH)_4]^{2-}$ and hence the CuO structures. It has been reported that the pH changes in response to the molar ratio of Cu^{2+} to OH^-, and that a higher pH can accelerate the transformation process.[128, 129] The initial CuO particles were assembled and formed needle-like structures, such as those shown in the TEM image in Figure 4-6, because of the large surface energy and van der Waals forces. Needle-like structures grew on the leaf-like structures via Ostwald ripening.[130, 131] When $NH_3 \cdot H_2O$ was added, the synthesis of CuO proceeded via $[Cu(NH_3)_4]^{2+}$ (eq. (3)). A larger ratio of NH_3 can accelerate crystal formation; furthermore, NH_3 contributes to growth along specific directions.[132] Cu^{2+} can be replaced Cu^+. The Cu^+ existing in plasma formed $[Cu(OH)_4]^-$ and $[Cu(NH_3)_4]^+$ as intermediate phase, respectively. Cu_2O particles were formed by its intermediate phase. Cu_2O has a strong tendency to reduce CuO. It would be less concentration of Cu_2O than CuO. Through these reactions, 3D structures were synthesized via anisotropic growth, as shown in Fig. 6. All of these processes occurred over a very short time scale corresponding to the duration of the explosions.
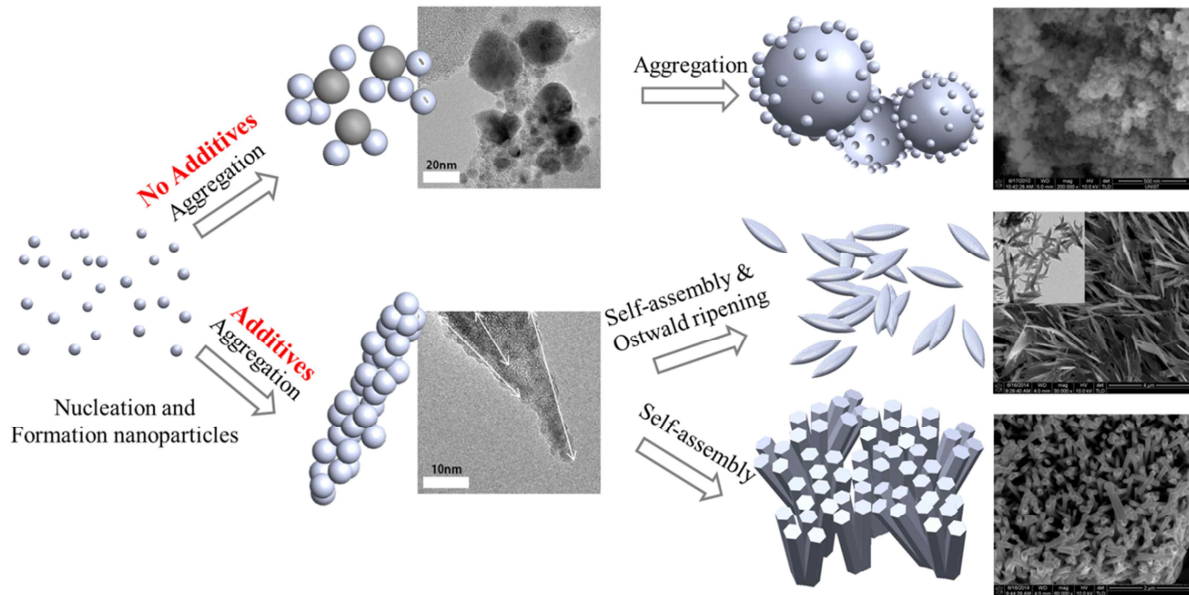
Figure 4-6. Schematic diagrams showing the formation of copper oxide particles in the plasma

4.3.3. Optical properties

The UV-vis spectra of the copper oxide nanofluids in different alkaline solutions are shown in Figure 4-7. The absorption bands for copper oxide nanoparticles have been reported to be in the range 500–600 nm,[133, 134] because of the effects of surface plasmon resonance, which is strongly dependent on the size and morphology of the particles. A broad absorption peak of the copper oxide nanoparticles was observed at 493 nm. The absorption band can be expected to exhibit a blue shift as the particle size decreases, due to quantum size effects.[135] The band gap of the hierarchical copper oxide microspheres was obtained using Tauc's relation[136]; i.e.,

$$(\alpha h v)^{n} = B(h v - E_{g}),$$ (4.5)

where α is the absorption coefficient, hv is the photon energy, the superscript n represents the nature of the transition, E_{g} is the optical band gap of the material and B is a constant related to the material and the matrix element for the transition. The inserts in Figure 4-7 show $(\alpha h v)^{2}$ as a function of hv. The band gap was determined by extrapolating to $\alpha = 0$, and was found to be 1.04eV, which is smaller than the value of 1.2eV reported.[1] Figure 4-7 (b) shows absorption spectra of the leaf-like and flower-like copper oxide structures formed in an aqueous NaOH solution. The maximum absorption peaks were observed at 370, 615, and 624 nm for quantities of NaOH of 5, 10 and 15 ml, respectively. With

60

10 and 15 ml of NaOH, two plasmon bands were observed at 370 and 620 nm, respectively.

The band gap was approximately 1.85–2.10eV; i.e., red-shifted known as band gap of CuO (1.2 eV of CuO and 2.2. eV of Cu_2O). The higher-energy band corresponds to oscillations of electrons perpendicular to the long axis. Figure 4-7 (c) shows absorption spectra of the hierarchical copper oxide structures with various morphologies formed in $NH_3 \cdot H_2O$ solutions. The maximum absorption peaks were observed at 627, 606, and 615 nm for structures formed in 5, 10 and 15 ml of $NH_3 \cdot H_2O$, respectively. The band gap was approximately 3.64–4.75eV. The synthesized copper oxide particles were approximately 1 μm in size, and this increase in size compared with those formed in DI water led to the red shift. NH_3 ligand in copper oxide colloids increases the stability of the complex particles and separation of energy levels[137].
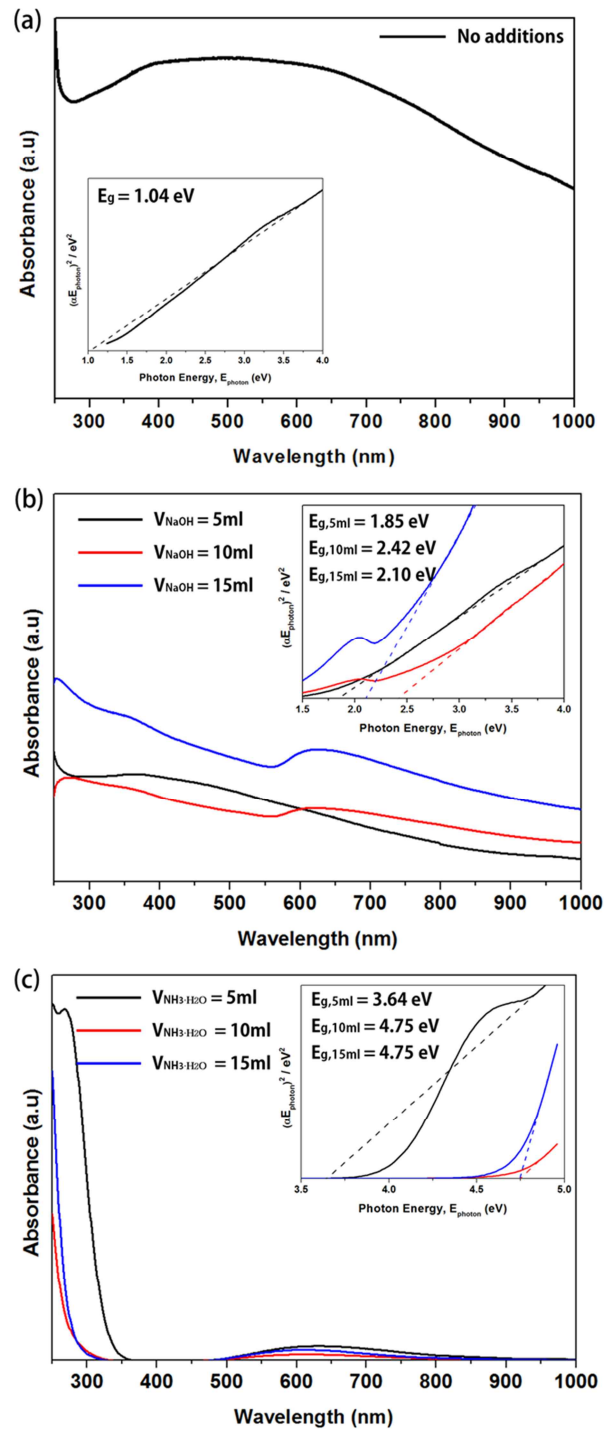
Figure 4-7. UV-vis absorption spectra of (a) spherical copper oxide nanoparticles formed using DI water, (b) leaf-like copper oxide structures formed in NaOH, and (c) flower-like and rod structures formed in $NH_3 \cdot H_2O$ solution. The inserts show the corresponding $(\alpha h\nu)^2$ as a function of the photon energy.

4.4. Summary

Copper oxide structures with various morphologies were synthesized via EEWL, with no surfactants or templates. $Cu/CuO/Cu_2O$ composited particles prepared using DI water were of nanometer-scale and spherical. Hierarchical copper oxide particles were obtained by adding NaOH or $NH_3 \cdot H_2O$, to obtain an alkali solution. Cu^+ and Cu^{2+} ions combined with OH^- and NH_3 to form agglomerates with various morphologies. Leaf-like 2D copper oxide structures were synthesized by adding NaOH, and increasing the quantity of NaOH accelerated growth of the agglomerate structures. When $NH_3 \cdot H_2O$ was added, the nucleation and growth of hierarchical 3D structures was observed. Uniform copper oxide rods were obtained by adding 15 ml of $NH_3 \cdot H_2O$, and the size of the copper oxide rods could be controlled by varying the amount of energy provided to the wire via Joule heating. The growth of the hierarchical copper oxide structures was attributed to aggregation and Ostwald ripening. The optical properties varied with the morphology of copper oxide structures, and the surface plasmon resonance of the self-assembled copper oxide nanoparticles was affected by the agglomeration of neighboring nanoparticles.

Chapter 5. Synthesis of nanofluids produced by the electrical explosion of the wire in liquid method

5.1. Introduction

There are several synthesis parameters that attribute to size and dispersion of nanofluids produced by the electrical explosion of the wire in liquid method. Investigation should be carried out the effect of various experimental parameters of EEWL on the characteristics of nanofluids synthesized. Characteristics of the nanofluids are controllable by volume of explosion wire, induced energy for explosion, and liquid type.

In this present work, design of experiments (DOE) and analysis of the voltage and current oscillograms method have been used for optimization of process parameters. DOE can analyze the effects of the parameters on the size and dispersion stability of nanofluids. And, we are understandable the explosion phenomenon through the examination of the voltage and current oscillograms.

Cooling is one of the most important technical issues for many industries. Alumina (Al_2O_3) nanoparticles are ceramics having outstanding engineering properties; they are being used in various industries. Elemental aluminum, especially as nanosized particles, is too reactive chemically to be found in nature as the pure metal. Because of this reactivity, oxidation of aluminum can be easily preceded by diffusion of oxygen through the oxide shell. Therefore, alumina is the most common nanoparticle used by many researchers. Most of studies on the thermophysical properties of nanofluids have used alumina nanofluids, with those nanofluids have been prepared primarily by the two-step method. In this study, the water-based and ethanol-based aluminum oxide nanofluids were prepared using the electrical explosion of the wire in liquid technique. The thermal conductivity and the viscosity of the aluminum oxide nanofluids were studied.

5.2. Optimization of Process Parameters

5.2.1. Design of Experiment

Design of experiment (DOE) is a systematic method to determine to obtain the maximum of information in the minimum number of experiments. A factorial design is the most important design for experimentation. It is used in most experiments because it is simple, versatile and can be used for

many factors.

DOE was used to compare the discharge features and to optimize process parameters on EEWL process. Silver nanofluids used in this study because silver is no phase change with liquid type. There are 4 parameters of interest in the size and dispersibility of particles, such as capacitance, wire length, liquid volume, and liquid type. Each parameter had two levels or values. The experiments were set up using Minitab tool. Designs with factors that are usually set at two levels assume that the effects of the factors are linear. Generally, a factor is only evaluated at the low and high points. Ideally, there should be one or more center-points to improve the reliability. Further analysis can compare the measurements of the dependent variable at the center point with the average values of the design. The DOE used a 1/2 fractional factorials design of the full factorial design on 4 parameters. Table 5-1 represents the result in 12 experiments.

Table 5-1. Experimental conditions by design of experiment and the size and zeta potential results of silver nanofluids

RunOrder	Capacitance (μF)	Wire length (mm)	Liquid volume (mℓ)	Liquid	Particle size (nm)	Zeta potential (mV)
1	7.5	28	500	Water	115.8	-29.30
2	30	28	500	Ethanol	239.8	-23.60
3	7.5	38	500	Ethanol	277.6	-19.20
4	30	38	500	Water	123.5	-37.00
5	7.5	28	1000	Ethanol	262.5	-19.70
6	30	28	1000	Water	726.0	-10.70
7	7.5	38	1000	Water	1283.0	-11.80
8	30	38	1000	Ethanol	1873.0	1.43
9	18.75 (15)	33	500	Water	123.7	-45.70
10	18.75 (15)	33	1000	Water	116.1	-41.70
11	18.75 (15)	33	500	Ethanol	1644.0	-2.71
12	18.75 (15)	33	1000	Ethanol	1476.0	-9.14

There are no parameters that has impact on the size and zeta potential because all parameters are closed to the normal probability plot as shown in Figure 5-1 (a) and 5-2 (b). The level of impact on particle size is liquid>liquid volume>wire length>capacitance+liquid>capacitance+liquid volume>capacitance>capacitance+wire length as indicated in Preto chart in Figure 5-1 (b). In the case of zeta potential, the level of impact is liquid>liquid volume>capacitance+liquid volume> capacitance+liquid> capacitance+wire length>wire length>capacitance as shown in Figure 5-2 (b).
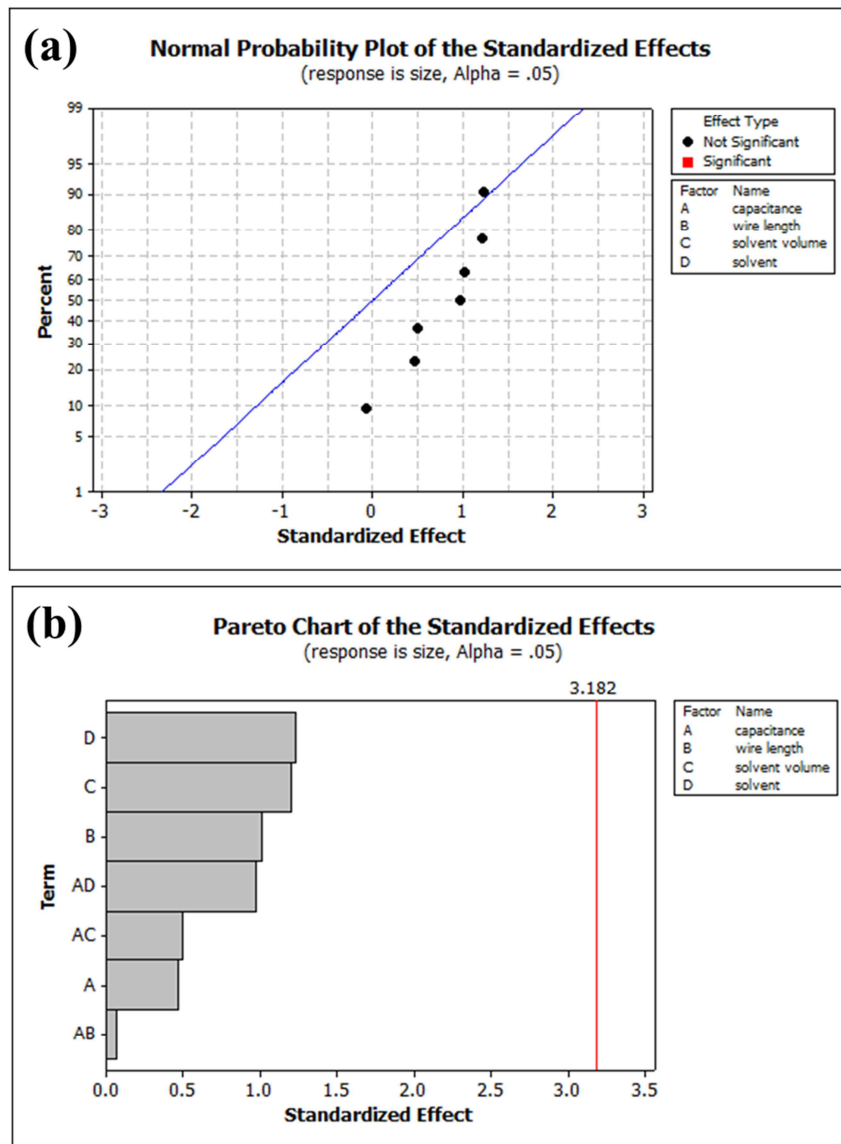
Figure 5-1. Normal probability plot and Pareto chart of the standardized effects for particle size

(a) **Normal Probability Plot of the Standardized Effects**
(response is zeta, Alpha = .05)

Effect Type
● Not Significant
■ Significant

Factor	Name
A	capacitance
B	wire length
C	solvent volume
D	solvent

(b) **Pareto Chart of the Standardized Effects**
(response is zeta, Alpha = .05)

3.182

Factor	Name
A	capacitance
B	wire length
C	solvent volume
D	solvent
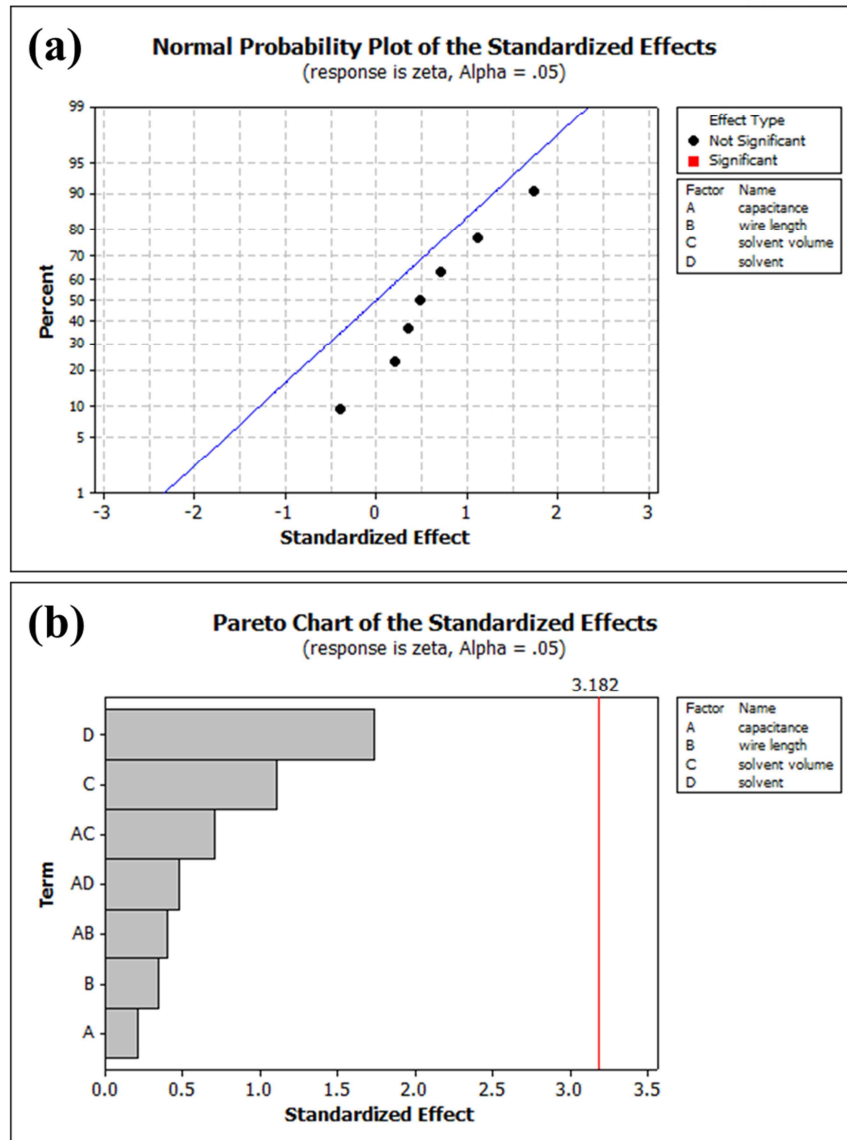
Figure 5-2. Normal probability plot and Pareto chart of the standardized effects for zeta potential

Figure 5-3 shows the main effect plot for particles size and zeta potential. When the capacitance and wire length decrease, particles size decreases and zeta potential increases. And, the smaller nanoparticles and the higher dispersed nanofluids can be produced in 500ml water.
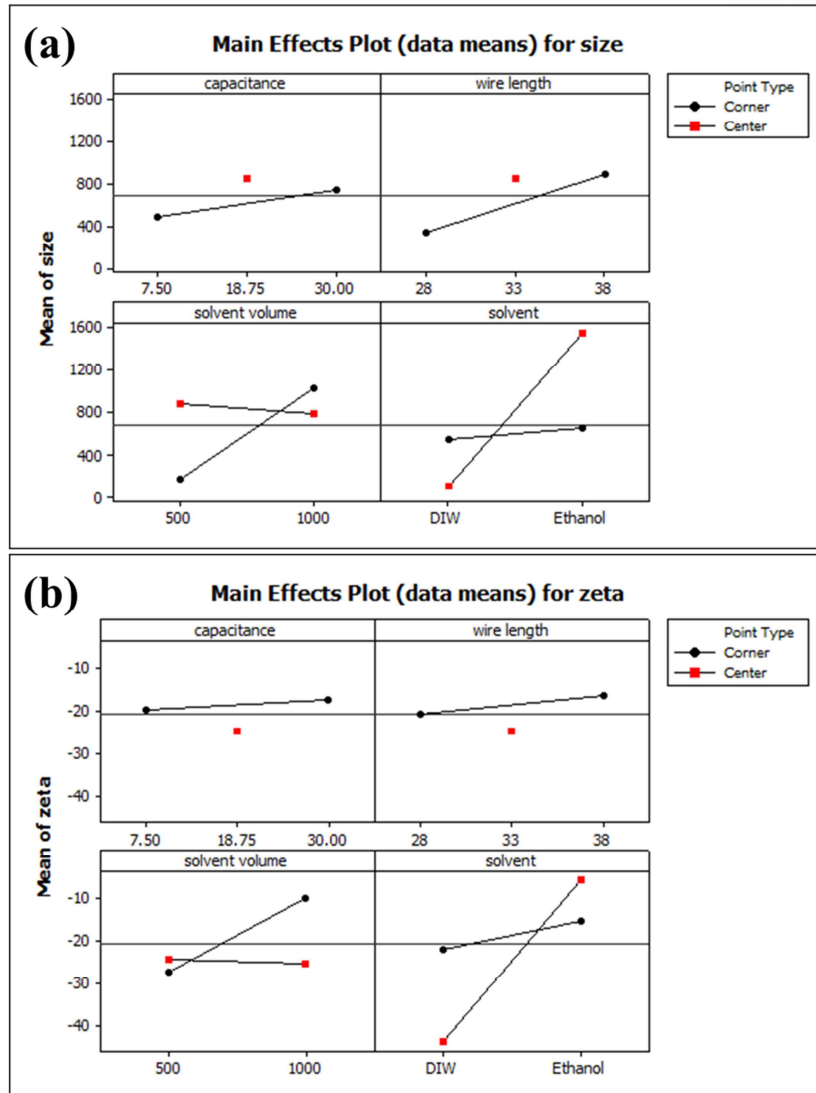
Figure 5-3. Main effects plot for (a) particle size and (b) zeta potential
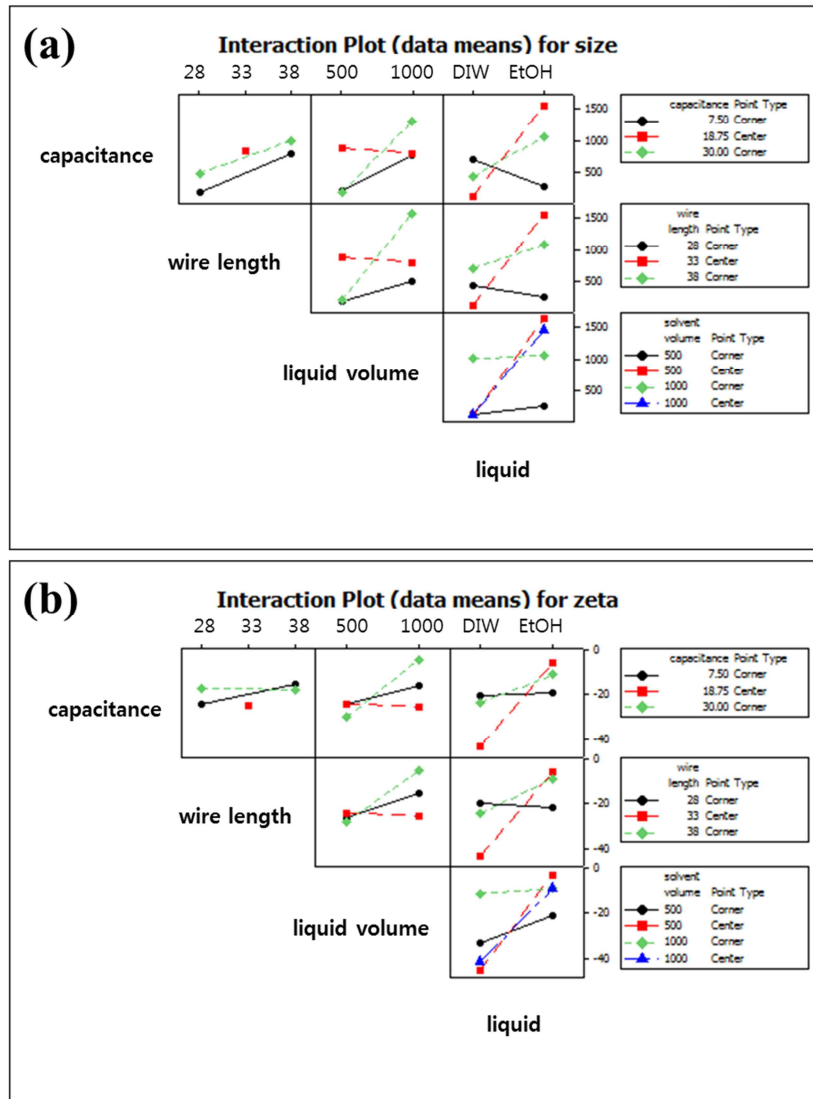
Figure 5-4. Interaction plot for (a) particle size and (b) zeta potential

Response optimizer was conducted to determine the optimized parameter conditions. The process was optimized when capacitance was 30 µF, wire length was 38 mm, liquid volume was 500 mL, and liquid type was deionized water. These conditions corresponded to a particle size of 49 nm and zeta potential of -39.15 mV as shown in Figure 5-5. These predicted optimized parameters were confirmed by repeating the experiment, and the results for particle size and zeta potential were 118.9 nm and -42.5 mV, respectively. There were differences between the prediction and the experimental results.

Optimal D 1.0000	Hi Cur Lo	capacita 30.0 30.0 7.50	wire len 38.0 38.0 28.0	solvent 1000 500 500	solvent Ethanol DIW DIW
size Minimum y = 49.0833 d = 1.0000					
zeta Minimum y = -39.1571 d = 1.0000					
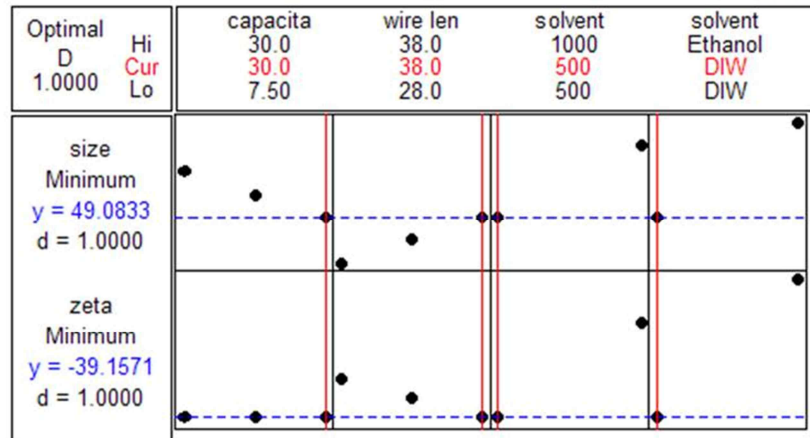
Figure 5-5. Response optimization conditions

5.2.2. Calculation of Electrical Phenomenon

Energy stored in the capacitors is used to explosion energy of the wire. The parameter conditions of the explosion are selected on the basis of the use energy efficiency charged in the capacitors and the energy density applied in the wire. The energy applied in the wire is one of the important parameters to determine the resistance change and thermodynamic state of the wire when the wire explodes and characterize of the nanoparticles. The energy used in the explosion has to be quantified experimentally using the voltage and current oscillograms because it is difficult to calculate in theory. The energy stored for capacitance of the 7.5 μF is 33.75 J. However, the energy value exceed much higher than 33.75J as shown in Table 5-2. The reason can be explained by sublimation energy of the materials. Sublimation energy is the internal energy of the transition from the solid to the vapor state. Because the solid-state wire is vaporized by the instantaneous current rise, sublimation energy of the materials is also an important parameter of the explosion process. The sublimation energy of aluminum is 33 J/mm^3. To investigate the relationship of the stored energy and sublimation energy was investigated in a wider range process condition.

The unstable region in Figure 5-6 is due to the energy used in the explosion is exceeded the energy stored in capacitors. The energy stored in capacitor does not reach the sublimation energy and the energy used in the explosion is exceeded the stored energy in capacitor. In Figure 5-6, the point of the explosion in unstable region is delayed than stable region. As the time delay the explosion, the current through the wire continues to rise. In other words, the energy stored in the capacitor, as well as additional energy during the current flowing is accumulated on the wire. However, when the energy stored in capacitor is much smaller than the sublimation energy, the explosion will not happen.

The explosion energy is used as follows,

Stable explosion;

$$E_{explosion} \geq E_{sublimation} \quad , \qquad E_{ex} = E_{capacitor} - E_{bss}$$

Unstable explosion;

$$E_{explosion} \leq E_{sublimation} , \qquad E_{ex} = E_{capacitor} + E_{additional \; current} - E_{bss}$$

Non-explosion

$$E_{explosion} < E_{sublimation}$$

Table 5-2. Deposited in the wire under various parameter conditions

Capacitance (Stored energy in capacitor)	Wire length / Diameter	23 mm	28 mm	30 mm
7.5 μF (33.75 J)	0.05 mm	15.9 J	17.2 J	15.6 J
	0.1 mm	94.2 J	103.2 J	106.9 J
	0.2 mm	449.5 J	598.1 J	467 J
30 μF (135 J)	0.05 mm	12.6 J	16.30 J	14.6 J
	0.1 mm	71.4 J	83.8 J	87.3 J
	0.2 mm	663.1 J	756.5 J	698 J
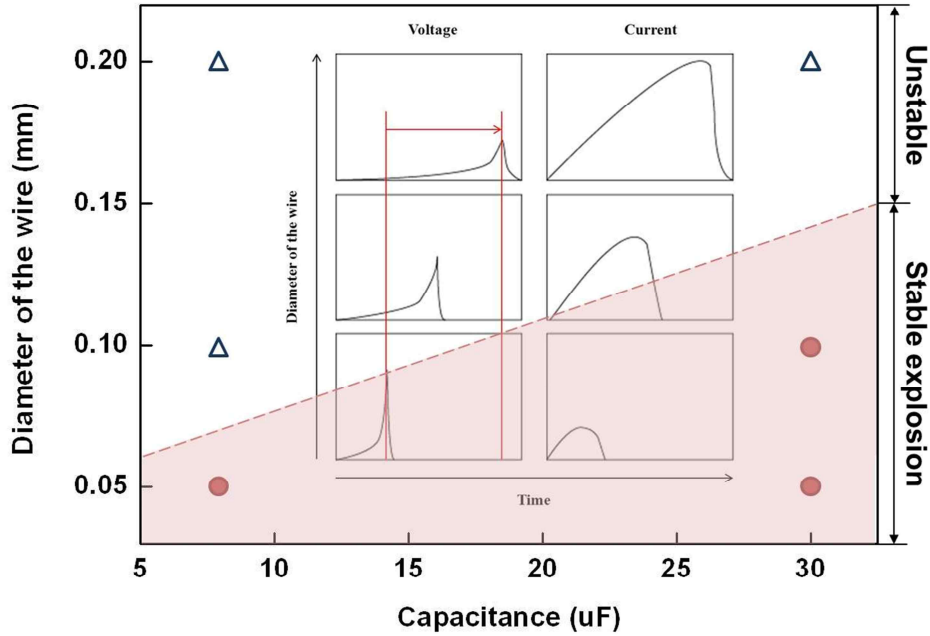
Figure 5-6. Explosion profile based on voltage and current oscillograms

5.3. Thermophysical Properties

5.3.1. Prediction models for thermal conductivity and viscosity of nanofluids

Some predictive models based on effective medium theory have been developed for the thermal conductivity of two-phase fluids. The experimental results of this study were analyzed using two of these models, i.e., the Maxwell[138] and Kenneth[139] models. The Maxwell model for thermal conductivity for nanofluids containing relatively large particles is appropriate for low particle concentrations. The Maxwell model is as follows:

$$k_{eff} = \frac{k_p + 2k_b + 2(k_p - k_b)\phi}{k_p + 2k_b - (k_p - k_b)\phi} k_b \tag{5.1}$$

where k_p is the thermal conductivity of the particle, k_b is the thermal conductivity of the base fluid, and Φ is the particle volume fraction in the liquid. The Kenneth model considers all major effective parameters including size, density, volume concentration, fluid temperature, and fluid viscosity. The Kenneth model is as follows:

72

$$k_{eff} = 1 + C \frac{f^a k_b \rho_p c_p T^{1.5}}{k_{BF} h \mu^{0.5} d_p^{0.5}} \exp\left(-\frac{3.8 T_b}{T}\right) \left(\frac{c_{BF}}{c_p}\right)^b k_b \qquad (5.2)$$

where C is a modified constant and c_{BF} is the specific heat of the base fluid. The a and b are empirical constants that represent the effects of nanoparticle coagulation and nanoparticle heat dissipation, respectively. These values provides [140] a = 0.7, b = 1.5, and C = 1.33×10^{-25}. The f, ρ_p, μ, and d_p are the volume fraction, particle density, base fluid viscosity, and particle diameter, respectively. C_{BF}/C_p is the ratio of the heat capacity of the base fluid to that of the nanoparticles. This model is considered all major effective parameters including size, density and volume concentration, the temperature of fluid, and viscosity.

There are some prediction models of viscosity of nanofluids. Einstein was the first to develop the model relating to nanofluids viscosity. The model is based on the nanofluids containing spherical particles at a very low concentration. The Einstein model is as follow:

$$\mu_{nf} = \mu_f (1 + 2.5\phi) \qquad (5.3)$$

Where μ_{nf} is the viscosity of nanofluids, μ_f is the viscosity of the base fluid and φ is the volume fraction of the particles. The Batchelor modified Einstein's model considering the Brownian motion and spherical particles. The model is given as follows.

$$\mu_{nf} = \mu_f (1 + 2.5\phi + 6.5\phi^2) \qquad (5.4)$$

These models are known as the classical model of viscosity of nanofluids.

5.3.2. Experimental Setup

The thermal conductivity of nanofluids was measured with a LAMBDA system. The LAMBDA system is based on the in-stationary hot-wire method. And this system consists of 3 components, the microprocessor unit for control and evaluation, the measuring head and the software controlled heating/cooling device. So, a completely homogeneous temperature distribution inside the sample can be provided.

The viscosity of the nanofluids was measured with Vibro Viscometer model SV-10 (A&D Company, Japan) under changing of temperature. The viscosity was calibrated with deionized water (DIW) from 25 to 60°C, as shown in Figure 5-7. Accurate viscosity data for aqueous nanofluids depend on measured data for DIW compared to the following correlation[141]:

73

$$\mu = \frac{e^{(1.1265-0.0396T)/(1-0.0073T)}}{10^4} \tag{5.5}$$

where μ is the viscosity of DIW (mPa·s) and T is the absolute temperature (K). The experimental uncertainty for the viscosity was 7.96%. The prediction of Einstein[142] and Batchelor[143] are compared with the experimental results.
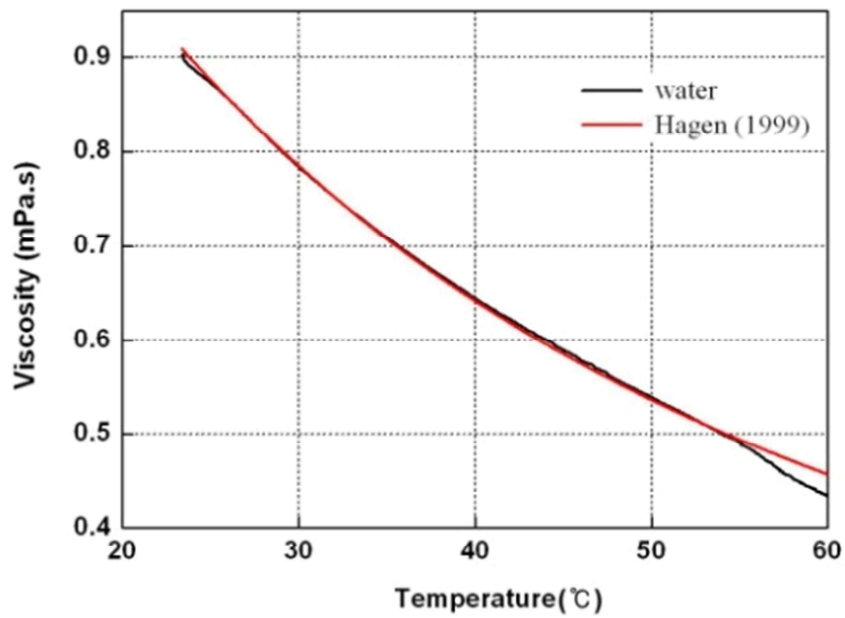
Figure 5-7. Viscosity-fluid temperature curve of water and calibration

5.3.3. Viscosity and thermal conductivity
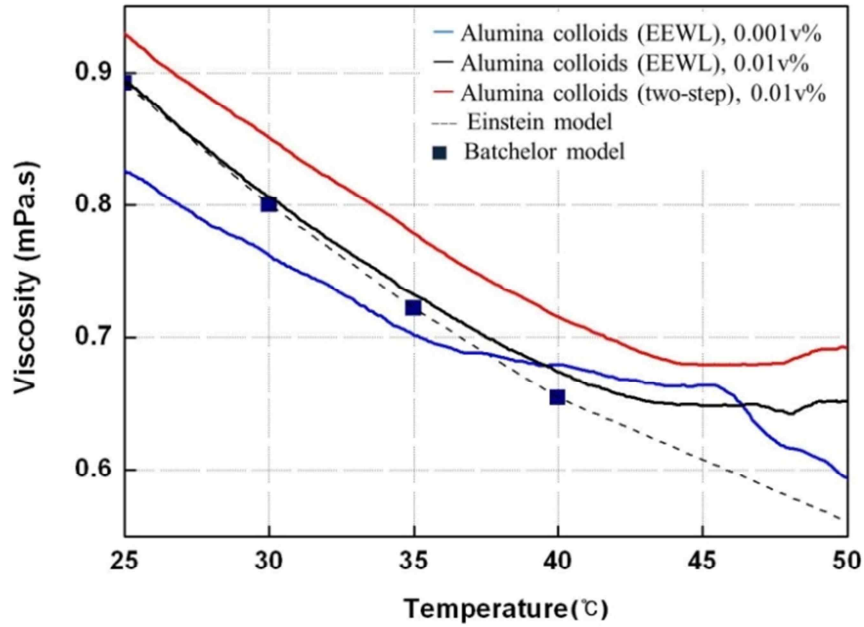
Figure 5-8. Variation in viscosity of the aluminum oxide nanofluids as a function of temperature

The viscosity of the aluminum oxide nanofluids was measured from 25–50°C. The viscosity of aluminum oxide nanofluids prepared by EEWL is lower than for those prepared by the two-step method (Figure 5-8). Viscosity decreased with increasing temperature.

The experimental results were compared with predictions from the Einstein and Batchelor models at 0.001 vol% concentration. They followed a similar trend. 0.01% of the alumina nanofluids by one-step method are the most consistent with two models, but as a result of different samples, it is hard to say whether the viscosity will increase or decrease.

Experimental and theoretical thermal conductivities were compared. Figure 5-9 shows that the thermal conductivity increased with increasing temperature for both sets of data. Experimental results showed that the 0.01 vol% aluminum oxide nanofluids prepared by the EEWL process behaved differently. Predictions by the Maxwell model agreed with the experimental results. However, the experimental and predicted values from the Kenneth model differed at high temperatures; this is because coagulation of the nanoparticles is not considered in this model.

75
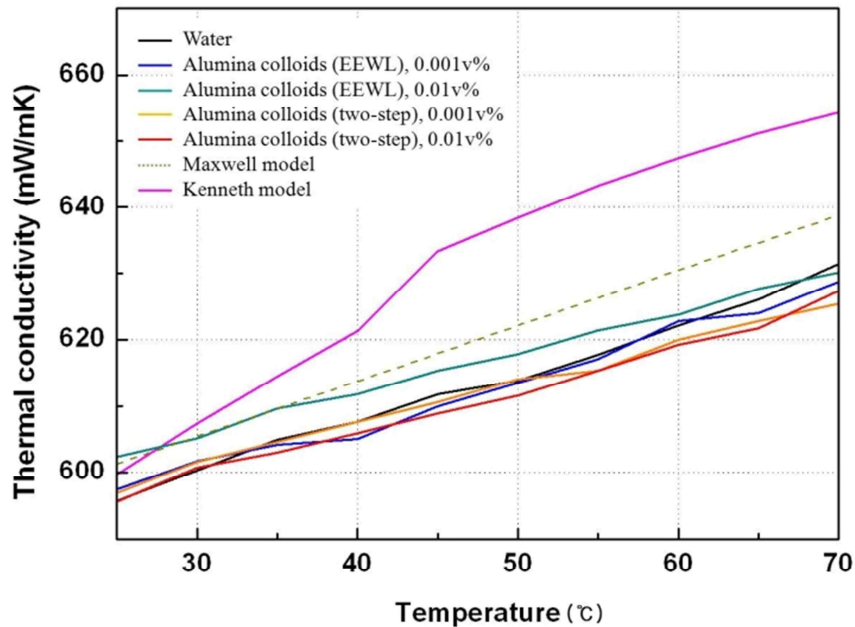
Figure 5-9. Experimental and theoretical thermal conductivities of water-based aluminum oxide nanofluids

5.4. Summary

In this study, we produced silver nanofluids by electrical explosion of wires in liquids. The particle size and zeta potential are strongly influenced by the basefluid. By optimizing control parameters, we decreased the particle size under fast explosion conditions and long plasma duration with low-viscosity media. A low viscosity decreased the particle size and dispersion stability due to greater expansion in the plasma volume. The process was optimized by response optimization conditions (ROC) when capacitance was 30 μF, wire length was 38 mm, liquid volume was 500 mL, and the liquid type was deionized water. For the repeated experiment, the average particle size of the Ag nanoparticles in water was 118.9 nm, and the zeta potential was -42.5 mV.

The energy deposition in the aluminum wire during EEWL process was evaluated as a function of the length of the wire, capacitance, and basefluid. A large capacitance increased the current rise. The high energy is stored with increasing of capacitance according to the relationship 0.5 CV^2. Increasing of the deposited energy in the wire is out of proportion to decreasing of the size of the aluminum nanoparticles in a given base liquid. This means that the explosion time affects the production of

nanoparticles more than the amount of energy deposited in the wire.

The thermal conductivity and the viscosity of aluminum oxide nanofluids were measured compared to prediction model. The nanofluids prepared under conditions of 7.5 μF and 38 mm had a lower viscosity than that predicted by the theoretical model at temperatures below 40°C. The experimental results show that the thermal conductivity of alumina nanofluids is affected by the base fluid. However, the enhancement of the thermophysical properties is not significant because of the extremely small concentration of the nanoparticles.

Chapter 6. Pool Boiling CHF Enhancement of Nanofluids

6.1. Introduction

One of the most interesting characteristics of nanofluids is their enhancement of the critical heat flux (CHF). The CHF is the thermal limit of the phase change during heat and its enhancement contributes to an increased performance and safety margins of thermal system. CHF enhancement has been studied extensively using different nanofluids and concentrations, including Al_2O_3, TiO_2, and ZrO_2. However, although parametric trends of CHF have been widely investigated for a wide range of geometrical and flow conditions, our fundamental understanding of the physical mechanisms of CHF is still inadequate. In these studies, researchers typically used low concentrations (< 0.1 vol%) of nanoparticles in water as a base fluid, where the thermal properties of the nanofluids were unaffected.

Nanofluids produced via EEWL have a higher dispersion stability compared to nanofluids produced by two-step method such as sonication. Thus, we can examine the influence of dispersion stability on CHF enhancement using silver, copper oxide, aluminum oxide nanofluids produced by EEWL. In present research is also conducted pool boiling experiments using xGnPs and xGnPs oxide nanofluids. Carbon-based nanomaterials are of interest due to their superior thermal and electrical properties. Among them, exfoliated graphite nanoplatelets (xGnPs) enhance the CHF of nanonfluids, and are of greater economic benefit than CNTs and graphene. CHF enhancement is contributed by the morphology change of the wire surface after pool boiling experiment, as one of the largest factor. The investigation of surface morphologies is conducted using SEM and AFM images intensively.

6.2. Experimental Setup

6.2.1. Preparation of silver, copper oxide and aluminum oxide nanofluids by EEWL

The silver, copper oxide and aluminum oxide nanofluids for pool boiling experiment were prepared by electrical explosion of the wire in liquid method. The preparation of nanofluids was progressed the identical process. Detailed experimental conditions are summarized in Table 6-1. The systemic conditions were based on the design of experiment (DOE) methodology of a previous study in chapter 5. And, two copper oxide nanofluids were more prepared with adding 10ml of $NH_3 \cdot H_2O$ under same experimental conditions.

Table 6-1. Summary of the EEWL process conditions

Capacitance	30 μF
Charging voltage	3 kV
Material / type	Aluminum, copper, or silver / wire
Wire diameter	0.1 mm
Wire length	3.8 mm
Liquid	Deionized water
Liquid volume	500 mL
Concentration	0.001 vol%

6.2.2. Preparation of xGnPs and xGnPs oxide nanofluids

xGnPs (M-5) particles were purchased from XG Sciences, Inc. The xGnPs combines a lower price and layered structure with superior thermal and electrical properties. The xGnPs used in this study displayed an average thickness of ~6-8nm and were synthesized by alkali metal intercalation. The material properties of the xGnPs powders are summarized in Table 3-2.

xGnPs oxide was synthesized from natural xGnPs (M-5) by the method of Hummers and Offeman[15]. The xGnPs (M-5) (5g) was put into and 80℃ solution of concentrated H_2SO_4 (30mL), $K_2S_2O_8$ (2.5g), and P_2O_5 (2.5g). The mixture was thermally isolated and allowed to cool to room temperature over a period of 6h. The mixture was then carefully diluted with distilled water, filtered, and washed on the filter until the rinse water pH became neutral. The product was dried in air. The oxidized xGnPs (M-5) powder(5g) was put into cold (0℃) concentrated H_2SO_4(115mL). $KMnO_4$ (15g) was added gradually with stirring and cooling, so that the temperature of the mixture was not allowed to reach 20℃. The mixture was then stirred at 35℃ for 2h, and distilled water (230mL) was added. The reaction was terminated by the addition of a large amount of distilled water (700mL) and 30% H_2O_2 solution (12.5mL), after which the color of the mixture changed to bright brown. The mixture was filtered and washed with 1:10 HCl solution (1.25L) in order to remove metal ions. Then, the GO product was suspended in distilled water, which was subjected to dialysis to completely remove metal ions and acids.

The high-resolution-transmission electron microscopy (HR-TEM) and field emission-scanning electron microscopy (FE-SEM) images of xGnPs and xGnPs oxide particles are shown in Figure 6-1.

The thickness of xGnPs (M-5) and xGnPs oxide particles are about 15.3nm and 11.5nm, respectively.

Table 6-2. Material properties of xGnPs

Physical structure	Interaction	Thermal conductivity	Density
Platelet	π-π	3000W/mK ll, 6W/mK ⊥	~2.2 g/㎤
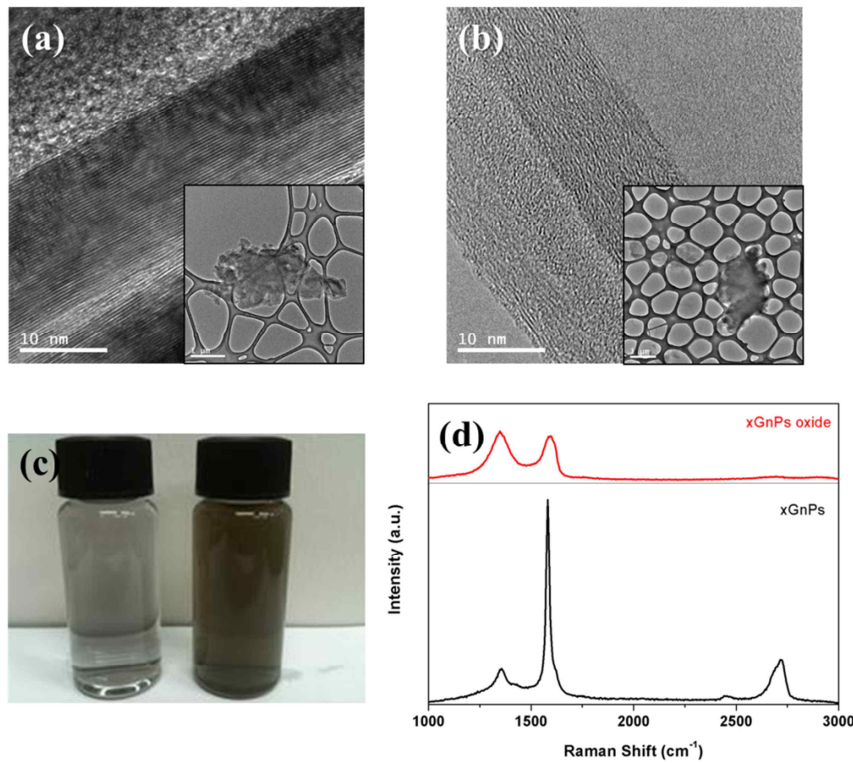
Figure 6-1. TEM images of (a) xGnPs, (b) xGnPs oxide powders dispersed in water, and (c) xGnPs(left)/xGnPs oxide(right) nanofluids with concentration of 0.001vol%

The two different nanofluids, including xGnPs and xGnPs oxide, were prepared by a two-step method: xGnPs and xGnPs oxide powders were added to distilled water with no surfactant. To stably disperse the particles, sonication was used. The xGnPs particles consist of a higher number of graphene sheets that form a platelet. The xGnPs and xGnPs oxide particles dispersed in deionized water are shown in

Figure 6-1 (c). The zeta potential of the nanofluids (Nano ZS, Malvern, UK) were -53.5 mV for xGnPs nanofluids and -62.5 mV for xGnPs oxide nanofluids at a particle concentration of 0.001 vol%.

Figure 6-1 (d) shows the Raman spectrum of the xGnPs and xGnPs oxide particles. The spectrum of the xGnPs oxide shows a broadened and blue shifted G-band at 1597 cm-1 and the D-band at 1353 cm-1. The G-band arises from the E_{2g} vibrational mode of sp2-carbon systems. The spectrum of the xGnPs shows a strong G-band at 1585 cm^{-1} with a small shoulder, identified as the D'-band at 1626 cm^{-1}, and a D-band at 1353 cm^{-1}. The D-band is caused by disordered structure into sp2-carbon systems. The intensity ratio of the D-band to the G-band is determined the quality of xGnPs structures. D'-band is also proportional to the concentration of defects. If there are some disordered impurities or surface charges, the G-band is split into two bands, G-band (1585 cm^{-1}) and D'-band (1626 cm^{-1}). All kinds of sp2-carbon materials have a strong 2D-band in the range of 2500 - 2800 cm-1. 2D-band is a second-order two-phonon assisted double resonant processes. 2D-band can be also used to determine the number of layer of graphene. The single-layer graphene exhibits a sharper 2D-peak located below 2700 cm^{-1} while bilayer have a broader peak. Multi-layer has a milder and broader peak located above 2700 cm^{-1}. 2D-band of xGnPs (M-5) particles shows around 2720 cm^{-1}, it can be explained that xGnPs (M-5) is probably consisted with five or more layers.

6.2.3. Pool boiling experiment

A schematic illustration of the experimental apparatus is shown in Figure 6-2. The apparatus consisted of a rectangle vessel, a Teflon cover, a reflux condenser to maintain the volume concentration of the working fluid during boiling, two electrodes, and a power supply. A horizontally suspended NiCr wire was located between two copper electrodes. The voltage, current, and temperature signals were collected by a data acquisition system (DAQ). The experiments were conducted in a stabilized atmosphere at a saturated temperature of about 100°C. Power was supplied to the wire heater until the CHF was reached. The power was increased in small steps as the heat flux approached the CHF.

The CHF was calculated using the following equation:

$$q_{CHF}^{"} = \frac{VI}{A} \qquad (6.1)$$

where I and V are the current and the voltage of the heater, respectively, and A is the heat-transfer area of the heater.
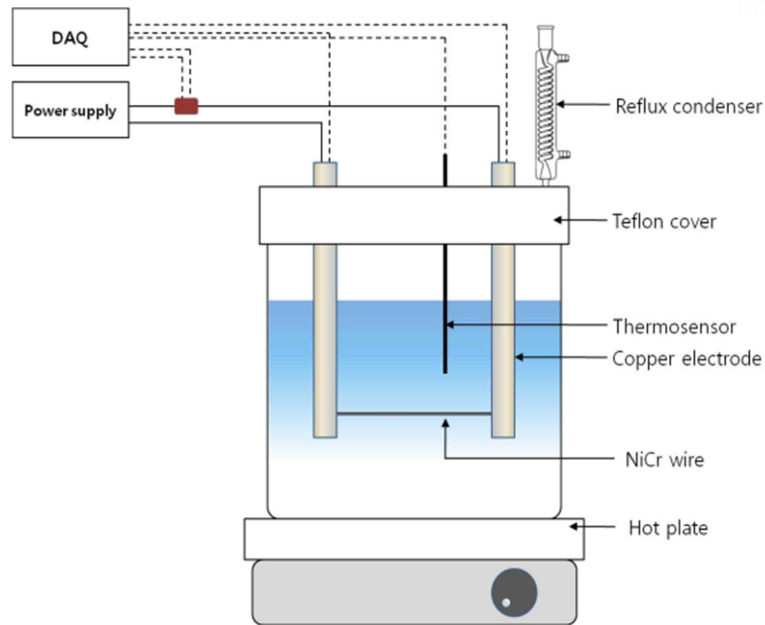
Figure 6-2. Schematic illustration of the pool boiling experimental apparatus

6.3. Results and Discussion

6.3.1. CHF enhancement using silver, copper oxide and aluminum oxide nanofluids by EEWL

Figure 6-3 shows the CHF enhancement ratio of nanofluids with different nanoparticles in pool boiling experiments compared with CHF values of water. Nanofluids except aluminum oxide (two-step) were produced by EEWL process. The aluminum oxide nanofluids prepared by EEWL showed the largest CHF enhancement of 187% at 0.001 vol% in concentration. The CHF of the Ag nanofluids was enhanced by 58% over pure water, while the CHF of the copper oxide nanofluids was enhanced by 99%. Two samples with different concentration marked in blue were prepared adding 10ml of ammonia ($NH_3 \cdot H_2O$) by EEWL process. Copper oxide nanofluids adding ammonia of 0.001vol% and 0.005vol% concentration enhanced in 56% and 75% CHF, respectively.
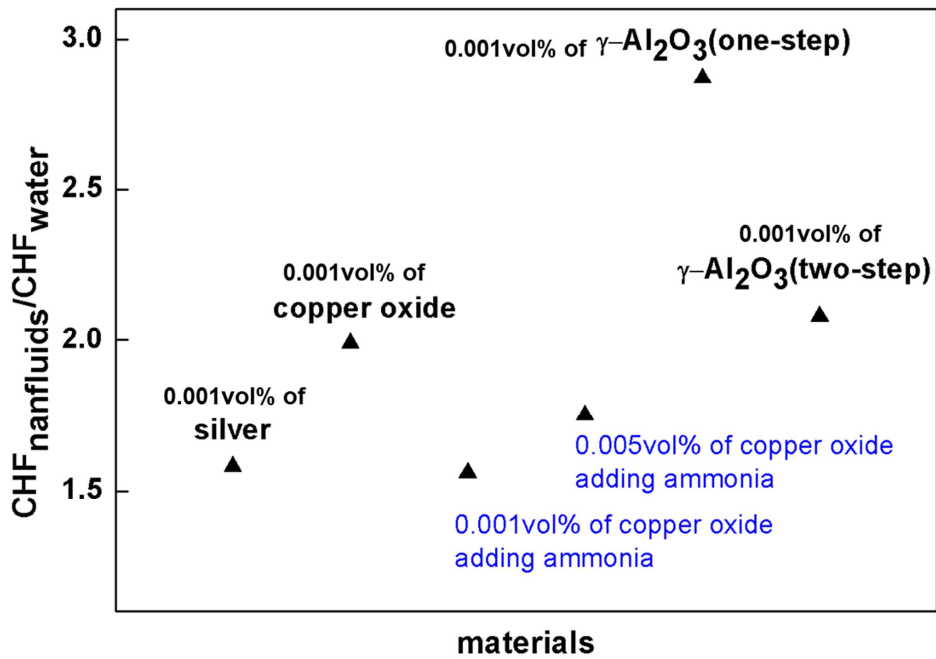
Figure 6-3. CHF enhancement ratio for various nanoparticles prepared in the water

The CHF enhancement can be explained by the roughness and structure of the heater surface and the wettability [89, 144]. Applying materials on the surface can affect to change the wettability due to their surface energy. Three materials show different CHF enhancement, because metal oxide can increase the wettability. Metal oxide is more hydrophilic increased surface energy than pure metal. The CHF of aluminum oxide by the EEWL and aluminum oxide by two-step are influenced by the surface roughness and geometry. Figure 6-4 shows the characteristics of the surface-deposited nanoparticles after pool boiling. The topology of the heating surface after the experiments was affected by the deposited nanoparticles. The wire surfaces showed build-up and disordered structures. The nanoparticle deposition was caused by nucleate boiling. Changing the surface structure can improve the CHF by separating the liquid and vapor paths[145].
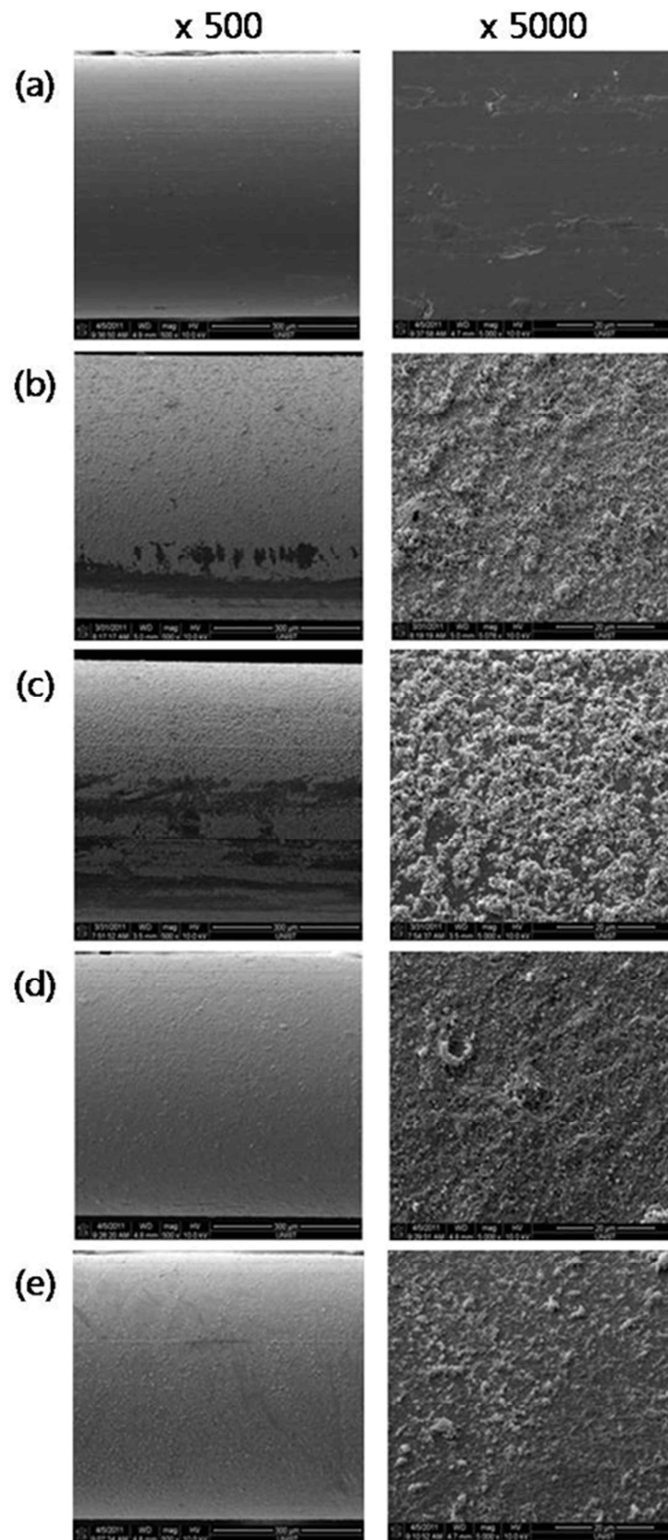
Figure 6-4. FE-SEM images of the heater surface after pool boiling

Figure 6-5 shows the surface deposited by copper oxide particles adding ammonia. The particles were formed to rocks with the edge structure. There was the bump on each face. The bumps were decreased and the size of rocks was increased with increasing volume concentration. CHF values of copper oxide nanofluids adding ammonia are enhanced with increasing volume concentration of particles. However, enhancement ration is low than copper oxide prepared in only water due to the effect of additives. Therefore, from now on, surface properties are investigated on nanofluids prepared without additives.
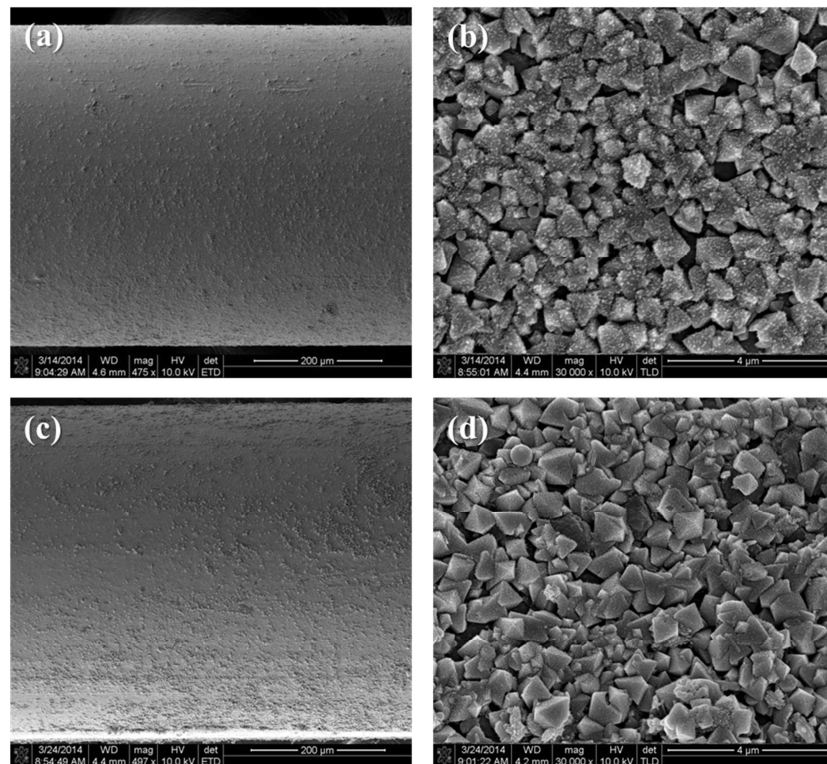
Figure 6-5. FE-SEM images of the heater surface deposited with copper oxide particles adding ammonia after pool boiling (a), (b) 0.001vol% and (c), (b) 0.005vol% in volume concentration
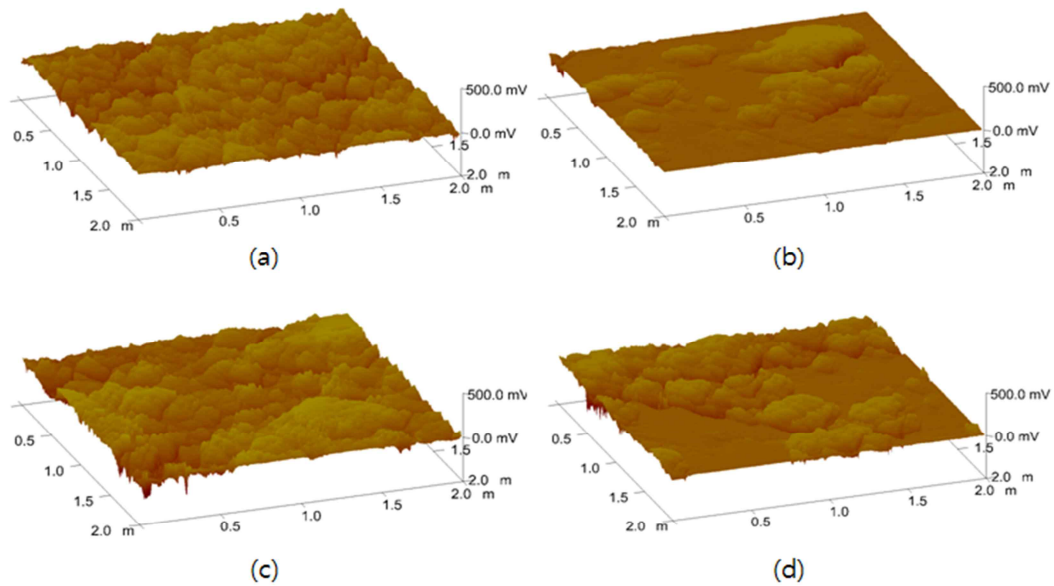
Figure 6-6. Profilometer images of the heater surface after boiling (a) silver, (b) copper oxide, (c) aluminum oxide nanofluids with 0.001vol% produced by EEWL, and (d) 0.001 vol% aluminum oxide nanofluids by two-step. The roughness values are 67.4, 44.4, 74.7, and 52.1 nm, respectively.

The roughness of the heater surface was analyzed using atomic force microscopy (AFM) (Multimode V, USA), as shown in Figure 6-6. For the EEWL aluminum oxide nanofluids, the deposited surface was relatively uniform compared with that of the two-step aluminum oxide nanofluids. In Figure 6-6 (b) and (d), part of surface of the pure wire was exposed by the agglomeration of nanoparticles during boiling. Several properties of surface are listed in Table 6-3.

Figure 6-7 shows the variation of height of deposited nanoparticles into AFM images. It is difficult to discuss about deep of pore due to exposed surface. The surface on the wire is composed with micro, nano, and micro/nanostructures because of the aggregation of nanoparticles. The micro/nanostructured surface showed the greatest increase in CHF compared with the micro or nanostructures by Kim et al. EEWL aluminum oxide surface has the most uniform hill distribution composited with nano- and micro/nanostructure compared to other surface and it can lead to delay the CHF.
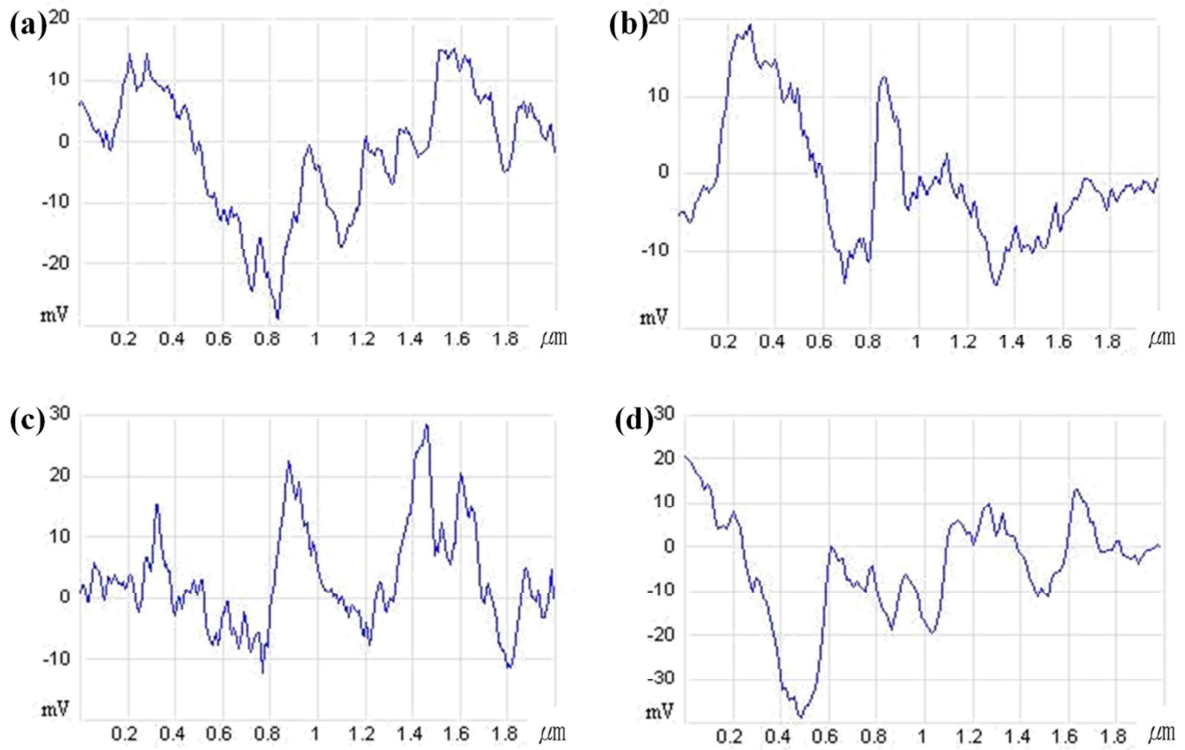
Figure 6-7. Height of deposited surfaces for (a) silver, (b) copper oxide, (c) aluminum oxide by EEWL, and (d) aluminum oxide by two-step

Table 6-3. Summary of surface properties from AFM, contact angle, and CHF

	Roughness (nm)	Average height (mV)	Projected area (μm^2)	Contact angle (°)	CHF (kW/m^2)
Water	-	-	-	70	948
Silver NFs	67.4	54	4	50	1498
Copper oxide NFs	44.4	33.7	4	36	1892
Aluminum oxide NFs by EEWL	74.7	44.1	4	16	2730
Aluminum oxide NFs by two-step	52.1	28.3	4	18	1976

Surface oxidation decreased the wettability, while the deposited nanoparticles on the heater surface significantly improved the wettability. To characterize surface wettability, the contact angle measurements is conducted as primary parameter. To measure static equilibrium contact angle of deposited surface with nanoparticles, a 1.5 μl-volume deionized water droplet was placed on the wire. The images of the droplet on the wire were taken by a charge-coupled device (CCD) camera. The angle between the solid-liquid boundary shows in Figure 6-8. The contact angles results are summarized in Table 6-3 and Figure 6-8. The wettability of deposited wires was significant improved compared to the bare wire. The contact angle on the bare wire was 70°, and the contact angles of deposited wires decreased with the larger CHF enhancement ratio. Silver nanofluids had the largest contact angle among the produced nanofluids. The aluminum oxide nanofluids by EEWL had the smallest contact angle. However, the difference between the two aluminum oxide nanofluids was quite small. According to the Wenzel model[146], the contact angle was affected by the surface tension, σ, the adhesion tension, γ_{SV}-γ_{SL}, and the roughness factor r (the ratio of the effective contact area to the smooth contact area).

$$\cos\theta = \frac{\gamma_{SV} - \gamma_{SL}}{\sigma} r \qquad (6.2)$$

There is probably not a great difference between nanofluids used in experiments on the surface tension, because very small concentration nanofluids were used. A porous surface with oxide nanoparticles increase the adhesion tension and decrease the contact angle. And the porous surface also increases the roughness factor, γ.
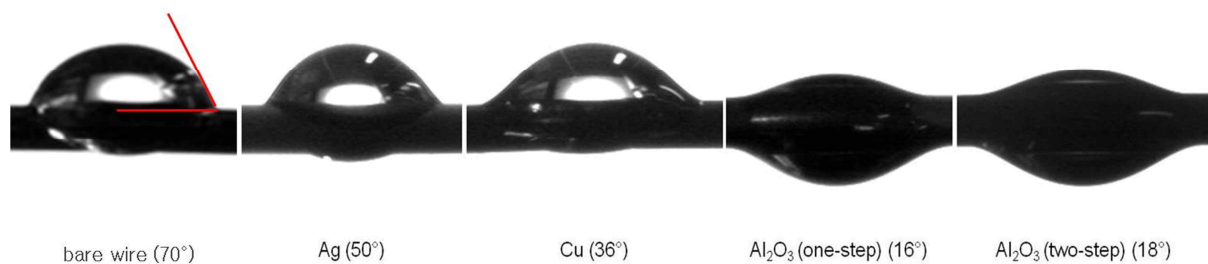
Figure 6-8. Contact angle on the wire surface after boiling

There is representable criterion whether increase or decrease rewetting upon bubble departure on the wire. It is the 'thermal activity', S:

$$S = \delta\sqrt{\rho_h c_h k_h}$$

(6.3)

Which, δ is the heater dimension and $\sqrt{\rho_h c_h k_h}$ is the heater material effusivity. The thermo-physical properties of the materials used in these experiments is reported in Table 6-4. Deposited surface increase the heater thermal activity and it can delay departure from nucleate boiling.

Table 6-4. Thermo-physical properties of materials

Material	ρ_h (kg/m^3)	c_h (J/kg K)	k_h (W/m K)	$\sqrt{\rho_h c_h k_h}$ (J/(m K s$^{1/2}$))
Silver	10,490	233	429	~32,000
Copper oxide	8,960	385	401	~37,000
Aluminum oxide	4,000	760	~40	~11,000

Kandlikar's CHF model is a well known prediction model that incorporates surface conditions. This model is based on the force balance on a bubble[100]. Thus, Kandlikar's model includes both bubble and contact angle parameters, according to the following equation:

$$q_{CHF}^{"} = K\rho_v h_{fg}\left[\frac{\sigma g(\rho_l - \rho_v)}{\rho_v^2}\right]^{1/4}$$

(6.4)

where $K = \left(\frac{1+cos\theta}{16}\right)\left[\frac{2}{\pi} + \frac{\pi}{4}(1+cos\theta)cos\varphi\right]^{1/2}$, ρ_v is the gas density, ρ_l is the liquid density, h_{fg} is the latent heat from the liquid state to the gas state, σ is the surface tension, and θ and φ are the receding contact angle and heater surface angle, respectively.

Computational results based on Kandlikar's model support CHF enhancement due to increased surface wettability. Surfaces with deposited nanoparticles exhibit increased wettability compared to bare surfaces, and the extent of the increase in wettability can be determined by measuring the

decrease in the contact angle of a liquid droplet on the surface. If the surface is rough, the solid-liquid contact area is effective. According to the definition of Wenzel [146], the contact angle is affected by a roughness factor, the surface tension, and the adhesion tension. If the surface is not smooth, the roughness factor is greater than unity. Thus, the porous buildup layer increases the effective contact area on the surface of the heating wire, which also contributes to a reduction in the contact angle on its surface.

Figure 6-9 compares the experimental and theoretical CHF results. The hot/dry spot theory of Kandlikar supports the idea of CHF enhancement due to increasing surface wettability. This result is in accord with the trend of the theoretical results. Although the wettability of the aluminum oxide nanofluids by EEWL was similar to that of the aluminum oxide by two-step, the CHF enhancement was much higher because the aluminum oxide nanofluids by EEWL was very pure and well dispersed. Therefore, the deposited layer on the wire after pool boiling was more uniform, which is a key contributor to the CHF enhancement.
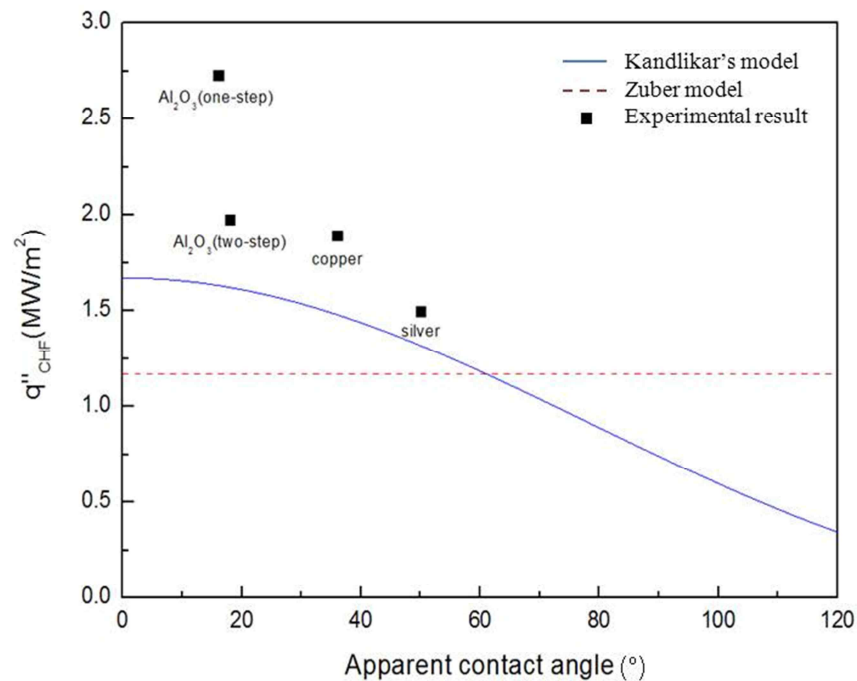
Figure 6-9. Comparison between experimental data and theoretical model

6.3.2. CHF enhancement using xGnPs and xGnPs oxide nanofluids

To investigate the effects of thermal conductivity and the concentration of nanofluids on the CHF enhancement, the thermal conductivity of xGnPs and xGnPs oxide were measured using a thermal conductivity measuring system (LAMBDA, Germany) according to particle concentrations ranging from 0.001 vol% to 0.5 vol%. The LAMBDA system used in this study was based on the in-stationary hot-wire method. The thermal conductivity of xGnPs/xGnPs oxide varied with increasing particle concentrations as shown in Figure 6-10 (a). The thermal conductivity was highest at 0.01 vol% for both nanofluids. The thermal conductivity decreased at volume concentrations > 0.01%.
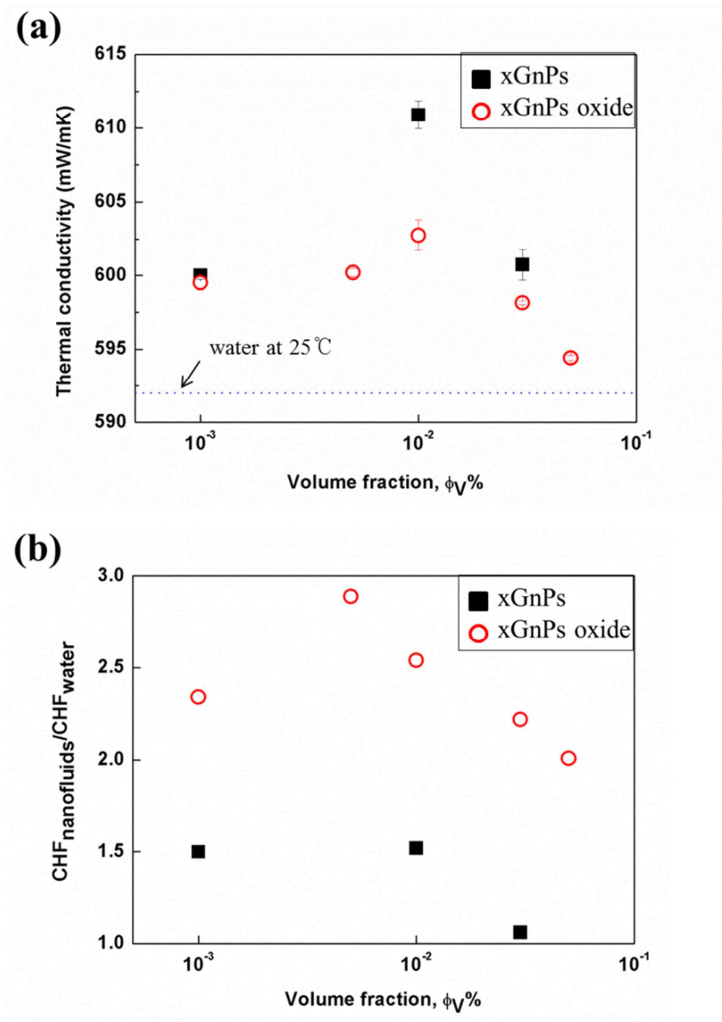
Figure 6-10. (a) Thermal conductivity and (b) CHF values of xGnPs and xGnPs oxide according to the different concentrations

The xGnPs and xGnPs oxide nanofluids exhibited significantly CHF enhancement. The xGnPs oxide nanofluids exhibited more enhanced CHF than xGnPs nanofluids. In the case of the xGnPs nanofluids with a minimum concentration of 0.001 vol%, the CHF was enhanced by only 50% compared with the CHF of pure water. However, in the case of the xGnPs oxide nanofluids with a concentration of 0.001 vol%, the CHF increased up to 130%. Therefore, the CHF enhancement was unaffected by the thermal conductivity of the nanofluids with varying concentrations, as shown in Figure 6-10. Rather, the type of material and the dispersion conditions of the nanofluids affected the CHF enhancement. Additionally, the xGnPs-oxides exhibited the most enhanced CHF, specifically 189% at a particle concentration of 0.005%, which is consistent with previous results. A decline in the CHF enhancement was observed when nanoparticle concentrations were greater than 0.01 vol%. Similar results were observed in pool boiling experiments with ZrO_2/water. Even in the Al_2O_3 [88] and CNT/water nanofluids [90], the CHF decreased with increasing particle concentration.

Following the pool boiling experiments, a buildup of nanoparticles was evident on the heating wire. Figure 6-11 shows the characteristics of the surface nanoparticles deposited on the heating surface. The topology of the surface following pool boiling changed due to deposited nanoparticles. The xGnPs oxide nanofluids exhibited a relatively uniform, thin layer of xGnPs oxide on the entire surface of the heating wire compared with the less-ordered buildup structure of the xGnPs nanofluids. Although the surface of the heating wire was partially and thinly covered by xGnPs particles in the presence of low concentration xGnPs nanofluids, the buildup created by the deposited nanoparticles became thicker. Deposition of nanoparticles on the heating wire surface led to enhanced CHF by changing the surface properties.
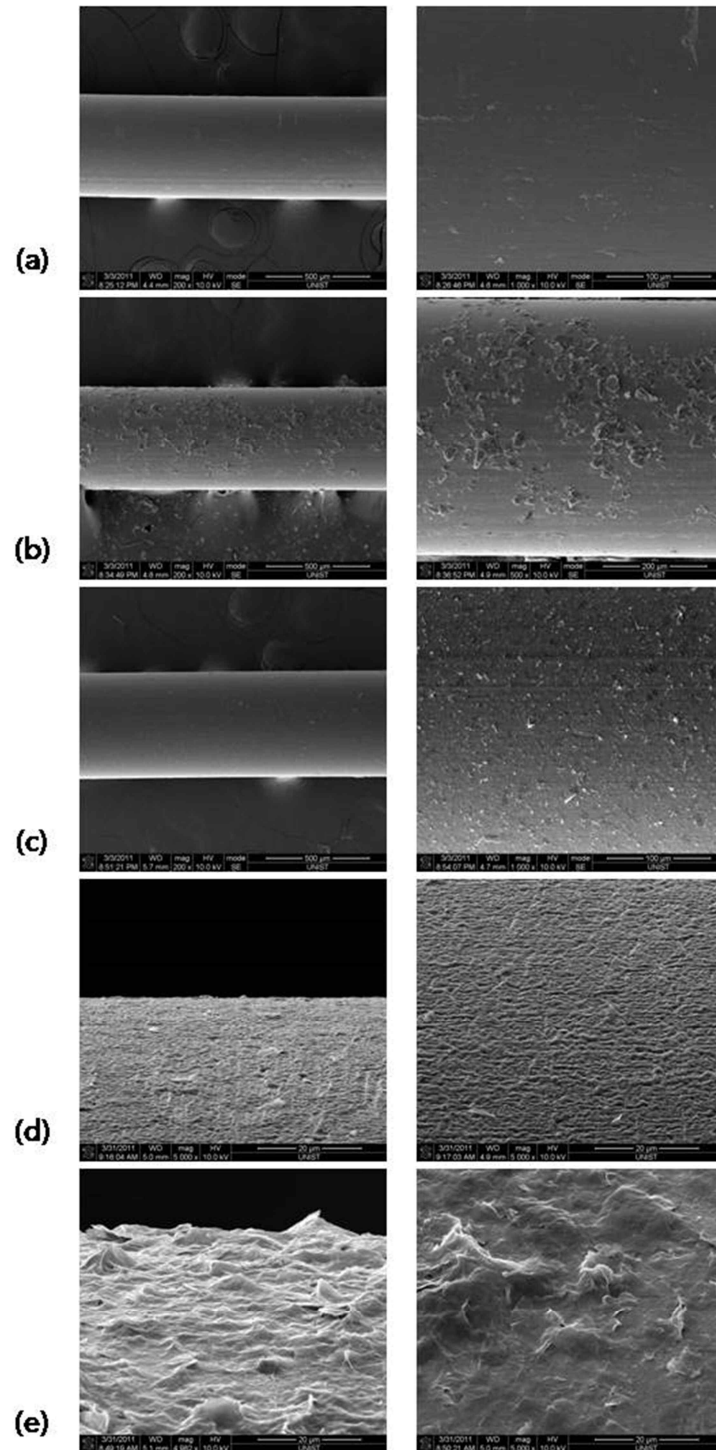
Figure 6-11. FE-SEM images of the heating wire surface boiled in (a) pure water, (b) 0.001 vol% xGnPs, (c) 0.001 vol% xGnPs-oxide, (d) 0.03 vol% xGnPs, and (e) 0.03 vol% xGnPs oxide nanofluids

Changing of heater surface lead to transition the nucleation site density, departure diameter and growing of bubble. Figure 6-12 presents the atomic force microscopy (AFM) images of the deposited surface after boiling for xGnPs and xGnPs oxide nanofluids. Heater surfaces with deposited xGnPs and xGnPs oxide particles exhibited greater roughness values than bare wire. Additionally, xGnPs oxide nanofluids led to a rougher surface than did xGnPs nanofluids, because of partially existent edges and folded areas in the oxide nanoparticles. However, in both cases, the resulting surfaces were not as rough as those reported in other studies [88] .
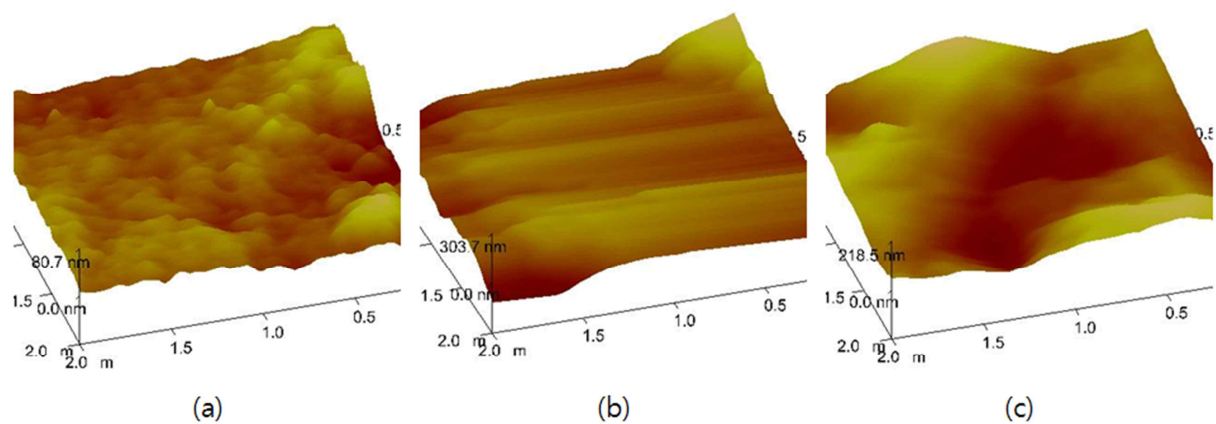
Figure 6-12. AFM images of the wire surface with deposited nanoparticles after boiling (a) bare wire in water, (b) 0.005 vol% xGnPs nanofluids, and c) 0.005 vol% xGnPs oxide nanofluids. The roughness values (Ra) were 8.34 nm, 28.8 nm, and 40.8 nm, respectively.

In general, the CHF enhancement could be explained by increasing the wettability of the surface. However, a small CHF enhancement of 0.03 vol% for the xGnPs oxide nanofluids tended not to match the computational results of Kandlikar's model, in which a lower contact angle contributed to the high CHF. In the case of xGnPs and xGnPs oxide nanofluids, the wettability effect for the CHF enhancement conflicted with the prediction model, as shown in Figure 6-13. Although the CHF enhancement of the 0.005 vol% xGnPs oxide nanofluids was 189%, its contact angle (72°) was close to that of the pure wire (70°). The 0.03 vol% xGnPs nanofluids displayed the greatest reduction in the contact angle, and the least CHF enhancement.

In cases of xGnPs and xGnPs oxide nanofluids, the heating wire surface was covered in a relatively flat manner compared to that observed for aluminum oxide nanofluids by EEWL (Figure 6-9). This result was attributed to the platelet shape of the nanoparticles, and to the hydrophobicity of the surface. Contrary to what is observed for hydrophilic surfaces, when the surface is hydrophobic, surface

roughness enhances the droplet contact angle.

To explain the disagreement with the model and experimental data, some researchers such as Liter and Kaviany[145] and Park et al.[87] tried to explain the reasons with reduction of Talyor unstable wavelength based on surface geometrical structures while Kim et al.[147] also reports the capillary wicking effect based on deposition structures. Therefore, the deviation from the Kandlikar's model seems to be reasonable for deposition characteristics.

In cases of high concentrations, above 0.005 vol%, nanoparticles were deposited on the electrodes in addition to the heating wire. Thus, the deposited xGnPs and xGnPs oxides impart thermal resistance, which prevents the dissipation of hot/dry spots. In other words, the thicker buildup layer of the deposited nanoparticles influences the connection region between the wire and the electrode.
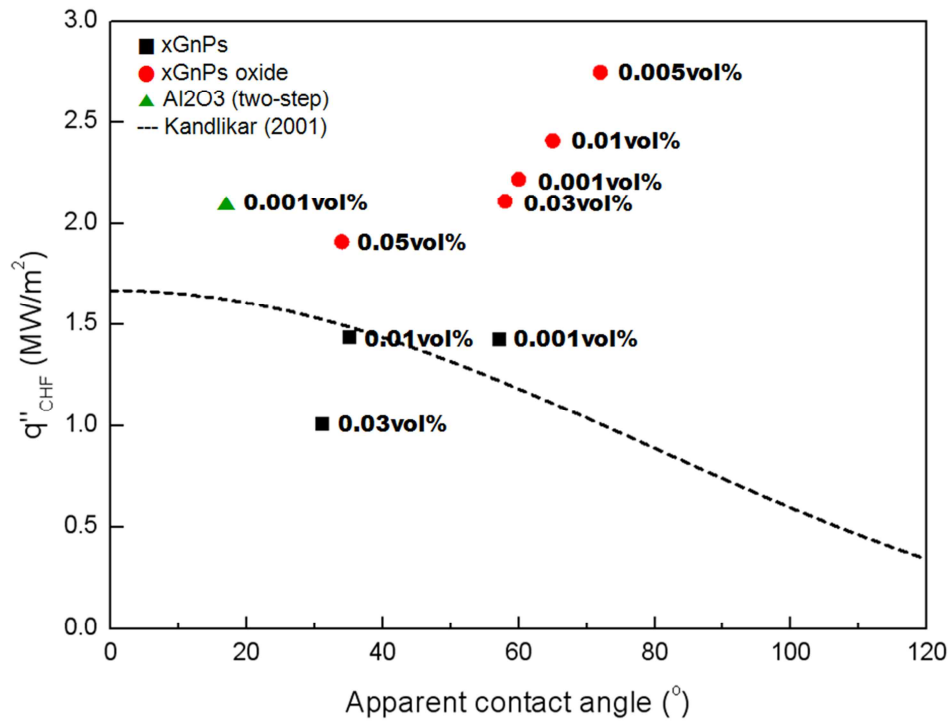
Figure 6-13. Comparison between experimental data and the prediction model of the pool boiling experiments.

6.4. Summary

We performed pool-boiling experiments using the silver, copper oxide, and aluminum nanofluids produced by EEWL. The silver, copper oxide and aluminum nanofluids caused significant CHF enhancement during boiling experiments: 187% at 0.001 vol% for aluminum oxide by EEWL, 58% at 0.001 vol% for silver, and 99% at 0.001 vol% for copper oxide nanofluids. Nanoparticles were deposited on the heater during pool boiling. Nanoparticles reduce the number of active nucleation sites while changing the surface roughness. The deposited surface has micro/nanostructure by aggregation of nanoparticles. Micro/nanostructure surface increases more wetting compared micro-, nano- and bare surface. And the constant height of protrusion is effective for increasing the wettability. Therefore, the deposited nanoparticles improved the wettability, as shown by the reduced contact angles of the surfaces after nanofluids boiling compared with surfaces after pure water boiling. Furthermore, metal oxide surface leads to increase the wettability by high surface energy. The higher wettability increased the CHF enhancement, according to both theoretical and experimental observations. The more dispersed nanofluids produced by EEWL exhibited greater CHF enhancement than nanofluids produced by the two-step method.

We also performed pool-boiling experiment using the nanofluids containing xGnPs and xGnPs oxide with different particle concentrations. The CHF of nanofluids when boiled over a NiCr wire increased with increasing concentrations of xGnPs/xGnPs oxide particles in the base fluid. The xGnPs oxide nanofluids dispersed with 0.005 vol% particles showing the largest CHF enhancement (189%). The surface morphology of the heated wire was analyzed using FE-SEM. Although the largest CHF enhancement was for the 0.005 vol% xGnPs oxide nanofluids, no reduction in the contact angle was evident. This trend conflicted with the prediction model. Thus, the excellent thermal conductivity of xGnPs and xGnPs oxide and their dispersion conditions affect such conflicting tendencies.

Chapter 7. Conclusions and Recommendations

7.1. Conclusions

This dissertation presents a technique to produce and optimize silver, copper oxide and aluminum oxide nanofluids for CHF enhancement. Synthesis of nanofluids by the EEWL process is as a function of the capacitance of the experimental circuit, wire properties, materials, and the kind of liquid. The effects of parameters on nanofluids are described in Chapter 3.

The following conclusions were obtained from Chapter 3.

- The size of nanoparticles decreases with increasing induced energy in the wire. The induced energy is proportional to the increasing of capacitance.

- The nanofluids can be produced to be spherical and highly dispersed nanoparticles by the EEWL process without any chemical additives. Most of the zeta potential of water-based nanofluids shows more than an absolute value of 30mV. The surface charge is related to boing of O^{2+} ions or H_2O molecules decomposing deionized water by explosion of the wire.

- The nanoparticles have a different oxygen portion with a kind of liquid. The composition ratio of water-based aluminum nanofluids is 3:2 for oxygen and aluminum. Copper oxide and silver nanofluids have little or no oxygen portion.

Spherical copper oxide nanofluids can be synthesized without additives. However, adding little additives can synthesize hierarchical copper oxide microsphere in shape. The following conclusions are obtained from Chapter 4.

- Water-based Cu/CuO/Cu$_2$O composited particles synthesized by EEWL are on the nanometer scale and are spherical in shape. Hierarchical copper oxide particles were synthesized under NaOH or NH$_3$·H$_2$O/deionized water solution.

- Leaf-like 2D copper oxide structures were synthesized by adding NaOH. When NH$_3$·H$_2$O was added, the copper oxide is flower-like and rods structure with increasing of additives amounts.

- The band gaps of hierarchical copper oxide particles are 1.85-4.7eV, red-shifted known as the

band gap of copper oxide (1.2eV of CuO and 2.2.eV of Cu_2O)

It is important to understand and optimize the effect of parameter on the characteristics of nanofluids. In this dissertation, Design of Experiments (DOE) and the analysis of VI oscillograms method have been used for the optimization of process parameters. Furthermore, the effect of various EEWL experimental parameters on thermophysical properties of nanofluids is described in Chapter 5.

The following conclusions can be drawn from Chapter 5.

- By optimizing control parameters, we decreased the particle size under fast explosion conditions and long plasma duration with low-viscosity media. A low viscosity decreased the particle size and dispersion stability due to a greater expansion in the plasma volume.

- From Response Optimization Technique, the experimental condition results in the size and zeta potential of 49nm and -39.1mV, respectively. For the repeated experiment, the average particle size was 118.9 nm, and the zeta potential was -42.5 mV.

- The explosion of the wire is related to the sublimation energy of material. The sublimation energy of aluminum is 33 J/mm^3. The induced energy in the wire should be greater than sublimation energy of metal. When the energy stored in the capacitor is similar, or a bit slower than the sublimation energy, the current through the wire continues to rise. When the energy stored in the capacitor is much smaller than the sublimation energy, the explosion will not happen.

- Enhancement of thermal conductivity and viscosity at 0.001vo% concentration of nanoparticles is not significant because of the extremely small concentration of the nanoparticles.

One of the most interesting characteristics of nanofluids is their enhancement of the critical heat flux (CHF). The common consensus of CHF enhancement mechanism is the morphology changing of the heater surface by nanoparticles. The research about the effect of nanoparticles on CHF enhancement is described in Chapter 6.

The following conclusions were obtained from Chapter 6.

- The silver, copper oxide and aluminum nanofluids caused significant CHF enhancement during the boiling experiments: 187% at 0.001 vol% for aluminum oxide by EEWL, 58% at 0.001 vol% for silver, and 99% at 0.001 vol% for copper oxide nanofluids. The xGnPs oxide nanofluids

dispersed with 0.005 vol% particles showing the largest CHF enhancement (189%).

- Micro/nanostructure surface increases wettability compared to micro-, nano- and bare surface. The deposited nanoparticles improve the wettability, especially on metal oxide surfaces.

- CHF of the silver, copper oxide and aluminum oxide nanofluids increases with the decreasing contact angle of the surface. It is in accord with the trend of the Kandlikar's CHF model. However, the results of xGnPs and xGnPs oxide

7.2. Recommendations

The current research provides the production of nanofluids and the optimization of the process parameters. The formation mechanism of the nanoparticles phase is still limited because it is impossible to analyze compositions in plasma. The recommendations for future work are described.

7.2.1. Synthesis of nanofluids by the EEWL process

The phase of particles is determined by condensation rate of the dissolved phase in the plasma. The synthesized nanoparticles in various base liquid were investigated in this study. The copper oxide nanoparticles have three compositions such as Cu, CuO and Cu_2O. Therefore, there is a need to develop adjusting techniques for compositions. Another aspect is that the measuring of the condensation rate can decrease the particle size and can synthesize in uniform size.

The measurement of the compositions of ions in the plasma is needed to investigate the chemical reaction between them. The concentrations of hydrogen and oxygen are important for determining the phase and dispersion stability of the nanoparticles.

The synthesis of the metallic and metallic oxide nanoparticles by the EEWL process has been pursued for several years. New attempts are needed. One of the most important advantages of the EEWL process is that all conductive materials are available in the synthesis of the nanofluids. Carbon materials have a superior electrical conductivity. The graphene/copper oxide composites are prepared by the EEWL process (Figure 7-1).
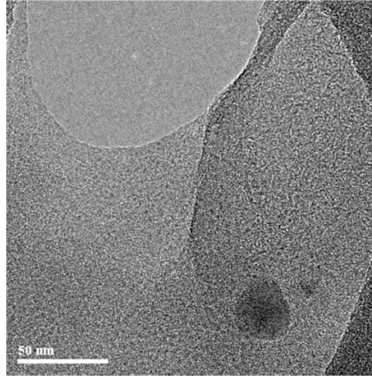
Figure 7-1. Graphene/Copper oxide synthesized by the EEWL process

7.2.2. Thermophysical properties of nanofluids

There are no significant enhancements of thermal conductivity and viscosity in this study. We measured of thermal conductivity and viscosity used nanofluids with very low concentration (~0.001 vol%). To investigate nanofluids synthesis by a one-step process, there is a need to increase the nanoparticles concentration. The thermal properties of nanofluids synthesized by an automated system can compare with nanofluids prepared by a two-step method with the same compositions.

7.2.3. Optimization of the EEWL process

In this study, optimization of the EEWL process was conducted by DOE and the measuring of voltage and current. We can calculate the parameters value influenced on particle size through the measuring of the voltage and the current oscillograms. The particle size can be optimized by numerical techniques using the parameter values.

7.2.4. Enhancement of CHF using nanofluids

CHF of copper oxide adding ammonia is enhanced less than copper oxide. If additives can be removed from the fluid after particle synthesis, the effect of particle shape on heat transfer can be investigated. The CHF performance may be affected by changing of the surface roughness with the concentration of nanoparticles.

8. REFERNCES

[1]   S. Kim and H.-J. Kim, "Anti-bacterial performance of colloidal silver-treated laminate wood flooring," *International Biodeterioration & Biodegradation,* vol. 57, pp. 155-162, 2006.

[2]   O. P. Siwach and P. Sen, "Fluorescence properties of Fe nanoparticles prepared by electro-explosion of wires," *Materials Science and Engineering: B,* vol. 149, pp. 99-104, 2008.

[3]   D.-C. Tien, K.-H. Tseng, C.-Y. Liao, and T.-T. Tsung, "Colloidal silver fabrication using the spark discharge system and its antimicrobial effect on Staphylococcus aureus," *Medical Engineering & Physics,* vol. 30, pp. 948-952, 2008.

[4]   D. P. Kulkarni, R. S. Vajjha, D. K. Das, and D. Oliva, "Application of aluminum oxide nanofluids in diesel electric generator as jacket water coolant," *Applied Thermal Engineering,* vol. 28, pp. 1774-1781, 2008.

[5]   M. Abu-Zaid, "Performance of single cylinder, direct injection Diesel engine using water fuel emulsions," *Energy Conversion and Management,* vol. 45, pp. 697-705, 2004.

[6]   N. Güngör, S. Işçi, E. Günister, W. Miśta, H. Teterycz, and R. Klimkiewicz, "Characterization of sepiolite as a support of silver catalyst in soot combustion," *Applied Clay Science,* vol. 32, pp. 291-296, 2006.

[7]   J. Buongiorno, D. C. Venerus, N. Prabhat, T. McKrell, J. Townsend, R. Christianson, Y. V. Tolmachev, P. Keblinski, L.-w. Hu, J. L. Alvarado, I. C. Bang, S. W. Bishnoi, M. Bonetti, F. Botz, A. Cecere, Y. Chang, G. Chen, H. Chen, S. J. Chung, M. K. Chyu, S. K. Das, R. Di Paola, Y. Ding, F. Dubois, G. Dzido, J. Eapen, W. Escher, D. Funfschilling, Q. Galand, J. Gao, P. E. Gharagozloo, K. E. Goodson, J. G. Gutierrez, H. Hong, M. Horton, K. S. Hwang, C. S. Iorio, S. P. Jang, A. B. Jarzebski, Y. Jiang, L. Jin, S. Kabelac, A. Kamath, M. A. Kedzierski, L. G. Kieng, C. Kim, J.-H. Kim, S. Kim, S. H. Lee, K. C. Leong, I. Manna, B. Michel, R. Ni, H. E. Patel, J. Philip, D. Poulikakos, C. Reynaud, R. Savino, P. K. Singh, P. Song, T. Sundararajan, E. Timofeeva, T. Tritcak, A. N. Turanov, S. Van Vaerenbergh, D. Wen, S. Witharana, C. Yang, W.-H. Yeh, X.-Z. Zhao, and S.-Q. Zhou, "A benchmark study on the thermal conductivity of nanofluids," *Journal of Applied Physics,* vol. 106, pp. -, 2009.

[8]   E.Nairne, "Electrical experiments by Nr.Edward Nairne," *Philos.Trans.R.Soc.London,* pp. 79-89, 1774.

[9]   R.Abrams, "Production and analysis of radioactive aerosols," *ch3629,* 1946.

[10]   Y. Kotov, "Electric Explosion of Wires as a Method for Preparation of Nanopowders," *Journal of Nanoparticle Research,* vol. 5, pp. 539-550, 2003/12/01 2003.

[11]   R. Sarathi, K. Murai, R. Kobayashi, H. Suematsu, W. Jiang, and K. Yatsui, "Production and

Characterization of Nano Copper Powder Using Pulsed Power Technique," *Synthesis and Reactivity in Inorganic, Metal-Organic, and Nano-Metal Chemistry (formerly Synthesis and Reactivity in Inorganic and Metal-Organic Chemistry),* vol. 36, pp. 127-130, 2006.

[12]   T. Sindhu, S. Chakravarthi, R. Jayaganthan, and R. Sarathi, "Studies on Generation and Characterization of Nano Aluminium Nitride Using Wire Explosion Technique," *Synthesis and Reactivity in Inorganic, Metal-Organic, and Nano-Metal Chemistry (formerly Synthesis and Reactivity in Inorganic and Metal-Organic Chemistry),* vol. 36, pp. 53-58, 2006.

[13]   T. K. Sindhu, R. Sarathi, and S. R. Chakravarthy, "Generation and characterization of nano aluminium powder obtained through wire explosion process," *Bulletin of Materials Science,* vol. 30, pp. 187-195, 2007.

[14]   S. I. Tkachenko, V. S. Vorob'ev, and S. P. Malyshenko, "The nucleation mechanism of wire explosion," *Journal of Physics D: Applied Physics,* vol. 37, p. 495, 2004.

[15]   A. G. W. a. N. F.W., *Use of the "action integral" in exploding wire studies*, New York:Plenum ed. vol. 1, 1959.

[16]   M. Keiichi, T. Yoshinori, S. Hisayuki, J. Weihua, Y. Kiyoshi, and N. Koichi, "Particle Size Controllability of Ambient Gas Species for Copper Nanoparticles Prepared by Pulsed Wire Discharge," *Japanese Journal of Applied Physics,* vol. 47, p. 3726, 2008.

[17]   S. Tsuneo, K. Komson, J. Weihua, and Y. Kiyoshi, "Nanosize Al 2 O 3 Powder Production by Pulsed Wire Discharge," *Japanese Journal of Applied Physics,* vol. 40, p. 1073, 2001.

[18]   T. Yoshinori, S. Tsuneo, N. Tadachika, S. Hisayuki, J. Weihua, and N. Koichi, "Synthesis of TiO 2 Nanosized Powder by Pulsed Wire Discharge," *Japanese Journal of Applied Physics,* vol. 47, p. 760, 2008.

[19]   S. Channarong, K. Yoshiaki, S. Tsuneo, J. Weihua, and Y. Kiyoshi, "Synthesis of Nanosize Powders of Aluminum Nitride by Pulsed Wire Discharge," *Japanese Journal of Applied Physics,* vol. 40, p. 1070, 2001.

[20]   K. Hokamoto, N. Wada, R. Tomoshige, S. Kai, and Y. Ujimoto, "Synthesis of TiN powders through electrical wire explosion in liquid nitrogen," *Journal of Alloys and Compounds,* vol. 485, pp. 573-576, 2009.

[21]   K. Y. A. a. Y. N.A., "Investigation of particles preparing by electrical explosion of wires," *J.Sov.Phys.Chem.Mater.Treatment B,* vol. 4, pp. 24-29, 1978.

[22]   V. V. Valevich and V. S. Sedoi, "Producing highly disperse powder in fast electrical explosion," *Russian Physics Journal,* vol. 41, pp. 569-574, 1998/06/01 1998.

[23]   V. S. Sedoi and V. V. Valevich, "Production of highly dispersed metal powders by electrical explosion in reduced-pressure nitrogen," *Technical Physics Letters,* vol. 25, pp. 584-585,

1999/07/01 1999.

[24]   K. V. P. Iazunov G.P., Kornienko L.A., Kosik N.A., Mitin R.V and Shevstusev A.P., "Some properties of fine powders produced by electrical explosion of conductors in a high pressure gas," *J.Sov.Questions Atom.Mater.Sci.Tech.,* vol. 1, pp. 21-24, 1978.

[25]   C. Chuhyun, K. Murai, T. Suzuki, H. Suematsu, J. Weihua, and K. Yatsui, "Enhancement of energy deposition in pulsed wire discharge for synthesis of nanosized powders," *Plasma Science, IEEE Transactions on,* vol. 32, pp. 2062-2067, 2004.

[26]   Y. S. Lee, B. Bora, S. L. Yap, and C. S. Wong, "Effect of ambient air pressure on synthesis of copper and copper oxide nanoparticles by wire explosion process," *Current Applied Physics,* vol. 12, pp. 199-203, 2012.

[27]   T. K. Sindhu, R. Sarathi, and S. R. Chakravarthy, "Understanding nanoparticle formation by a wire explosion process through experimental and modelling studies," *Nanotechnology,* vol. 19, p. 025703, 2008.

[28]   B. Bora, C. S. Wong, H. Bhuyan, Y. S. Lee, S. L. Yap, and M. Favre, "Understanding the mechanism of nanoparticle formation in wire explosion process," *Journal of Quantitative Spectroscopy and Radiative Transfer,* vol. 117, pp. 1-6, 2013.

[29]   J. K. Antony, N. J. Vasa, S. R. Chakravarthy, and R. Sarathi, "Understanding the mechanism of nano-aluminum particle formation by wire explosion process using optical emission technique," *Journal of Quantitative Spectroscopy and Radiative Transfer,* vol. 111, pp. 2509-2516, 2010.

[30]   B. Debalina, M. Kamaraj, B. S. Murthy, S. R. Chakravarthi, and R. Sarathi, "Generation and characterization of nano-tungsten carbide particles by wire explosion process," *Journal of Alloys and Compounds,* vol. 496, pp. 122-128, 2010.

[31]   K. Song, W. Kim, C.-Y. Suh, D. Shin, K.-S. Ko, and K. Ha, "Magnetic iron oxide nanoparticles prepared by electrical wire explosion for arsenic removal," *Powder Technology,* vol. 246, pp. 572-574, 2013.

[32]   N. Wada, K. Akiyoshi, K. Morita, and K. Hokamoto, "Reaction synthesis of several titanium oxides through electrical wire explosion in air and in water," *Ceramics International,* vol. 39, pp. 7927-7933, 2013.

[33]   A. Grinenko, V. Gurovich, A. Saypin, S. Efimov, Y. Krasik, and V. Oreshkin, "Strongly coupled copper plasma generated by underwater electrical wire explosion," *Physical Review E,* vol. 72, 2005.

[34]   C. Cho, Y. W. Choi, C. Kang, and G. W. Lee, "Effects of the medium on synthesis of nanopowders by wire explosion process," *Applied Physics Letters,* vol. 91, pp. -, 2007.

[35]   E. K. Ya, A. Fedotov, D. Sheftman, S. Efimov, A. Sayapin, V. T. Gurovich, D. Veksler, G. Bazalitski, S. Gleizer, A. Grinenko, and V. I. Oreshkin, "Underwater electrical wire explosion," *Plasma Sources Science and Technology,* vol. 19, p. 034020, 2010.

[36]   F. G. Karioris and B. R. Fish, "An exploding wire aerosol generator," *Journal of Colloid Science,* vol. 17, pp. 155-161, 1962.

[37]   R. F. Phalen, "Evaluation of an exploded-wire aerosol generator for use in inhalation studies," *Journal of Aerosol Science,* vol. 3, pp. 395-406, 1972.

[38]   R. Sugunakar Reddy, M. Kamaraj, U. Kamachi Mudali, S. R. Chakravarthy, and R. Sarathi, "Generation and characterization of zirconium nitride nanoparticles by wire explosion process," *Ceramics International,* vol. 38, pp. 5507-5512, 2012.

[39]   G. Goloverda, B. Jackson, C. Kidd, and V. Kolesnichenko, "Synthesis of ultrasmall magnetic iron oxide nanoparticles and study of their colloid and surface chemistry," *Journal of Magnetism and Magnetic Materials,* vol. 321, pp. 1372-1376, 2009.

[40]   I. V. Beketov, A. P. Safronov, A. V. Bagazeev, A. Larrañaga, G. V. Kurlyandskaya, and A. I. Medvedev, "In situ modification of Fe and Ni magnetic nanopowders produced by the electrical explosion of wire," *Journal of Alloys and Compounds,* vol. 586, Supplement 1, pp. S483-S488, 2014.

[41]   D.-W. Joh, T.-K. Jung, H.-S. Lee, and D.-H. Kim, "Synthesis of Nanoparticles Using Electrical Explosion of Ni Wire in Pt Solution," *Journal of Nanoscience and Nanotechnology,* vol. 13, pp. 6092-6094, 2013.

[42]   Y.-S. Kwon, A. A. Gromov, and J. I. Strokova, "Passivation of the surface of aluminum nanopowders by protective coatings of the different chemical origin," *Applied Surface Science,* vol. 253, pp. 5558-5564, 2007.

[43]   W. J. a. K. yatsui, "Pulsed Wire Discharge for Nanosize Powder Synthesis," *IEEE Transactions on Plasma Science,* vol. 26, pp. 1498-1501, 1998.

[44]   C. H. Cho, S. H. Park, Y. W. Choi, and B. G. Kim, "Production of nanopowders by wire explosion in liquid media," *Surface and Coatings Technology,* vol. 201, pp. 4847-4849, 2007.

[45]   J. A. Eastman, U. S. Choi, S. Li, L. J. Thompson, and S. Lee, "Enhanced Thermal Conductivity through the Development of Nanofluids," *MRS Online Proceedings Library,* vol. 457, pp. null-null, 1996.

[46]   X. Wang, Xu, XianfanChoi, Stephen U S, "Thermal conductivity of nanoparticle-fluid mixture " *Journal of Thermophysics and Heat Transfer,* vol. 13, pp. 474-480, 1999.

[47]   H. Xie, J. Wang, T. Xi, Y. Liu, F. Ai, and Q. Wu, "Thermal conductivity enhancement of suspensions containing nanosized alumina particles," *Journal of Applied Physics,* vol. 91, pp.

4568-4572, 2002.

[48]   R. Prasher, D. Song, J. Wang, and P. Phelan, "Measurements of nanofluid viscosity and its implications for thermal applications," *Applied Physics Letters,* vol. 89, pp. -, 2006.

[49]   P. K. Namburu, D. P. Kulkarni, A. Dandekar, and D. K. Das, "Experimental investigation of viscosity and specific heat of silicon dioxide nanofluids," *Micro and Nano Letters,* vol. 2, pp. 67-71, 2007.

[50]   L. Chen, H. Xie, W. Yu, and Y. Li, "Rheological Behaviors of Nanofluids Containing Multi-Walled Carbon Nanotube," *Journal of Dispersion Science and Technology,* vol. 32, pp. 550-554, 2011/03/23 2011.

[51]   M. Kole and T. K. Dey, "Viscosity of alumina nanoparticles dispersed in car engine coolant," *Experimental Thermal and Fluid Science,* vol. 34, pp. 677-683, 2010.

[52]   H. Masuda, A. Ebata, K. Teramae, and N. Hishinuma, "Alteration of Thermal Conductivity and Viscosity of Liquid by Dispersing Ultra-Fine Particles Dispersion of Al_2O_3, SiO_2 and TiO_2 Ultra-Fine Particles," *Netsu Bussei,* vol. 7, pp. 227-233, 1993.

[53]   S. Lee, S. U. S. Choi, S. Li, and J. A. Eastman, "Measuring Thermal Conductivity of Fluids Containing Oxide Nanoparticles," *Journal of Heat Transfer,* vol. 121, pp. 280-289, 1999.

[54]   M.-S. Liu, M. C.-C. Lin, C. Y. Tsai, and C.-C. Wang, "Enhancement of thermal conductivity with Cu for nanofluids using chemical reduction method," *International Journal of Heat and Mass Transfer,* vol. 49, pp. 3028-3033, 2006.

[55]   X. Wang, X. Xu, and S. U. S. Choi, "Thermal conductivity of nanoparticle-fluid mixture," *Journal of thermophysics and heat transfer,* vol. 13, pp. 474-480, 1999.

[56]   C. H. Li and G. P. Peterson, "Experimental investigation of temperature and volume fraction variations on the effective thermal conductivity of nanoparticle suspensions (nanofluids)," *Journal of Applied Physics,* vol. 99, pp. -, 2006.

[57]   S. K. Das, N. Putra, P. Thiesen, and W. Roetzel, "Temperature Dependence of Thermal Conductivity Enhancement for Nanofluids," *Journal of Heat Transfer,* vol. 125, pp. 567-574, 2003.

[58]   W. J. Tseng and K. C. Lin, "Rheology and colloidal structure of aqueous TiO2 nanoparticle suspensions," *Materials Science and Engineering A,* vol. 355, pp. 186-192, 2003.

[59]   C. T. Nguyen, F. Desgranges, G. Roy, N. Galanis, T. Maré, S. Boucher, and H. Angue Mintsa, "Temperature and particle-size dependent viscosity data for water-based nanofluids - Hysteresis phenomenon," *International Journal of Heat and Fluid Flow,* vol. 28, pp. 1492-1506, 2007.

[60]   S. W. Lee, S. D. Park, S. Kang, I. C. Bang, and J. H. Kim, "Investigation of viscosity and thermal conductivity of SiC nanofluids for heat transfer applications," *International Journal of Heat and Mass Transfer,* vol. 54, pp. 433-438, 2011.

[61]   H. Chen, Y. Ding, Y. He, and C. Tan, "Rheological behaviour of ethylene glycol based titania nanofluids," *Chemical Physics Letters,* vol. 444, pp. 333-337, 2007.

[62]   S. M. S. Murshed, K. C. Leong, and C. Yang, "Investigations of thermal conductivity and viscosity of nanofluids," *International Journal of Thermal Sciences,* vol. 47, pp. 560-568, 2008.

[63]   K. B. Anoop, S. Kabelac, T. Sundararajan, and S. K. Das, "Rheological and flow characteristics of nanofluids: Influence of electroviscous effects and particle agglomeration," *Journal of Applied Physics,* vol. 106, pp. -, 2009.

[64]   Y. He, Y. Jin, H. Chen, Y. Ding, D. Cang, and H. Lu, "Heat transfer and flow behaviour of aqueous suspensions of TiO2 nanoparticles (nanofluids) flowing upward through a vertical pipe," *International Journal of Heat and Mass Transfer,* vol. 50, pp. 2272-2281, 2007.

[65]   Y. Yang, Z. G. Zhang, E. A. Grulke, W. B. Anderson, and G. Wu, "Heat transfer properties of nanoparticle-in-fluid dispersions (nanofluids) in laminar flow," *International Journal of Heat and Mass Transfer,* vol. 48, pp. 1107-1116, 2005.

[66]   S. M. You, J. H. Kim, and K. H. Kim, "Effect of nanoparticles on critical heat flux of water in pool boiling heat transfer," *Applied Physics Letters,* vol. 83, pp. 3374-3376, 2003.

[67]   M. H. Shi, M. Q. Shuai, Z. Q. Chen, Q. Li, and Y. Xuan, "Study on Pool Boiling Heat Transfer of Nano-Particle Suspensions on Plate Surface," vol. 14, pp. 223-231, 2007-11-07 2007.

[68]   D. Wen and Y. Ding, "Experimental investigation into the pool boiling heat transfer of aqueous based γ-alumina nanofluids," *Journal of Nanoparticle Research,* vol. 7, pp. 265-274, 2005/06/01 2005.

[69]   B. H.Truong, "Determination of pool boiling critical heat flux enhancement in nanofluids," MIT, 2007.

[70]   H. Kim and M. Kim, "Experimental study of the characteristics and mechanism of pool boiling CHF enhancement using nanofluids," *Heat and Mass Transfer,* vol. 45, pp. 991-998, 2009/05/01 2009.

[71]   Z.-h. Liu, J.-g. Xiong, and R. Bao, "Boiling heat transfer characteristics of nanofluids in a flat heat pipe evaporator with micro-grooved heating surface," *International Journal of Multiphase Flow,* vol. 33, pp. 1284-1295, 2007.

[72]   B. Jo, P. S. Jeon, J. Yoo, and H. J. Kim, "Wide range parametric study for the pool boiling of

nano-fluids with a circular plate heater," *Journal of Visualization,* vol. 12, pp. 37-46, 2009/03/01 2009.

[73]   J. H. Lienhard and V. K. Dhir, "Hydrodynamic Prediction of Peak Pool-boiling Heat Fluxes from Finite Bodies," *Journal of Heat Transfer,* vol. 95, pp. 152-158, 1973.

[74]   Z.-H. Liu, X.-F. Yang, and J.-G. Xiong, "Boiling characteristics of carbon nanotube suspensions under sub-atmospheric pressures," *International Journal of Thermal Sciences,* vol. 49, pp. 1156-1164, 2010.

[75]   H. J. Van Ouwerkerk, "Burnout in pool boiling the stability of boiling mechanisms," *International Journal of Heat and Mass Transfer,* vol. 15, pp. 25-34, 1972.

[76]   D. Milanova and R. Kumar, "Role of ions in pool boiling heat transfer of pure and silica nanofluids," *Applied Physics Letters,* vol. 87, pp. -, 2005.

[77]   D. Milanova and R. Kumar, "Heat Transfer Behavior of Silica Nanoparticles in Pool Boiling Experiment," *Journal of Heat Transfer,* vol. 130, pp. 042401-042401, 2008.

[78]   S.Witharana, "Boiling of refrigerants on enhanced surfaces and boiling of nanofluids," Ph.D, The Royal Institute of Technology, 2003.

[79]   P. Vassallo, R. Kumar, and S. D'Amico, "Pool boiling heat transfer experiments in silica–water nano-fluids," *International Journal of Heat and Mass Transfer,* vol. 47, pp. 407-411, 2004.

[80]   N. D. J.P. Tu, T.Theofanous, "An experimental study of nanofluid boiling heat transfer," in *6th International Symposium on Heat Transfer*, Beijing, China, 2004.

[81]   I. C. Bang and S. Heung Chang, "Boiling heat transfer performance and phenomena of Al2O3–water nano-fluids from a plain surface in a pool," *International Journal of Heat and Mass Transfer,* vol. 48, pp. 2407-2419, 2005.

[82]   J. S. Coursey and J. Kim, "Nanofluid boiling: The effect of surface wettability," *International Journal of Heat and Fluid Flow,* vol. 29, pp. 1577-1585, 2008.

[83]   A. Hee Seok, V. Sathyamurthi, and D. Banerjee, "Pool Boiling Experiments on a Nano-Structured Surface," *Components and Packaging Technologies, IEEE Transactions on,* vol. 32, pp. 156-165, 2009.

[84]   H. Kim, H. S. Ahn, and M. H. Kim, "On the Mechanism of Pool Boiling Critical Heat Flux Enhancement in Nanofluids," *Journal of Heat Transfer,* vol. 132, pp. 061501-061501, 2010.

[85]   S. M. Kwark, G. Moreno, R. Kumar, H. Moon, and S. M. You, "Nanocoating characterization in pool boiling heat transfer of pure water," *International Journal of Heat and Mass Transfer,* vol. 53, pp. 4579-4587, 2010.

[86]   S. M. Kwark, M. Amaya, R. Kumar, G. Moreno, and S. M. You, "Effects of pressure,

orientation, and heater size on pool boiling of water with nanocoated heaters," *International Journal of Heat and Mass Transfer,* vol. 53, pp. 5199-5208, 2010.

[87] S. D. Park, S. Won Lee, S. Kang, I. C. Bang, J. H. Kim, H. S. Shin, D. W. Lee, and D. Won Lee, "Effects of nanofluids containing graphene/graphene-oxide nanosheets on critical heat flux," *Applied Physics Letters,* vol. 97, p. 023103, 2010.

[88] S. J. Kim, I. C. Bang, J. Buongiorno, and L. W. Hu, "Surface wettability change during pool boiling of nanofluids and its effect on critical heat flux," *International Journal of Heat and Mass Transfer,* vol. 50, pp. 4105-4116, 2007.

[89] H. Kim, J. Kim, and M. Kim, "Effect of nanoparticles on CHF enhancement in pool boiling of nano-fluids," *International Journal of Heat and Mass Transfer,* vol. 49, pp. 5070-5074, 2006.

[90] R. Kathiravan, R. Kumar, A. Gupta, R. Chandra, and P. K. Jain, "Pool boiling characteristics of multiwalled carbon nanotube (CNT) based nanofluids over a flat plate heater," *International Journal of Heat and Mass Transfer,* vol. 54, pp. 1289-1296, 2011.

[91] H. Kim, "Enhancement of critical heat flux in nucleate boiling of nanofluids: a state-of-art review," *Nanoscale Research Letters,* vol. 6, pp. 1-18, 2011/06/09 2011.

[92] I. C. Bang and S. Heung Chang, "Boiling heat transfer performance and phenomena of Al2O3-water nano-fluids from a plain surface in a pool," *International Journal of Heat and Mass Transfer,* vol. 48, pp. 2407-2419, 2005.

[93] H. D. Kim, J. Kim, and M. H. Kim, "Experimental studies on CHF characteristics of nano-fluids at pool boiling," *International Journal of Multiphase Flow,* vol. 33, pp. 691-706, 2007.

[94] Z.-H. Liu and Y.-H. Qiu, "Boiling heat transfer characteristics of nanofluids jet impingement on a plate surface," *Heat and Mass Transfer,* vol. 43, pp. 699-706, 2007.

[95] S. Das, G. Prakash Narayan, and A. Baby, "Survey on nucleate pool boiling of nanofluids: the effect of particle size relative to roughness," *Journal of Nanoparticle Research,* vol. 10, pp. 1099-1108, 2008.

[96] G. P. Narayan, K. B. Anoop, and S. K. Das, "Mechanism of enhancement/deterioration of boiling heat transfer using stable nanoparticle suspensions over vertical tubes," *Journal of Applied Physics,* vol. 102, pp. 074317-7, 2007.

[97] S. M. Kwark, R. Kumar, G. Moreno, J. Yoo, and S. M. You, "Pool boiling characteristics of low concentration nanofluids," *International Journal of Heat and Mass Transfer,* vol. 53, pp. 972-981, 2010.

[98] M. N. Golubovic, H. D. Madhawa Hettiarachchi, W. M. Worek, and W. J. Minkowycz, "Nanofluids and critical heat flux, experimental and analytical study," *Applied Thermal Engineering,* vol. 29, pp. 1281-1288, 2009.

[99] K. Sefiane, D. Benielli, and A. Steinchen, "A new mechanism for pool boiling crisis, recoil instability and contact angle influence," *Colloids and Surfaces A: Physicochemical and Engineering Aspects,* vol. 142, pp. 361-373, 1998.

[100] S. G. Kandlikar, "A Theoretical Model to Predict Pool Boiling CHF Incorporating Effects of Contact Angle and Orientation," *Journal of Heat Transfer,* vol. 123, p. 1071, 2001.

[101] T. G. Theofanous, T. N. Dinh, J. P. Tu, and A. T. Dinh, "The boiling crisis phenomenon: Part II: dryout dynamics and burnout," *Experimental Thermal and Fluid Science,* vol. 26, pp. 793-810, 2002.

[102] Z. N, "Hydrodynamic aspects of heat transfer," UCLA, 1959.

[103] H. D. Kim and M. H. Kim, "Effect of nanoparticle deposition on capillary wicking that influences the critical heat flux in nanofluids," *Applied Physics Letters,* vol. 91, pp. -, 2007.

[104] L. Stobiński and R. Duś, "Atomic hydrogen adsorption on thin gold films," *Surface Science,* vol. 269–270, pp. 383-388, 1992.

[105] L. Stobiński and R. Duś, "Atomic hydrogen solubility in thin gold films and its influence on hydrogen thermal desorption spectra from the surface," *Applied Surface Science,* vol. 62, pp. 77-82, 1992.

[106] L. Stobiński, R. Nowakowski, and R. Duś, "Atomic hydrogen adsorption on thin discontinuous and continuous gold films—similarities and differences," *Vacuum,* vol. 48, pp. 203-207, 1997.

[107] N. Saliba, D. H. Parker, and B. E. Koel, "Adsorption of oxygen on Au(111) by exposure to ozone," *Surface Science,* vol. 410, pp. 270-282, 1998.

[108] A. Franceschetti, S. J. Pennycook, and S. T. Pantelides, "Oxygen chemisorption on Au nanoparticles," *Chemical Physics Letters,* vol. 374, pp. 471-475, 2003.

[109] S. D. Puckett, J. A. Heuser, J. D. Keith, W. U. Spendel, and G. E. Pacey, "Interaction of ozone with gold nanoparticles," *Talanta,* vol. 66, pp. 1242-1246, 2005.

[110] A. E. Rakhshani, "Preparation, characteristics and photovoltaic properties of cuprous oxide—a review," *Solid-State Electronics,* vol. 29, pp. 7-17, 1986.

[111] C. Zhang, J. Chen, Y. Zeng, X. Rui, J. Zhu, W. Zhang, C. Xu, T. M. Lim, H. H. Hng, and Q. Yan, "A facile approach toward transition metal oxide hierarchical structures and their lithium storage properties," *Nanoscale,* vol. 4, pp. 3718-3724, 2012.

[112] X. P. Gao, J. L. Bao, G. L. Pan, H. Y. Zhu, P. X. Huang, F. Wu, and D. Y. Song, "Preparation and electrochemical performance of polycrystalline and single crystalline CuO nanorods as anode materials for Li ion battery," *Journal of Physical Chemistry B,* vol. 108, pp. 5547-5551, 2004.

[113] Y. Mu, J. Yang, S. Han, H. Hou, and Y. Fan, "Syntheses and gas-sensing properties of CuO nanostructures by using [Cu(pbbt)Cl2]2·CH3OH as a precursor," *Materials Letters,* vol. 64, pp. 1287-1290, 2010.

[114] K. Han and M. Tao, "Electrochemically deposited p-n homojunction cuprous oxide solar cells," *Solar Energy Materials and Solar Cells,* vol. 93, pp. 153-157, 2009.

[115] L. Li, J. Qin, S. A. Yin, and G. Tang, "Effects of mobile phase ratios on the separation of plant carotenoids by HPLC with a C30 column," *Chromatographia,* vol. 65, pp. 91-94, 2007.

[116] H. Zhu, J. Wang, and G. Xu, "Fast synthesis of Cu2O hollow microspheres and their application in DNA biosensor of hepatitis B virus," *Crystal Growth and Design,* vol. 9, pp. 633-638, 2009.

[117] F. Favier, E. C. Walter, M. P. Zach, T. Benter, and R. M. Penner, "Hydrogen sensors and switches from electrodeposited palladium mesowire arrays," *Science,* vol. 293, pp. 2227-2231, 2001.

[118] X. Zhang, D. Zhang, X. Ni, J. Song, and H. Zheng, "Synthesis and electrochemical properties of different sizes of the CuO particles," *Journal of Nanoparticle Research,* vol. 10, pp. 839-844, 2008.

[119] A. El-Trass, H. ElShamy, I. El-Mehasseb, and M. El-Kemary, "CuO nanoparticles: Synthesis, characterization, optical properties and interaction with amino acids," *Applied Surface Science,* vol. 258, pp. 2997-3001, 2012.

[120] Q. Liu, H. Liu, Y. Liang, Z. Xu, and G. Yin, "Large-scale synthesis of single-crystalline CuO nanoplatelets by a hydrothermal process," *Materials Research Bulletin,* vol. 41, pp. 697-702, 2006.

[121] M. A. Dar, Y. S. Kim, W. B. Kim, J. M. Sohn, and H. S. Shin, "Structural and magnetic properties of CuO nanoneedles synthesized by hydrothermal method," *Applied Surface Science,* vol. 254, pp. 7477-7481, 2008.

[122] N. Mukherjee, B. Show, S. K. Maji, U. Madhu, S. K. Bhar, B. C. Mitra, G. G. Khan, and A. Mondal, "CuO nano-whiskers: Electrodeposition, Raman analysis, photoluminescence study and photocatalytic activity," *Materials Letters,* vol. 65, pp. 3248-3250, 2011.

[123] M. Kaur, K. P. Muthe, S. K. Despande, S. Choudhury, J. B. Singh, N. Verma, S. K. Gupta, and J. V. Yakhmi, "Growth and branching of CuO nanowires by thermal oxidation of copper," *Journal of Crystal Growth,* vol. 289, pp. 670-675, 2006.

[124] T. Jiang, Y. Wang, D. Meng, X. Wu, J. Wang, and J. Chen, "Controllable fabrication of CuO nanostructure by hydrothermal method and its properties," *Applied Surface Science,* vol. 311, pp. 602-608, 2014.

[125]   H. Chen, G. Zhao, and Y. Liu, "Low-temperature solution synthesis of CuO nanorods with thin diameter," *Materials Letters,* vol. 93, pp. 60-63, 2013.

[126]   E. Park and H. W. Park, "Fabrication and synthesis of solvent-free aluminum oxide colloids by electrical explosion of wires in liquids method," *Colloids and Surfaces A: Physicochemical and Engineering Aspects,* vol. 459, pp. 100-108, 2014.

[127]   J. Liu, X. Huang, Y. Li, K. M. Sulieman, X. He, and F. Sun, "Hierarchical nanostructures of cupric oxide on a copper substrate: controllable morphology and wettability," *Journal of Materials Chemistry,* vol. 16, p. 4427, 2006.

[128]   S. Sun, X. Zhang, Y. Sun, S. Yang, X. Song, and Z. Yang, "Hierarchical CuO nanoflowers: water-required synthesis and their application in a nonenzymatic glucose biosensor," *Physical Chemistry Chemical Physics,* vol. 15, pp. 10904-10913, 2013.

[129]   D. P. Singh, A. K. Ojha, and O. N. Srivastava, "Synthesis of Different Cu(OH)2 and CuO (Nanowires, Rectangles, Seed-, Belt-, and Sheetlike) Nanostructures by Simple Wet Chemical Route," *The Journal of Physical Chemistry C,* vol. 113, pp. 3409-3418, 2009/03/05 2009.

[130]   S. Liu, R. Xing, F. Lu, R. K. Rana, and J. J. Zhu, "One-pot template-free fabrication of hollow magnetite nanospheres and their application as potential drug carries," *Journal of Physical Chemistry C,* vol. 113, pp. 21042-21047, 2009.

[131]   Y. S. Luo, X. J. Dai, W. D. Zhang, Y. Yang, C. Q. Sun, and S. Y. Fu, "Controllable synthesis and luminescent properties of novel erythrocyte-like CaMoO4 hierarchical nanostructures via a simple surfactant-free hydrothermal route," *Dalton Transactions,* vol. 39, pp. 2226-2231, 2010.

[132]   C. Lu, L. Qi, J. Yang, D. Zhang, N. Wu, and J. Ma, "Simple Template-Free Solution Route for the Controlled Synthesis of Cu(OH)2 and CuO Nanostructures," *The Journal of Physical Chemistry B,* vol. 108, pp. 17825-17831, 2004/11/01 2004.

[133]   M. Salavati-Niasari, F. Davar, and N. Mir, "Synthesis and characterization of metallic copper nanoparticles via thermal decomposition," *Polyhedron,* vol. 27, pp. 3514-3518, 2008.

[134]   Y. Kobayashi, S. Ishida, K. Ihara, Y. Yasuda, T. Morita, and S. Yamada, "Synthesis of metallic copper nanoparticles coated with polypyrrole," *Colloid and Polymer Science,* vol. 287, pp. 877-880, 2009.

[135]   S. Link and M. A. El-Sayed, "Shape and size dependence of radiative, non-radiative and photothermal properties of gold nanocrystals," *International Reviews in Physical Chemistry,* vol. 19, pp. 409-453, 2000/07/01 2000.

[136]   P. Chand, A. Gaur, and A. Kumar, "Structural, optical and ferroelectric behavior of CuO nanostructures synthesized at different pH values," *Superlattices and Microstructures,* vol. 60,

pp. 129-138, 2013.

[137]   B. Faust, *Modern Chemical Techniques*: Royal Society of Chemistry, 1997.

[138]   J. C. Maxwell, "A Treatise on Electricity and Magnetism, Oxford University Press, Cambridge " 1904.

[139]   K. D. Kihm, C. Chon, J. Lee, and S. U. S. Choi, "A new heat propagation velocity prevails over Brownian particle velocities in determining the thermal conductivities of nanofluids," *Nanoscale Research Letters,* vol. 6, p. 361, 2011.

[140]   C. H. Chon, K. D. Kihm, S. P. Lee, and S. U. S. Choi, "Empirical correlation finding the role of temperature and particle size for nanofluid (Al_2O_3) thermal conductivity enhancement," *Applied Physics Letters,* vol. 87, p. 153107, 2005.

[141]   K. D. Hagen, "Heat Transfer with Applications, Prentice-Hall, New Jersey, USA," pp. 637-638, 1999.

[142]   A. Einstein, "Rubber network formation Anal," *Phys,* vol. 19, p. 289, 1906.

[143]   G. K. Batchelor, "EFFECT OF BROWNIAN MOTION ON THE BULK STRESS IN A SUSPENSION OF SPHERICAL PARTICLES," *Journal of Fluid Mechanics,* vol. 83, pp. 97-117, 1977.

[144]   P. N. Das SK, Roetzel W, "Pool boiling characteristics of nano-fluids," *International Journal of Heat and Mass Transfer,* vol. 46, pp. 851-862, 2003.

[145]   M. K. Scott G. Liter, "Pool-boiling CHF enhanceent by modulated porous-layer coating: theory and experiment," *International Journal of Heat and Mass Transfer,* vol. 44, pp. 4287-4311, 2001.

[146]   R. N. Wenzel, "Surface Roughness and Contact Angle," *The Journal of Physical and Colloid Chemistry,* vol. 53, pp. 1466-1467, 1949.

[147]   S. J. Kim, I. C. Bang, J. Buongiorno, and L. W. Hu, "Effects of nanoparticle deposition on surface wettability influencing boiling heat transfer in nanofluids," *Applied Physics Letters,* vol. 89, p. 153107, 2006.

Acknowledgement

I would never have been able to finish my thesis without the help, support, guidance and effort of a lot of people.

Firstly, I would like to express my deepest gratitude to my advisor, Prof. Hyung Wook Park, for all the support, guidance and encouragement throughout the course of my graduate study. I would also like to appreciate the members, Prof. In Cheol Bang, Young-Bin Park, Sung Soo Park and Hae-Jin Choi for their valuable time and thoughtful insight.

In addition, I would like to thank Dr. Deka and Dr. Ravi for his knowledge and for useful discussion throughout my research work. I would also like to thank our lab members, kyungil Kong, Dongmin kim, jisu Kim, Ieon Lee, Jaeu Seo and Doyoung Kim for their help and support during my stay at UNIST.

Finally, I would like to appreciate my parents, Sanggeun Park and Sunhee Kim, and my younger sister, Eunjung Park for their endless love, understanding and support throughout my graduate study.